博士論文

The effect of the extreme wet event on the larch forest ecosystem in northeastern Siberia
(北東シベリアのカラマツ林生態系に及ぼす湿潤イベントの影響)

Division of Earth System Science,
Graduate School of Environmental Science,
Hokkaido University
北海道大学大学院環境科学院地球圏科学専攻

Aleksandr NOGOVITCYN

February 2023

Table of Contents

Abstract

Extreme wet events are predicted to be more frequent and intensive worldwide, especially in northern regions under Arctic amplification. The taiga ecosystem in northeastern Siberia, a nitrogen-limited ecosystem on permafrost with a dry climate, has changed under such event in 2007. This study aims to investigate how larch forest conditions varied historically and spatially a decade after the extreme wet event in 2007.

Observations were conducted at the Spasskaya Pad Forest station (62°25' N, 129°62' E) near Yakutsk, Russia. In the summer of 2018, a transect (60 m × 510 m) with 34 plots (30 m × 30 m) was set. The plots were divided into four forest types visually using photographs. The first one is a typical larch forest (TF) with no visible effect from the extreme wet event. The other three types are forests affected by the event in order of damage level: regenerating forests RF-1 and RF-2 and damaged forest (DF), where all trees died. The conditions of these four forest types were determined by normalized difference vegetation index (NDVI), a proxy of above-ground production, which was calculated from satellite data (Landsat images with a spatial resolution of 30 m), and the field-observed data. To examine spatial variations in the forest conditions, NDVI in the four forest types were investigated during the summer of 2018 and compared with carbon and nitrogen stable isotopes ($\delta^{13}C$ and $\delta^{15}N$) and the ratio of carbon and nitrogen contents (C/N) of larch needles from mature trees. To study historical variations, the seasonal maximum NDVI in the transect was observed in 1999-2019 and compared with the ecosystem parameters at typical forest out of the transect, such as tree-ring width index (RWI), soil moisture water equivalent (SWE), $\delta^{13}C$, $\delta^{15}N$ and C/N of larch needles.

The spatial variations in NDVI in 2018 revealed a large difference in NDVI among the forest types in June: the TF plots showed the highest values, followed by the RF-1, RF-2, and the most damaged DF. During the summer, the highest and lowest NDVI values were found in the unaffected TF and affected DF, respectively, suggesting that larch tree stand density affected NDVI. In addition, the stand density may be a controlling factor in the spatial variations in the needle C/N and $\delta^{13}C$ values based on their significant relationships with the NDVI in June. It

was concluded that the larch trees from the RF have higher levels of nitrogen and light availability (relatively low C/N and high $\delta^{13}C$) because of the slight competition for the resources, owing to a low-stand density.

The historical variations in NDVI showed that there was generally no difference among the forest types before the extreme wet event in 2007, suggesting that all the forests within the transect were typical larch forests (TF). On the other hand, after the event, NDVI in the RF-2 and DF decreased and the difference in NDVI increased because of high tree mortality under an extremely high SWE and the presence of surface water, lowering NDVI.

Before the extreme wet event in 2007, the TF NDVI was positively correlated with the SWE in the previous summer and current June. In this dry region, this result suggested that larches used the previous-year soil water to make photosynthate (carbon assimilated by photosynthesis) for preparing needles in the current year and used the early-summer soil water for elongation of needles in the current year. On the other hand, after the wet event, the correlations between the TF NDVI and SWE in the previous summer and current June changed to negative. It was suggested that the wet environment in such a dry region may have reduced needle production after the event, resulting in a lower NDVI. The process of photosynthesis depended on soil moisture during the entire observation period, since there was a correlation between the needle $\delta^{13}C$ and previous-August SWE in 1999-2019. The needle C/N was negatively correlated with the TF NDVI in 1999-2006, i.e., high soil moisture may lead to an increase in production of soil inorganic nitrogen and, as a result, an increase in larch needle production. But in 2008-2018, the correlation between the TF NDVI and C/N remained negative, while there was the negative effect of SWE on the TF NDVI after the event. The needle $\delta^{15}N$ and TF NDVI showed a positive correlation before 2007 but no correlation after 2007. Herewith, the $\delta^{15}N$ was generally decreasing after the event, indicating larches may use less inorganic soil nitrogen from deeper layers, which usually have higher soil $\delta^{15}N$ than a surface layer. Based on a positive correlation between the TF NDVI and RWI in 1999-2006, the tree growth and needle production showed synchronous responses to environmental changes before 2007, but the correlation was disturbed after 2007.

The above results showed that, in this dry region, the correlation between the TF NDVI and soil moisture changed from positive to negative before and after the wet event, and the production of larch needles may have decreased in the wet environment. An extremely high soil moisture may had caused an inactive soil inorganic N, anaerobic-stress-induced root damage and/or production of soil phytotoxins, which decreased nitrogen uptake by larches. In the future, more intense and frequent extreme wet events may change the larch forest by reducing not only the production of larch needles but also the wood production.

Chapter 1. General introduction

1.1. Global climate change and extreme weather

In recent years, the surface temperature has increased on a global scale, but the rate of temperature increase has not been spatially uniform (Serreze and Barry 2011). In the high latitudes of the northern hemisphere, the temperature rate is significantly higher than the global average, that makes the northern regions to be more vulnerable to global climate change (Stocker et al. 2013). Under warming, reductions in sea ice, glaciers, and snow, thawing of permafrost and consequent land subsidence have also been observed in such regions (Constable et al. 2022). It has been pointed out that such environmental changes have a significant impact on terrestrial ecosystems (Callaghan et al. 2010; McGuire et al. 2009), so warming in the future could significantly alter carbon and nitrogen cycles not only in Arctic but also at global scale.

Beside warming, extreme precipitation events, such as heavy rainfall and drought, have been observed to become more frequent and intensive worldwide (Douville et al. 2021). These events have different impacts on hydrological and ecological processes in ecosystems with different soil water availabilities (Knapp et al. 2008). Although vegetation responses to drought have been widely studied (e.g. Anderegg et al. 2012; Barber et al. 2000; Kannenberg et al. 2019; Liu et al. 2017; Michaelian et al. 2011), effects of extreme wet events are comparatively less well known. In water-limited regions, dendrochronological data show increased tree growth after extreme wetness, which offsets the negative impact of drought conditions in previous years (Jiang et al. 2019). However, in some regions, extreme moist conditions cause a reduction in vegetation productivity (Heisler-White et al. 2009) and, in severe cases, plant dieback (e.g. Iwasaki et al. 2010; Rozas and Garcia-Gonzalez 2012). The northern regions stand out because extreme events are expected to be more pronounced under Arctic amplification. Therefore, the boreal forest on permafrost, one of the main components of the global carbon cycle, will face changes (e.g. Richardson et al. 2013).

1.2. Importance of taiga ecosystem

Boreal forest in northern regions of N. America and Eurasia, including islands, occupies a large forest area, about 27 % (FAO 2020). Under conditions of increasing atmospheric CO_2 concentrations (e.g. Friedlingstein et al. 2022), a role of taiga and other terrestrial ecosystems as carbon sinks becomes more important. Among the taiga areas, Alaska, Canada and Siberia are distinguished by permafrost soil, which is one of the main components of global carbon cycle. Siberian taiga is covered with coniferous trees, mainly larches, which grow under severe conditions, such as continental climate, i.e. cold winters, hot summers and low precipitation (Archibold 1995), and limited nitrogen availability (Popova et al. 2013). Permafrost and seasonal ice are important sources of water for larches during drought (Sugimoto et al. 2003; Sugimoto et al. 2002). These conditions make this ecosystem vulnerable to environmental changes. Under warming, permafrost may be declined, and that can trigger huge amounts of carbon emission (Schuur et al. 2015) and change the ecosystem.

In eastern Siberia, a role of the taiga ecosystem and its responses to climate change have been studied at the Spasskaya Pad Forest station near Yakutsk. This larch forest is a net CO_2 sink, but quantitative estimations of the flux from tower measurements and various models differ (Takata et al. 2017). For the past decades, tree ring growth has been decreased, and according to tree-ring width index (RWI)-based statistical model, the radial growth of tree expected to have a negative trend because of high temperature induced drought (Tei et al. 2017). On the other hand, precipitation extremes, which are predicted to be more intensive and frequent (Douville et al. 2021), also can negatively affect the forest. Roots of larch, which usually uptake water from seasonal ice in active layer (above the permafrost) under dry conditions, are able to adapt to wet conditions by decreasing vertical distribution (Takenaka et al. 2016). But the extreme wet event in 2007, when soil moisture was the highest for the past century (Tei et al. 2013), was fatal for a large number of trees in the forest, especially in depressions (Iijima et al. 2014; Ohta et al. 2014). Beside high tree mortality, affected sites are distinguished by secondary succession of the understory and floor vegetation communities to water-resistant species (Ohta

et al. 2014). Such sites in the forest are supposed to emit methane, that makes the ecosystem to be net CH_4 source, according to estimations of open-path eddy covariance measurements (Nakai et al. 2020). The wet event was caused by continuously heavy precipitation, including an extremely large snowfall. Snow manipulation experiment in the forest showed an influence of interannual variation in winter precipitation on the phenology and production of soil inorganic nitrogen (Shakhmatov et al. 2022). After the extreme moist conditions formed in 2005-2009, eddy-covariance flux measurements showed no significant trends in CO_2 exchange at ecosystem scale, but a contribution of understory and floor vegetations to CO_2 fluxes has increased with their biomass, while that of overstory larch has decreased (Kotani et al. 2019). High mortality of larches in 2007 could be caused by two consecutive extreme events – drought and wetness (Tei et al. 2019b). Severe drought and moist conditions occurred in the forest lead to changes in normalized difference vegetation index (NDVI) (Nagano et al. 2022; Tei et al. 2019a), which is considered to be a proxy of vegetation productivity. However, gross primary production (GPP) was found to be more related with larch tree-ring width index (RWI) in 2004-2014, but not with NDVI, because of changes of the understory and floor vegetation composition (Tei et al. 2019a). Although a large number of papers studying the larch forest in eastern Siberia have been published, there was no study on relationships between historical NDVI and foliar parameters in eastern Siberia.

1.3. Approaches to monitor ecosystem changes

In this study, remote sensing data and field-observed ecosystem parameters were used as approaches to monitor ecosystem changes. Advantages of using remote sensing data is a large temporal and spatial coverage of the study area. One of widely applied remote sensing methods is the satellite-derived normalized difference vegetation index (NDVI) as an indicator of photosynthetically active greenness to determine vegetation changes owing to shifts in environmental parameters. The NDVI is based on the red and near-infrared (NIR) radiation reflected from the study area:

$$NDVI = (NIR – Red)/ (NIR + Red). \quad (1.1)$$

This vegetation index has been identified to correlate with structural traits, the leaf area index (LAI), i.e. leaf area per unit ground area (Chen and Cihlar 1996; Gamon et al. 1995; Wang et al. 2005), and fractional vegetation cover (Blok et al. 2011). It is also considered to be a tool used to estimate a fraction of photosynthetically active radiation (fPAR) absorbed by plants owing to their relationship (Myneni and Williams 1994), which can be converted to net primary production at either the regional or global scale (Lambers et al. 1998). Because NDVI can be a proxy for above-ground production, many studies have attempted to compare it with field-observed ecosystem parameters, for example, foliar biochemical traits and isotopic signatures.

The red-edge and NIR spectral regions have been shown to be sensitive to leaf nitrogen (Clevers and Gitelson 2013; Wang et al. 2016), which is one of the most essential biochemical leaf traits. Thus, foliar nitrogen content (g N/100 g dry leaf weight, %N) as an indicator of nitrogen availability is suggested to correlate with the vegetation index. Previously, %N was found to be spatially correlated with NDVI (Dyer et al. 1991; Santos et al. 2017; Turner et al. 1992) and seasonally (Lee et al. 2008; Zhu et al. 2007) in grasslands and crops for agricultural purposes. The relationship between NDVI and %N is predominantly positive (Dyer et al. 1991; Lee et al. 2008; Santos et al. 2017; Zhu et al. 2007). At the Siberian taiga-tundra boundary, it has been found that the needle N content of larch trees is an important indicator of nitrogen availability, because it is positively correlated with inorganic nitrogen in soil (ammonium NH_4^+) (Liang et al. 2014). Similarly, Matsushima et al. (2012) revealed a positive effect of increased soil N availability after understory removal and N fertilization experiments on leaf N content in white spruce in Canada. Instead of nitrogen content, the ratio of foliar carbon to nitrogen content (C/N ratio) has been investigated in many regions to estimate the nitrogen use efficiency of plants (Li et al. 2007; Liu et al. 2005).

Another approach involves the leaf isotopic signatures, such as carbon and nitrogen stable isotope compositions ($\delta^{13}C$ and $\delta^{15}N$), which are widely applied to determine how environmental conditions affect plant physiology. The $\delta^{13}C$ and $\delta^{15}N$ are calculated by:

$$\delta^{13}C \text{ (or } \delta^{15}N) \text{ ‰} = (R_{sample}/R_{std} - 1) \times 1000, \quad (1.2)$$

where R_{sample} and R_{std} are isotope ratios ($^{13}C/^{12}C$ or $^{15}N/^{14}N$) of sample and standard, respectively: Vienna Peedee Belemnite (VPDB) for carbon or atmospheric N_2 for nitrogen.

The $\delta^{13}C$ was found to be sensitive to changes in weather conditions, such as drought and solar radiation (Farquhar et al. 1989), resulting in $\delta^{13}C$ increase under smaller stomatal conductance and enhanced photosynthesis. After treatment of a white spruce plantation in Canada, leaf $\delta^{13}C$ increased along with soil N availability (and leaf N content and $\delta^{15}N$) through enhanced carboxylation rate (Matsushima et al. 2012). Spatial NDVI and $\delta^{13}C$ have been reported to be negatively correlated in crops (Stamatiadis et al. 2010; Yousfi et al. 2016), because low biomass production was observed in dry areas. Similar results have been shown in regional-scale studies on natural ecosystems, where the spatial variability in leaf carbon isotope composition (or discrimination) is explained by the amount of precipitation in different parts of the study region (Ale et al. 2018; del Castillo et al. 2015; Guo and Xie 2006). However, in addition to the negative relationship between NDVI and leaf $\delta^{13}C$ in the southern part of the Tibetan Plateau, Guo and Xie (2006) also revealed a positive relationship in northern Tibet; therefore, NDVI is influenced by soil. Light condition also affects photosynthetic activity and thus leaf $\delta^{13}C$. In Siberian larch, and most plants, shaded leaves have lower $\delta^{13}C$ than sunlit leaves. However, not many papers discussed the relationship between NDVI and $\delta^{13}C$ responding to light condition. So, I expect the correlation of between NDVI and $\delta^{13}C$ can be an indicator of environmental variation in soil N and water availability (dry-wet gradient).

Leaf $\delta^{15}N$ serves as an indicator of nitrogen sources for plants, such as organic or inorganic soil nitrogen and atmospheric nitrogen deposition (Michelsen et al. 1996). In many studies, foliar $\delta^{15}N$ has been associated with soil $\delta^{15}N$ (Handley et al. 1999a), which can vary spatially (e.g. Fujiyoshi et al. 2017) and vertically in depth (e.g. Makarov et al. 2008).

1.4. Objective

Taiga in eastern Siberia is one of the main biomes in the world because it covers a large area. This forest ecosystem spreads over the permafrost under a continentally dry climate, but

the extreme wet event of 2006-2007 changed forest conditions. But there are not many papers, which studied how the forest changed in terms of nitrogen and water availabilities and forest production. I believe that the extreme wet event had not only visual effect, that is the forest damage (the tree mortality), but also effect, which cannot be visually detected, such as changes in the physiological response of larches. Since the extreme wet events in the region are expected to be more frequent and intense, it is important to understand the effects of such events on the taiga forest in the future. The objective was to understand how the larch forest at the Spasskaya Pad changed and what factors impacted the changes for the past two decades. Firstly, spatial variations in satellite-derived NDVI and physiological condition of larch trees by observing foliar $\delta^{13}C$ and $\delta^{15}N$, and C/N were investigated along a transect including sites unaffected and affected by the wet event a decade after the wet event. Secondly, historical variations in NDVI of affected and unaffected sites was investigated in 1999-2019, in order to understand effects of extreme wet event on NDVI. Besides, historical variation in the NDVI of unaffected forest was compared with the historical variations in the ecosystem parameters observed at visually unaffected forest, such as tree-ring width index (RWI), soil moisture, needle $\delta^{13}C$, $\delta^{15}N$, and C/N, and with those in the climatic parameters, such as air temperature and precipitation, to understand how larch forest production (NDVI and RWI) varied depending on climate, soil moisture, and N availability.

Chapter 2. Materials and Methods

2.1. Study site and transect

The study was carried out in the Spasskaya Pad Experimental Forest (62°15’18’’N, 129°37’08’’E, alt. 220 m a.s.l.), Institute of Biological Problems of Cryolothozone, Siberian Branch of the Russian Academy of Sciences (IBPC SB RAS), near Yakutsk, Russia (Figure 2.1a). The region in Eastern Siberia is established on a continuous permafrost and has a continental climate (dry climate) with extremely high annual temperature range. The forest is located on a relatively plain terrain with a slight inclination to the north. During the observation period 1991-2020 at Yakutsk, the average annual precipitation is 233 mm and the average monthly temperature ranges from -37˚C to +20˚C in cold January and warm July, respectively. The overstory (forest canopy) consists of deciduous species, dominant coniferous larch (*Larix cajanderi*) (Abaimov et al. 1998) mixed with broadleaved birch (*Betula pendula*), the understory are small shrubs, such as evergreen cowberry (*Vaccinium vitis-idaea*) and deciduous bearberry (*Arctous alpina),* and other grasses.

Although this area has a continuously dry climate, an extreme wet event occurred in 2007. The water year precipitation (from October to September) was very large in 2005 (285 mm) and 2006 (340 mm), and the snowfall in the 2006-2007 winter (October to April) was extremely large (106 mm), which was 1.4 times higher than the average (77 mm from 1971 to 2000). This large amount of precipitation causes high soil moisture (Sugimoto 2019), resulting in high tree mortality (Iwasaki et al. 2010). After abnormal wet conditions occur, the floor vegetation changed to moisture-tolerant grasses and shrubs in some areas, and the stand density of tall trees decreased (Iijima et al. 2014; Iwasaki et al. 2010; Ohta et al. 2014).

Figure 2.1 b,c show the vegetation cover (Landsat 7 ETM+ Natural Color Images) 1 km north of the Spasskaya Pad Forest Station before (2006) and after (2008) the extreme wet event, respectively. To investigate a long-term effect of the extreme wet event on the forest, in the summer of 2018 (a decade after the event), 60 m × 510 m transect was set using wooden pegs and plastic strings, including both intact and affected areas. It was divided into 30 m × 30 m

plots (in total, 34 plots, red polygons in Figure 2.1 b,c), and these plots were visually classified based on forest conditions from the photographs. Four forest types were distinguished along the transect, as shown in Figure 2.2: typical mature forest (TF; number of plots in the transect, n = 17), regenerating-1 (RF-1: many/few mature trees and many young trees; n = 11), regenerating-2 (RF-2: few/no mature trees and many young trees; n = 4), and damaged (DF: no mature trees, few young trees; n = 2) forests. The first, TF, consisted of mature larches of approximately 180 years old with a height of approximately 22 m (Kotani et al. 2019) and had no visible damage from the wet event. The plots discerned as regenerating forest, RF-1, had many dead mature larches and formed forest gaps in the overstory where there were a large number of young larches (seedlings and saplings with a height of up to 3 m) and shrubs. After a wet event for several years, larch seeds germinated and formed a large number of young trees in RF-1. Damaged forest DF, where all mature trees died, was covered predominantly by moisture-tolerant grasses, and there were much smaller numbers of young larches than in RF-1. The DF plots were located on the depression in a trough-and-mound topography (shown by a dark-brown color in Figure 2.1c), and some patches of the DF plots were flooded. Regenerating forest RF-2 plots had a moderate forest condition between RF-1 and DF. The geographical coordinates (longitude and latitude) of the pegs defining the boundaries of each plot were measured using a handheld GPS (Garmin) with a horizontal accuracy of 3 m to estimate satellite-derived NDVI for the plots.

2.2. NDVI for spatial and historical variations

The raster normalized difference vegetation index (NDVI) was computed based on the atmospherically corrected Landsat Collection-1 Level-2 image products with a spatial resolution of 30 m with the QGIS software (v. 3.2.2-Bonn) based on the equation 1.1, where NIR and Red are near-infrared and red surface reflectance bands of the products, respectively. The image products were provided by the United States Geological Survey (USGS) website (https://earthexplorer.usgs.gov/). The image products georeferenced to WGS-84 UTM 52N

coordinate system were selected corresponding to the location of the study transect. NDVI value was extracted for each transect plot with the zonal statistics function. The transect plots which consist of pixels not attributed as quality pixels (clear-terrain, low confidence cloud, low confidence cirrus) in the quality assessment bit index band according to Landsat Surface Reflectance product guides were excluded from the analysis.

To investigate the seasonal variation in NDVI in 2018, I obtained the image products that were acquired from June to September 2018. After calculating raster NDVI, the mean NDVI value was extracted for each transect plot using the zonal statistics function, wherein a transect plot was presented in the QGIS as a polygon vector layer created from the geographical coordinate data. Only the transect plots with pixels showing "clear-terrain, low confidence cloud and low confidence cirrus" in Quality Assessment band were used in the analysis. During June–September 2018, images were acquired on 15 days in total, but only 5 days (June 4, July 31, August 7, August 23, and September 17) were cloud-free. Therefore, NDVI on these five observation days were analyzed in this study.

To investigate the historical variation in NDVI, I considered seasonal maximum of mean NDVI of the transect for the long-time period 1999-2019. The longest time-series data available for the study area have been obtained by Landsat 7 satellite with Enhanced Thematic Mapper Plus (ETM+) image sensor since 1999. However, its sparse temporal resolution (16 days) and scan-line corrector failure in 2003 force to consider additional data from other satellites, such as Landsat 5 Thematic Mapper (TM) (available until 2011) and Landsat 8 Operational Land Imager (OLI) (available since 2013) (Figure S1). Since the last two have different sensors in contrast to Landsat 7, NDVI values calculated from the TM and OLI images were converted to ETM+ using the linear equations 2.1 and 2.2:

$$NDVI_{ETM+} = 1.037 * NDVI_{TM}, \quad (2.1)$$

$$NDVI_{ETM+} = 0.9589 * NDVI_{OLI} + 0.0029 \quad (2.2)$$

developed by Ju and Masek (2016) and Roy et al. (2016) for boreal forests, respectively. For each year, paired sample t-test was applied to determine a difference among mean NDVI of the

transect on observation days (Figure S2). In case of statistically insignificant difference among observation days, the day with a higher number of quality pixels was selected. To verify the historical variation in NDVI of the transect, a larger area, 10 km x 10 km (here after 10-km plot), including the Spasskaya Pad Forest was used to compare with the transect (the center of 10-km plot was located at 62°17'4''N, 129°32'44''E, Figure 2.1a). For each observation day, mean NDVI of the 10-km plot was calculated using only quality pixels with ENVI 5.1 (L3Harris Technologies, USA). For each year, seasonal maximum NDVI of the 10-km plot was determined as the highest mean NDVI among observation days, on which a number of quality pixels were more than 50% (totally, 111556 pixels). The seasonal maximums of transect and 10-km plot showed the same day about three fourth of the study period (15 years among 21), and showed the different day in 6 years: 2006 (August 7 and July 29), 2007 (July 1 and 25), 2010 (July 1 and 15), 2011 (August 5 and 12), 2015 (July 23 and 31), 2019 (July 1 and 9). Averaged NDVI values of the 10-km plot, the transect and each forest type (TF, RF-1, RF-2, and DF) in the transect were shown in Figures 4.1a and b.

2.3. Larch needle $\delta^{13}C$, $\delta^{15}N$ and C/N data for spatial variation

In the period from late July to early August 2018, one to two tree branches were cut in each plot, from one to four randomly located living mature larch trees, from a height of approximately 6 m in the lower crown, with the use of a pole tree pruner. The needles from each tree were placed in a paper bag and mixed thoroughly. A total of 105 needle samples were collected and oven-dried at 60 °C for 24 h.

The dried needle samples were brought to Hokkaido University, they were powdered with liquid nitrogen, and dried again at 60 °C for 24 h. Each sample was then wrapped in a tin capsule and analyzed for carbon and nitrogen contents and for their isotope compositions using a continuous flow isotope ratio mass spectrometry system consisting of Flash EA 1112 (Thermo Fisher Scientific, Milan, Italy) coupled to Delta V (Thermo Fisher Scientific, Bremen, Germany) via Conflo III interface (Thermo Fisher Scientific, Bremen, Germany). The stable

carbon and nitrogen isotopic compositions were reported with the standard δ notation (‰) relative to the VPDB (Vienna Peedee Belemnite) and atmospheric N_2 (air), respectively. The analytical precisions (standard deviation) of the carbon and nitrogen content measurements were better than 0.3% and 0.1%, respectively, and those for the isotopic compositions $\delta^{13}C$ and $\delta^{15}N$ were 0.1‰.

2.4. Field-observed parameters for historical variation

Several parameters of the ecosystem have been observed from 1998 at the typical forest. In order to monitor physiological response of larch to environmental changes, the $\delta^{13}C$ (‰), $\delta^{15}N$ (‰), and C/N of larch needles have been observed since 1999, except 2012 at a site located 0.2 km south of the transect (Figure 2.3). In the mid-August of every year, the same four to eight young larch trees close to each other were sampled. After sampling, the same procedures were done as described in Section 2.3 to obtain larch needle $\delta^{13}C$, $\delta^{15}N$ and C/N data. Average values of $\delta^{13}C$ (‰), $\delta^{15}N$ (‰), and C/N of these samples were used. Details of average calculations were shown in Figure S3 and S4. In 2015, there was no data for $\delta^{15}N$ and N content.

Larch ring-width index (RWI) for more than 100 years until 2016 was estimated by detrending and standardizing the raw time-series width data obtained from the collected paired cores (Tei et al. 2019a).

Soil moisture was observed with time-domain reflectometry (TDR), and soil moisture water equivalent (SWE; amount of liquid water contained within soil layer, mm) in the soil layer 0–60 cm was obtained for 1998–2019 in June, July, and August using the method described by Sugimoto et al. (2003) (near the transect, Figure 2.3). There was no data in June of both 2002 and 2011, August of 2003. Details of intra- and interannual variation of SWE were shown in Figure S5.

Among climate variables, summer air temperature and precipitation datasets recorded by the meteorological station at Yakutsk (62.02º N, 129.72º E) were obtained from All-Russia

Research Institute of Hydrometeorological Information - World Data Centre (RIHMI-WDC) website (http://aisori-m.meteo.ru/).

2.5. Statistical analysis

For spatial variations, for each transect plot, the mean and standard deviation of the needle $\delta^{13}C$, $\delta^{15}N$, and C/N values were calculated. In order to investigate the relationships between the datasets, simple linear regressions (function 'lm') were used in R statistics (v. 3.6.0). The regression models were described by the determination coefficient R^2 (degree of variance between the observed and fitted values) and *p* value (statistical significance level). In order to determine whether the NDVI in the same group (a forest type or the entire transect) on two observation days was different, either the parametric paired Student's *t*-test or the non-parametric Wilcoxon signed-rank test was used. If the mean difference between the pairs on two days was normally distributed, according to the Shapiro–Wilk test, the paired *t*-test was performed; otherwise, the Wilcoxon signed-rank test was used. In order to define a statistical difference between the means of either the plot NDVI or the individual foliar traits in two different groups (forest types), a parametric unpaired Student's two-sample *t*-test was applied in R. This test assumed that two groups of data (forest types) had normal distributions and equal variances, which were checked using the Shapiro–Wilk test and the F-test, respectively. If two normally distributed groups did not have equal variances, Welch's two-sample *t*-test was used. If at least one of the two groups was not normally distributed, the non-parametric Wilcoxon rank-sum test was used instead of the *t*-test.

For the historical variations, relationships between datasets were investigated using a simple linear regression model (function 'lm') and a Pearson correlation test ('cor.test'). Trends of NDVI change in 1999-2019 were estimated using Mann-Kendall test (package 'trend', function 'mk.test'). Differences in a parameter between two groups (forest types) were determined with two parametric unpaired two-sample tests, classical-Student's and Welch's t-tests, and one non-parametric Wilcoxon rank-sum test as it was described before. The results

of the statistical tests were shown in the Supplementary materials (Table S2-S9). The models and tests described by levels of statistical significance (p-values) less than 0.05 and 0.1 were considered to be “significant” and “moderately significant”, respectively.

Chapter 3. Spatial variations in NDVI and forest conditions

3.1. Results

3.1.1. Seasonal variation of NDVI and forest condition

Seasonal variations in NDVI along the transect are shown in Figure 3.1. The NDVI values of 34 plots varied from 0.42 to 0.73 (0.66 ± 0.09) on June 4, from 0.71 to 0.76 (0.74 ± 0.01) on July 31, from 0.73 to 0.81 (0.77 ± 0.02) on August 7, from 0.64 to 0.73 (0.70 ± 0.02) on August 23, from 0.39 to 0.47 (0.43 ± 0.02) on September 17 (Figure 3.1a-e). The highest values were observed on August 7 and decreased until September. It is important to note that the four forest types showed different NDVI values. The distribution of the forest types along the transect is displayed in Figure 3.1f. The TF had the highest values, followed by RF-1, RF-2, and DF (Figure 3.1g). A large difference in NDVI among the forest types was observed on June 4: TF, RF-1, RF-2, and DF were 0.71 ± 0.01 (n = 17), 0.66 ± 0.03 (n = 11), 0.51 ± 0.06 (n = 4), and 0.46 ± 0.01 (n = 2), respectively, but the difference was small on July 31 (Figure 3.1g). Subsequently, the mean NDVI values for the forest types TF, RF-1, RF-2, and DF changed uniformly (Figure 3.1g). As shown in Table 3.1, the statistical tests revealed the highest NDVI at TF and the lowest NDVI at RF-2 and DF; the difference between RF-2 and DF was statistically insignificant. RF-1 was between the highest (TF) and lowest (RF-2 and DF) in June, July, and August (Table 3.1).

3.2.2. Spatial variations in larch foliar traits

Spatial variations in foliar $\delta^{13}C$ and $\delta^{15}N$ values and C/N ratios along the transect are shown in Figure 3.2. Six of 34 plots had no data because no mature trees or other trees were available for sampling using the pole tree pruner. Foliar $\delta^{13}C$ averaged for all samples was -28.2 ± 0.7‰ (n = 105). Among the plots, the lowest $\delta^{13}C$ was found in TF plot No. 7 (-28.9 ± 0.3‰, n = 4), and the highest was in RF-2 plot No. 29 (-26.6 ± 0.5‰, n = 4) (Figure 3.2a). As seen in Figure 3.3a, when comparing the forest types, the mean $\delta^{13}C$ of RF-2 (-26.6 ± 0.5‰, n

= 4) was higher than that of TF (-28.2 ± 0.6‰, n = 68) and RF-1 (-28.2 ± 0.6‰, n = 33), but, according to Student's *t*-tests, no significant difference was observed among TF, RF-1, and RF-2.

As shown in Figure 3.3a, there were several outliers. Relatively high $\delta^{13}C$ values of individual trees were observed not only in the RF-2 plot but also in TF plot No. 1 (-25.9‰) and RF-1 plot No. 34 (-26.4‰). I describe these data later in the Discussion section.

The foliar $\delta^{15}N$ value averaged for all samples was -3.9 ± 0.9‰ (n = 105). Mean $\delta^{15}N$ at plots ranged from -5.0 ± 0.6 (RF-1 plot No. 23) to -2.3 ± 0.8‰ (RF-2 plot No. 29) (Figure 3.2b). Among the forest types, mean $\delta^{15}N$ values were statistically insignificant, although the TF (-4.0 ± 0.8‰, n = 68) and RF-1 (-3.9 ± 0.9‰, n = 33) had lower $\delta^{15}N$ than RF-2 (-2.3 ± 0.8‰, n = 4) (Figure 3.3b).

The foliar C/N ratio showed the mean value of 37.2 ± 6.4 (n = 105) for all samples, ranging from 24.0 to 58.3 was observed at trees in the RF-2 plot No. 29 and the TF plot No. 5, respectively. Among the forest types, no significant difference in C/N was observed, but the C/N ratio in TF (38.9 ± 6.3, n = 68) was higher than that in RF-1 (34.7 ± 5.2, n = 33), and RF-2 (28.4 ± 4.2, n = 4) showed the lowest C/N (Figure 3.2c and Figure 3.3c).

The C/N and $\delta^{13}C$ values for each tree sample were found to be linearly related, but with much variation (R^2 =0.18, $p < 0.05$; Figure 3.4). The other foliar traits showed no significant relationships.

3.2.3. Relationships between NDVI and foliar traits

The statistical parameters that describe linear regression models between foliar traits and NDVI are tabulated in Table 3.2. The NDVI on June 4 was linearly related to $\delta^{13}C$ and C/N (Figure 3.5). $\delta^{13}C$ showed a significant negative relationship with the June 4 NDVI, but there was significant variation in $\delta^{13}C$ (R^2 =0.15, $p < 0.05$; Figure 3.5a). June 4 NDVI values showed a significant increasing trend with the plot C/N ratio (R^2 =0.39, $p < 0.01$, Figure 3.5b). In

addition, C/N was positively correlated with NDVI on August 23 ($R^2 = 0.39$, $p < 0.01$) and September 17 ($R^2 = 0.15$, $p < 0.05$).

3.2. Discussion

3.2.1. Plant phenology and seasonality of the ecosystem of each forest type

In this study, one of the purposes of applying NDVI was to identify whether vegetation productivity varied among the four forest types formed after the damage by the wet event during the growing season. Unfortunately, the number of observation days for NDVI was limited by sparse data acquisition (every 16 days) and cloud-contaminated images. As a result, only five days (June 4, July 31, August 7, August 23, and September 17) were available to interpret the general trends in NDVI for better understanding phenology.

The transect NDVI increased from June 4 to August 7, and the seasonal peak was reached on August 7 for all forest types (Figure 3.1g). The maximum greenness in both the intact and affected areas at the beginning of August implied the highest foliar biomass production of the above-ground vegetation as a result of its growth. The timing and magnitude of peak NDVI in an ecosystem can vary spatially and annually. Previously, the phenology of Siberian forests was found to be controlled by precipitation and air temperature, and the peak NDVI was determined to occur usually in July (Suzuki et al. 2001). However, in our case, it was difficult to determine the date of the seasonal peak because of the sparse data acquisition. The NDVI peak in 2018 could have been reached earlier. After the vegetation green-up, NDVI subsequently decreased owing to leaf senescence (yellowing) (Figure 3.1g).

On all observation days, the NDVI values were the highest at TF and decreased due to the damage by the wet event, although the statistically similar (insignificant) RF-2 and DF data were the lowest (Figure 3.1g). The descending order of NDVI from the intact (TF) to the more affected areas can be explained by the differences in tree stand density. Although a typical forest is composed of a large number of larches making up the dense canopy, the damaged forest has no mature trees. In turn, the regenerating forests RF-1 and RF-2 had gaps in the forest canopy,

where many trees died after the wet event. The positive effect of stand density on NDVI can be associated with a positive relationship between NDVI and LAI (Bahru and Ding 2020; Will et al. 2005). A typical larch forest in the intact area is supposed to have higher foliar biomass production than other forest types, with a lower number of trees in the affected area. However, several studies conducted in northern boreal regions showed a negative relationship between NDVI and the attributes of above-ground biomass. In Siberian larch forests, Loranty et al. (2018) found that the mean seasonal NDVI was lower at sites with higher overstory stand density. In Canadian permafrost peatlands covered by black spruce and larch, both stand density and basal area are negatively correlated with the peak NDVI (Dearborn and Baltzer 2021). In those studies, this implicit phenomenon could be explained by shadowing both the understory and lower part of crowns in dense conifer stands, which decreases NDVI values (e.g. Hall et al. 1995). However, in our case, the foliar biomass of the forest canopy was the main factor controlling the spatial variation in the NDVI.

The difference in NDVI between the highest (TF) and the lowest (DF) forest types was the largest on June 4 and then significantly decreased by July 31, after which it remained small. As a result, the increase in NDVI from June 4 to July 31 was smallest at TF and largest at DF (Figure 3.1g). This can be associated with the phenological features of the above-ground vegetation for each type. The intact and affected areas differed in the ratio of the overstory and surface vegetation exposed to radiation. A small increase in NDVI at TF was mainly caused by the growth of needles and shoots of mature larches, whereas a large increase in DF was induced by the growth of grasses, shrubs, and young larches. In turn, the increases in NDVI at RF-1 and RF-2 resulted from the phenology of both the forest canopy and surface vegetation. Therefore, the production of surface vegetation, such as shrubs and grasses, is high during this period and causes higher NDVI. Chen and Cihlar (1996) reported a similar finding when they found a stronger relationship between NDVI and overstory LAI in open boreal conifer stands in late spring than in mid-summer. Because the understory and floor vegetation greatly contribute to NDVI in the middle of the growing season, it was reasonable to use NDVI in early summer to investigate the spatial variation in above-ground production of the overstory.

Thus, throughout the growing season, vegetation in the intact (TF) and affected (RF-1, RF-2, and DF) areas varied in phenology. At the beginning of the growing season, the large difference in NDVI between the areas was associated with mature larch tree stand density: NDVI was higher in the intact area with dense forest canopy than in the affected area. However, afterwards, the difference was smaller on the subsequent observation days because the surface vegetation in the gaps of the forest canopy in the affected area grew and showed high greenness. The maximum production in both areas was reached at the same time, at the beginning of August. NDVI then decreased uniformly because of leaf senescence.

3.2.2. Forest condition after the damage by the wet event

To understand the physiological responses of larch trees after the wet event, needle parameters, such as $\delta^{13}C$, $\delta^{15}N$, and C/N, were compared among the forest types, but the results were not statistically significant. These results could be derived from the sample size; namely, much smaller sample sizes at RF-1 (n = 33) and RF-2 (n = 4) than at TF (n = 66) may have produced non-significant relationships.

In our study, as seen in Figure 3.2a and Figure 3.5a, the highest $\delta^{13}C$ values in the transect were found in RF-2 plot No. 29 and RF-1 plot No. 23 near the depression, where tree stand density seemed to significantly decrease after the extreme wet event. There are two potential reasons for these high $\delta^{13}C$ values. The first was that high $\delta^{13}C$ was caused by water logging (Li and Sugimoto 2018), such as the extreme wet event that occurred in 2007, and the second was the light condition. For the first one, during waterlogging pot experiments, Li and Sugimoto (2018) reported an increase in foliar $\delta^{13}C$ values for the larch trees *Larix gmelini*. However, such high $\delta^{13}C$ values were photosynthesized only during water logging, and there was no water in RF-1 or RF-2. In addition, according to C/N data, at RF-1 and RF-2, there were favorable conditions in terms of nitrogen availability (low C/N ratio or high N content). Therefore, the high foliar $\delta^{13}C$ was caused by the second reason; that is, the high $\delta^{13}C$ in the low-density stand can be explained by higher light availability than in dense stands. The laboratory observations,

which were conducted by Ehleringer et al. (1986), support that the light level is the environmental parameter most likely responsible for the changes in intercellular CO_2 levels and, consequently, higher $\delta^{13}C$.

The results of vertical gradients in $\delta^{13}C$ have been reported in many studies (Duursma and Marshall 2006; Ehleringer et al. 1986; Garten and Taylor 1992). In dense stands, leaves in the lower part of the tree crown have lower $\delta^{13}C$ than those in the upper part owing to shading. Thus, regenerating forest stands with a low number of trees are supposed to be more exposed to light, resulting in higher $\delta^{13}C$ values than those in typical forests with a large number of trees.

It is necessary to mention that high $\delta^{13}C$ values were observed not only in regenerating forests but also in typical forests (Figure 3.3a). As shown in Figure 3.3a, $\delta^{13}C$ of the trees from TF plot No. 1 (-25.9‰) and RF-1 No. 34 (-26.4‰) was unusually high (outliers). The reason for this high $\delta^{13}C$ could be the same as that at RF-2, because the C/N ratio of these trees was relatively low (32.9 and 28.5, respectively), indicating high nitrogen availability. In addition to these outlier data, some of the trees at TF had relatively high $\delta^{13}C$, but there was a high C/N ratio (e.g., -28.2 ‰ and 58.3 for $\delta^{13}C$ and C/N in plot No. 5, Figure 3.4). This result indicates that the trees were under dry conditions.

The C/N averaged for each forest type varied: TF was the highest, RF-1 was intermediate, and the lowest value was observed at RF-2. As described before, NDVI was similarly different among TF, RF-1, and RF-2 (Figure 3.1g); therefore, the plot-averaged C/N was positively correlated with NDVI at different phenological stages in early June (leaf development) and at the end of August and September (senescence) (see Table 3.2). Thus, C/N varied significantly among the forest types, which means that forest density could affect nitrogen uptake by larch. Thus, the low foliar C/N values, that is, the high N content observed in the plots with regenerating forest, indicate higher nitrogen availability for larch trees. This was an unexpected result because nitrogen uptake was hypothesized to be limited in wet areas owing to high competition between plant roots and soil communities. Previously, spatial NDVI and mass-based N content were found to be negatively correlated only in grasslands (Turner et al. 1992). In *Bromus inermis* prairie, such negative relationships were found at the beginning and end of

the growing season, which are presumably controlled by tallgrass regrowth after grazing and senescence, respectively (Turner et al. 1992). I expected that N availability for a tree in the affected plots would be lower than that in the plots with a typical forest because of inactive nitrogen production in wet soil. However, our results show higher N availability for one mature tree in the affected forest owing to low competition among trees. In addition, the larch trees in the affected areas may be well supplied with water, which increased nitrogen uptake.

Our results regarding the foliar nitrogen isotopic composition were ambiguous. Plot $\delta^{15}N$ was not dependent on June NDVI, which was considered to represent tree stand density, but there was a significant positive relationship between plot $\delta^{15}N$ and NDVI in July. Generally, individual trees exhibited large variations in foliar $\delta^{15}N$ values. The high variability observed in our study demonstrates the spatial heterogeneity of the soil along the transect.

As a result, I found spatial variations in NDVI and foliar $\delta^{13}C$ and C/N depending on forest conditions formed after the wet event. Generally, a level of forest damage in our study site was controlled by microtopographic conditions (Iwasaki et al. 2010), thereby highest tree mortality was observed on the topographic depression in the northern part of the transect (DF). Besides, soil properties, such as water retention and porosity (Iwasaki et al. 2010), could have an influence on the formation of the forest types and, consequently, on the variations in NDVI and foliar $\delta^{13}C$ and C/N.

3.3. Summary

In the Chapter 3, spatial variations in NDVI and leaf-level indicators of the physiological response of the larch forest in eastern Siberia 10 years after the extreme wet event. Stand density seemed to be an important factor controlling changes in NDVI. In affected areas, i.e., regenerating (RF) and damaged (DF) forests, high tree mortality caused a lower NDVI on each observation day than that in the intact forest. The larch forest in RF (lower June NDVI) had higher light (higher $\delta^{13}C$) and nitrogen (lower foliar C/N) availabilities because of reduced competition for light and soil nitrogen among trees. Such favorable conditions and the presence of a large number of young larch trees may lead to further succession of RF after an extreme

wet event. However, the difference in soil nitrogen production between affected and unaffected areas was still not clear. Therefore, nitrogen availability per unit of area should be investigated. To understand how the larch forest in the affected areas will change, it is necessary to have a long-term observation of the forest conditions.

Chapter 4. Historical variation in NDVI of typical forest

4.1. Results

4.1.1. Year-to-year variation of seasonal maximum NDVI

Figure 4.1a shows historical variation in seasonal maximum NDVI of transect and 10-km plot in 1999-2019. Both NDVI time-series varied similarly. The date of seasonal maximum of each year was observed from June 25 to August 13 (shown in Table S1), except for 1999. The maximum transect NDVI in 1999 was observed on August 27 (0.75±0.02, n=34), because the Landsat data in 1999 were limited to only the latter half of August. Mean seasonal maximum NDVI for the entire transect varied from 0.72 to 0.80. During the period 1999-2001, NDVI of the transect was high from 0.75±0.02 (n=34) to 0.80±0.02 (n=34) (Figure 4.1a), but in 2002 and 2003, NDVI was much lower (0.73±0.02, n=34) than that in 2001. From 2003 to 2006, NDVI again increased from 0.73±0.02 (n=34) to 0.76±0.02 (n=34). During the wet event in 2007-2008, NDVI decreased to 0.73±0.04 (n=34). After 2009, NDVI was basically higher than in 2008 (0.72±0.03, n=34), except 2016 (0.72±0.03, n=31).

Both mean NDVI of the 10-km plot and transect decreased from 1999 to 2019 (-0.0009 and -0.0010 $year^{-1}$, respectively), but not with statistically significant trends. Generally, mean NDVI in the transect was higher than that in the 10-km plot, except 2000 and 2014.

4.1.2. NDVI of each forest type

The NDVI time-series for four forest types (typical forest TF, regenerating forests RF-1 and RF-2, damaged forest DF) in the transect during 1999-2019 are shown in Figure 4.1b. As seen in Figure 4.1b and Figure 4.2a, before 2007, NDVI of TF in 1999-2001 (0.75±0.02 to 0.79±0.01, n=17) was higher than in the subsequent period 2002-2006 (0.73±0.02 to 0.75±0.02, n=17). There was a significant decrease in TF NDVI between the period from 2002 to 2004 (Figure 4.1b, Figure 4.2a). During 1999-2006, NDVI of the four types were close each other, but after the wet event, NDVI values noticeably differed among the forest types (Figure 4.1b). In 2007, the NDVI of TF (0.76±0.02, n=17) was the highest, and those of other three types

decreased in the order of RF-1 (0.72±0.03, n=11), RF-2 (0.68±0.02, n=4), and DF (0.67±0.02, n=2) (Figure 4.1b). In 2008 the NDVI slightly decreased, and showed the same order of forest types as observed in 2007. After 2009, the difference among the forest types, especially between TF and DF, has still remained, although it has become smaller than that in 2007.

4.1.3. NDVI of the typical forest and ecosystem parameters of the study site

To consider the historical variation in NDVI of typical forest in our study area, TF NDVI and observed parameters were compared (Figure 4.1 and 4.2). In Figure 4.3, the linear relationships between NDVI and other parameters were investigated for two different temporal periods, before (1999-2006) and after (2008-2019), to compare them.

4.1.3.1. Climate parameters (temperature and precipitation) at Yakutsk

Interannual variations in climatic parameters, such as air temperature and precipitation, in 1999-2019 are displayed in Figure 4.1c and d. The average air temperature for June-August (the summer temperature) was relatively high in 1998, 2001-2002, 2008-2012 (Figure 4.1c). The TF NDVI did not show the correlation with the summer temperature. The amount of water year precipitation (from last year October to this year September) for the period from 1991 to 2020 averaged about 233 ± 47 mm. As seen in Figure 4.1d, larger water year precipitation, i.e., precipitation higher than 280 mm (one standard deviation above the mean for 1991-2020), was observed in 2003 (287 mm), 2005-2007 (285, 340, and 296 mm), 2013 (304 mm). The amount of water year precipitation in 2001 (124 mm) was the lowest in the whole observation period. This drought year (2001) showed high TF NDVI. Consecutive wet years in 2005-2007 showed slightly high TF NDVI values, but there was no correlation between the water year precipitation and NDVI.

4.1.3.2. RWI at the typical forest

The larch tree-ring width index (RWI) had a mostly similar trend with the transect TF NDVI in 1999-2007 (Figure 4.1a and b). The RWI and average TF NDVI showed high values

in 2000-2001 (0.95-1.08 and 0.78-0.79) followed by low values in 2002-2003 (0.33-0.55 and 0.73), herewith the RWI in 2003 was the lowest for the whole observation period. Then, both of them had increased by 2007 (1.21 and 0.76). After 2007, these two parameters showed a different behavior. During the period from 2010 to 2013, a one-year time lag in the TF NDVI was found: there was an increase in RWI from 2009 to 2011, and decrease in 2012, and one year later from 2010 to 2012 TF NDVI increase, and decrease in 2013. Statistically, a temporal correlation between the TF NDVI and RWI was positive at a moderate significant level for the period of 1999-2016 ($r=0.41$, $p<0.1$, Table S7), herewith a correlation was significantly positive before 2007 ($r=0.79$, $p<0.05$, Figure 4.3a, Table S5), but insignificantly negative after 2007 (Figure 4.3a, Table S6).

4.1.3.3. Soil moisture water equivalent (SWE) at the typical forest

The time series of the soil moisture water equivalent (SWE) and TF NDVI showed different correlations in the early and late halves of the observation period (Figure 4.2a and c). In 1999-2007, the SWE averaged for June-August (here after summer SWE) and TF NDVI showed mostly similar trends. High values of the TF NDVI in 2000 and 2001 corresponded to high values of the SWE in the current June (239 and 202 mm) and in the last summer (173 and 176 mm in 1999 and 2000). These high values of the TF NDVI and SWE were followed by low values during the drought period of 2002-2003. After that, as the summer SWE increased from 2004 (124 mm) to 2007 (218 mm), the TF NDVI also increased. So, before 2007, the TF NDVI showed the lowest values during dry years, but the highest in the wet years (Table 4.1). For the period from 2008 to 2019, the correlation between the TF NDVI and summer SWE was negative with a one-year time lag of the SWE (Figure 4.2a and c). A low value of the summer SWE was observed in 2011 (91 mm), and a high value of the TF NDVI was seen in the subsequent year 2012. After 2016, the TF NDVI showed an increasing trend, while the SWE decreased from 2015 to 2019. Statistically, the TF NDVI showed positive correlations with the SWE in current June ($r=0.83$, $p<0.05$) and previous summer ($r=0.79$, $p<0.1$), including previous July ($r=0.82$, $p<0.05$) and previous August ($r=0.69$, $p<0.1$), during the period from 1999 to 2006

(Figure 4.3b-d and S6d; Table S5), and negative correlations with the SWE in previous summer ($r=-0.65$, $p<0.05$) and in current summer at a stronger significance level ($r=-0.73$, $p<0.01$) after 2008 (Figure 4.3b-d and S6a-e; Table S6). While, during and after 2007, there was no change in the TF NDVI, slightly damaged RF-1 showed a decrease in NDVI to the levels like during the 2002 drought (Table 4.1).

4.1.3.4. Larch needle $\delta^{13}C$, $\delta^{15}N$, C/N at the typical forest

As seen in Figure 4.2a and d, the foliar $\delta^{13}C$ and TF NDVI moved in opposite directions in the early half of observation period (from 1999 to 2009) (Figure 4.2a and d). For example, in 2000 and 2001, the TF NDVI had large values, while the foliar $\delta^{13}C$ values were low (-29.5±0.5 and -28.9±0.9‰). During the period from 2002 to 2007, TF NDVI increased, and at the same time foliar $\delta^{13}C$ values decreased. The foliar $\delta^{13}C$ values higher than -28.0‰ were observed in 2002, 2003, 2011 and 2018, when low summer SWE and low TF NDVI were observed (Figure 4.2a and d). A correlation between the foliar $\delta^{13}C$ and TF NDVI was statistically insignificant without a time lag (Figure 4.2e, Table S5-7), but there was a significant correlation between the foliar $\delta^{13}C$ and TF NDVI with a time lag of the foliar $\delta^{13}C$ (Table S6). Besides, the foliar $\delta^{13}C$ was negatively correlated with the previous August SWE was found in 1999-2007 ($r=-0.79$, $p<0.05$) and 1999-2019 ($r=-0.63$, $p<0.01$) (Figure 4.4), but also with the SWE in current year June and July for the period from 1999 to 2007), and June to August for 2008 to 2019 (Table S8).

Similar to the $\delta^{13}C$, the foliar C/N and TF NDVI moved in opposite directions (Figure 4.2a and f). In 2000 and 2001, the foliar C/N had low values (25.6±1.1 and 28.8±3.4, respectively), while the TF NDVI was high. There was also a distinct negative correlation between trends in C/N and TF NDVI before and after 2007 but excluding 2019 (Figure 4.3f).

The foliar $\delta^{15}N$ was decreasing after 2005 (Figure 4.2e). Positive correlation was observed between the foliar $\delta^{15}N$ and TF NDVI before 2007 (Figure 4.3g).

4.2. Discussion

4.2.1. NDVI variation among forest conditions

Before 2007, there was a small difference in NDVI among four forest types (Figure 4.1b and Table S4). Most years before 2007, NDVI values at RF and DF were larger than that at TF. In 2007-2008, there was a large difference in NDVI among the forest types, especially between the TF and DF (Figure 4.1b). In this period, the soil moisture water equivalent (SWE) reached extremely high values (Figure 4.2c) caused by a large precipitation amount occurred in 2005-2008 (Figure 4.1d). Consequently, forest floor was partially waterlogged, resulting in a damage of the larch forest, especially at DF and RF in the transect. These data may indicate that, during the drought years (before 2007), wet sites such as DF and RF showed higher NDVI values than dry TF sites, because of higher water availability. However, after 2007, the TF, which was visually unaffected by the wet event, showed higher NDVI than the DF and RF. The presence of surface water in DF and the soil saturated with water in DF and RF could also reduce NDVI values.

After 2009, as soil was getting dry, the difference in NDVI among forest types was becoming small (Figure 4.1b). This may be caused by the change in vegetation at DF and RF, that is to say the change from mature larch tree to understory and floor vegetation such as water-tolerant species and seedlings of birch and larch trees via secondary succession. In 2016, the difference in NDVI between TF and DF became large again (Figure 4.1b). This may be caused by the high SWE observed in 2015 (Figure 4.2c), which lowered NDVI at RF and DF.

The difference in NDVI between TF and DF, however, still remained in the end of the observation period. In the section 3, the spatial variation in NDVI along the transect was investigated a decade after the wet event, in 2018. It was concluded that NDVI was higher in TF than in DF because of a difference in the stand density of mature trees, because NDVI indicates a leaf area index (LAI), which corresponded a number of mature trees in this forest.

4.2.2. Trends in NDVI of the transect and 10-km plot

The NDVI of the 10-km plot showed a similar trend with the transect NDVI during the observation period ($r=0.78$, $p<0.001$), as seen in Figure 4.1a, and the mean NDVI value of the 10-km plot was lower than that of the transect in most years. The year-to-year variations were found in both NDVI data, but no significant increasing or decreasing trends were observed, and that is consistent with previous studies in this site (Lloyd et al. 2011; Nagano et al. 2022; Tei et al. 2019a). Therefore, our observation data can be used for the analyses of ecosystem change not only for plot scale but also regional scale.

4.2.3. Water availability

As described in Results, soil moisture water equivalent (SWE) controls forest NDVI, because our observation site (northeastern taiga) is established in the continentally dry area. I found positive and negative correlations between NDVI and SWE. Before 2007, TF NDVI was correlated positively with June SWE in current year (Figure 4.3b), and positively with the SWE in last year June, July, August and the last year summer (JJA) (Figure 4.3 c,d and Figure S6 c,d, Table S5). These indicate the influence of hydrological conditions in the previous year and early summer in the current year on leaf productivity of larch trees in the current year.

Larches as deciduous trees assimilate carbon by photosynthesis (photoassimilate) during the summer to prepare the needles in the next year, and elongation of needles may be affected by hydrological condition in the early summer. In the Spasskaya Pad Forest, pulse-labeling experiment with $^{13}CO_2$ showed that stored carbon from previous year contributed about 50% to formation of new needles of *Larix gmelini* saplings (Kagawa et al. 2006). The high level of water availability in the summers of 1999 and 2000 contributed to the increased carbon storage and, as a result, the high formation of needles in 2000 and 2001. The followed significant NDVI decrease in 2002 was caused by a low level of soil moisture, i.e., dry conditions. The high summer air temperature (Figure 4.1c) and small amount of precipitation (Figure 4.1d) in 2001 and 2002 caused drought in 2002 and 2003. After that, the soil moisture was increasing due to

a large amount of water year precipitation (Figure 4.1d), that contributed an increase in NDVI until 2007.

It has been known that the NDVI was found to depend on the previous-year precipitation in arid and semi-arid regions (e.g., Burry et al. 2018; Camberlin et al. 2007). Besides, historical time-series of climate indices, based on both precipitation and temperature, had relations with one-year lagged NDVI (e.g., Liu et al. 2017; Verbyla 2015). In boreal interior Alaska, the summer moisture index showed correlation with maximum summer NDVI not only at one-year time lag in two 10-km climate station buffers, but also at two-year time lag in many other ones (Verbyla 2015). The possible reasons for the multi-year NDVI lag could be the long-term negative vegetation responses to drought events, such as decrease in carbon allocation by plants (e.g., Kannenberg et al. 2019) and plant mortality (e.g., Anderegg et al. 2012). The negative effects of the drought event also took place in our study (Table 4.1).

The effect of the preceding hydrological conditions on NDVI is also evidenced by the significant negative correlation between the foliar $\delta^{13}C$ and previous August SWE in 1999-2007 ($r = -0.79$, $p < 0.05$; Figure 4.4). The mechanism of plant $\delta^{13}C$ response to changes in light and water availabilities have been well explained in previous studies (e.g., Farquhar et al. 1989). Under drought stress in 2001-2002, there apparently was a decrease in needle stomatal conductance, resulting in a decrease in carbon assimilation. In the next years, 2002-2003, larches produced less needles (lower NDVI) from the previously photosynthesized carbon with low values of intercellular CO^2 pressure and, as a result, high $\delta^{13}C$ values.

Compared the decrease in TF NDVI for drought event, decrease in TF NDVI for wet event was not so large (Figure 4.2a), although wet event caused decrease in RF-1 and 2 NDVI significantly. However, the positive correlations between the TF NDVI and soil moisture, which were observed in 1999-2006, shifted to the opposite ones in 2008-2019 (Figure 4.3b-d and Figure S6a-e). After 2007, the TF NDVI was negatively correlated with the SWE of all months in previous (with one-year time lag) and current years (without a lag) (Table S6). This may indicate that, after the extreme wet event, the soil moisture in previous and current years seemed to negatively affect the current TF NDVI. So, a high level of the soil moisture may

affect needle production, i.e., carbon assimilation, needle formation and/or needle elongation. But based on the foliar $\delta^{13}C$ data, there was no evidence that the needle stomatal conductance, which is an indicator of the rates of transpiration and carbon assimilation, was disturbed by the event, because the correlation between the foliar $\delta^{13}C$ and SWE remained negative in 2008-2019 like in 1999-2007 (Table S8). Herewith, in 2008-2019, the foliar $\delta^{13}C$ may be mainly controlled by hydrological conditions in the current year rather than in the previous year (Table S8). In years with a high SWE, such as 2009 and 2015, stomatal conductance increased (a low foliar $\delta^{13}C$), that usually indicates a great potential of a plant to assimilate CO_2, a high C storage and a high needle production (a high TF NDVI) in the current and next years. Nevertheless, in these wet years and in their subsequent 2010 and 2016, TF NDVI values were low. Therefore, the decrease in the TF NDVI in the wet years may be due to factors other than the carbon assimilation process. Nitrogen availability for larches can control formation of needles in the beginning of the growing season and their elongation and, consequently, the TF NDVI.

4.2.4. Nitrogen availability

Before 2007, the TF NDVI showed a significant negative correlation with the foliar C/N (Figure 4.3f), which indicate a positive correlation with the foliar N content. In this ecosystem, there was no previous study on the temporal correlation between the NDVI and plant N content (or $\delta^{15}N$). The leaf nitrogen and chlorophyll (green pigment), where the nitrogen is one of the important elements, were found to be positively correlated with NDVI (Gamon et al. 1995). Previously, the relationship between NDVI and leaf N content was predominantly investigated in crops for agricultural purposes, but not in natural ecosystems. Besides, in coniferous forests, estimation of foliar nitrogen using remote-sensing methods showed the highest uncertainty due to complex structure of needleleaf canopies (reviewed by Homolova et al. 2013).

As leaf N content was considered to be an indicator of nitrogen availability for a plant in some boreal regions, where the ecosystem is usually poor in N (Liang et al. 2014; Matsushima et al. 2012), so it may be concluded that forest greenness (NDVI) was controlled by nitrogen uptake by larch trees. Herewith, soil moisture was suggested to play a crucial role in

maintaining the forest nitrogen status (Table S9). In 2000-2001, soil water was available for plants, and induced favorable conditions for soil nitrogen uptake by trees. Under a suitable soil moisture condition, production of soil inorganic N may be increased. These may lead a high production of larch needles (high NDVI). In 2002-2003, during drought years, the dry conditions caused the opposite effects, namely less productivity of soil inorganic N and less N uptake by trees. In the post-drought period of 2004-2007, an increase in the soil moisture was gradually recovering the forest conditions in terms of nitrogen uptake and needle production.

After 2007, the foliar C/N still showed a negative correlation with the TF NDVI in 2008-2018 but statistically weaker comparing to 1999-2006 (Figure 4.3f). At the same time, the positive correlations between the TF NDVI and SWE changed to the negative ones in 2008-2019. According to the results, a high soil moisture could lead to a low needle production under a low nitrogen availability. When an extremely high soil moisture, resulting in the soil saturated with water, caused less production of soil inorganic nitrogen, low TF NDVI and high C/N values may be observed, that is a negative correlation between them.

While the N content reflects the plant nitrogen status, the plant $\delta^{15}N$ is widely accepted to depend on the isotopic composition of nitrogen sources (e.g., Evans 2001). So, the $\delta^{15}N$ of soil inorganic ammonium NH_4^+, which is the main nitrogen source in the Spasskaya Pad forest (Popova et al. 2013), presumably determined the foliar $\delta^{15}N$ in larches. As seen in Figure 4.2e, the foliar $\delta^{15}N$ was decreasing since 2005. This data suggested that larch trees used less soil N, especially produced in deeper soil layer, which usually has a higher soil $\delta^{15}N$. It may be related with either change in soil N dynamics, or decreasing the vertical distribution of roots (Takenaka et al. 2016), or damaging lower roots by an extremely high soil moisture. Under root oxygen stress due to soil flooding, plant metabolism is changed from anaerobic one to fermentation characterized by energy-deficiency and ethanol production, both of which induce decreased nutrient uptake and plant growth (reviewed by Pezeshki and DeLaune 2012). Reduced soil conditions are also able to produce soil phytotoxins damaging the root system (Pezeshki 2001).

It should be noted that not only the extreme wet event in 2007 but also the extreme drought in 2001 may cause a change in N availability. There are many studies that the foliar

$\delta^{15}N$ increased during drought (Handley et al. 1999b; Lopes and Araus 2006; Ogaya and Penuelas 2008; Penuelas et al. 2000). But in this study, drought in 2001 and 2002 decreased the foliar $\delta^{15}N$. The exact reason was not identified, but drought in 2001 and 2002 might affected the N availability for larch trees.

4.2.5. NDVI and RWI of larch trees

Two parameters of above-ground biomass, the tree-ring width index (RWI) and TF NDVI, were positively correlated in 1999-2006 at a significant level ($r = 0.79$, $p<0.05$; Figure 4.3a). Similarly, in other northern regions, temporal patterns of the NDVI and dendrochronological data were similar for larch (Berner et al. 2013; Berner et al. 2011; Erasmi et al. 2021), pine (Berner et al. 2011), spruce (Andreu-Hayles et al. 2011; Beck et al. 2013; Berner et al. 2011; Lopatin et al. 2006). This means that the tree growth (RWI) and needle production (NDVI as an indicator of LAI) showed synchronous responses to environmental changes before 2007. However, there was no significant correlation between the TF NDVI and RWI after 2007. Thus, the extreme wet event in 2007 could change the physiological response of larch trees to the environment in terms of needle and wood production.

Correlation between the NDVI and RWI at our observation site was previously observed by Tei et al. (2019a). They used GIMMS-NDVI3g, and found its positive correlation with the RWI in the next year during 2004–2014 in the study site. These two parameters, the NDVI and RWI, reflect the carry-over of carbon, which is fixed via needles in previous year and used in the current year, as experimentally demonstrated by Kagawa et al. (2006). In our study, there was no significant correlation between the TF NDVI and RWI at one-year lag of the RWI (Figure S6g). In previous studies, dendrochronological data showed that tree growth responded to climate with a time lag (e.g., Tei and Sugimoto 2018). In our study, the soil moisture and nitrogen availability for trees seemed to be the key factors of environment affecting not only the NDVI, as mentioned above, but also the RWI. However, the TF NDVI and RWI were not significantly correlated after 2007, while there was a significant positive correlation before

2007. Thus, the extreme wet event in 2007 could change the physiological response of larch trees to the environment in terms of needle and wood production.

4.3. Summary

In the Chapter 4, to understand effects of the extreme wet event on the larch forest of northeastern Siberia, historical variations in the satellite-derived NDVI (forest greenness) and field-observed parameters of larch forest were investigated. The NDVI values of the plots visually unaffected (typical mature larch forest, TF) and affected (RF and DF) by the event were similar before 2007, but differed after 2007 because of a high tree mortality in the last plots caused by waterlogging and a presence of water on depression. And the TF, which was visually unaffected by the event, had also undergone changes. The soil moisture played an important role in the above-ground biomass production before and after the wet event. The SWE was correlated negatively with the needle C/N (Table S9) and positively with the TF NDVI (Table S5). So, before the event, a high level of water availability (high SWE) in the previous summer and current June for a plant showed positive effects on nitrogen uptake (low C/N or high N content), needle growth (high NDVI) and, consequently, stem growth (high RWI). But after the event, an excessively high soil moisture (high SWE) negatively affected on the nitrogen availability (high C/N; Table S9) and needle production (low NDVI; Table S5). The decrease in the needle $\delta^{15}N$ after the event may indirectly indicate either change in soil N dynamics, or decreasing the vertical distribution of roots, or damaging lower roots by an extremely high soil moisture.

5. General discussion and Conclusions

Tree mortality in DF and RF during the extreme wet event was controlled by soil properties and topographic features, i.e. depressions (Iwasaki et al. 2010). But among the effects of the event, there may be not only tree mortality but also invisible damages in living trees. In this study, NDVI, a potential indicator of needle production, in the typical forest was negatively related with the summer SWE in previous and current years in 2008-2019 and with the current-year needle C/N in 2008-2018 (Table S6). That may indicate that needle production for current and next years during the summer was disturbed by increased soil moisture and decreased soil N uptake by trees. We suggested that N uptake by larches might be reduced in wet soils by damaged lower roots, or decreased vertical distribution of roots (Takenaka et al. 2016), or changed soil N production.

Changes in the process of needle production may affect tree growth in the current and next years in the forest (Kagawa et al. 2006; Tei et al. 2019a). But we found no evidence that tree radial growth was disturbed after 2007: the RWI well responded to changes in the SWE (Figure 3b and c). Additionally, at ecosystem scale, there was no significant change in CO_2 exchanges measured by the 32-m flux tower in this larch forest (Kotani et al. 2019). However, observed increase in understory biomass was suggested to compensate negative changes in fluxes at overstory level (Kotani et al. 2019) and in NDVI of the forest (Nagano et al. 2022). That means that negative effects of the extreme wet event for the living larch trees were not excluded in the previous studies. Our study showed that limitation in N uptake at a high soil moisture level is one of the factors, which may potentially reduce tree growth in the future.

The spatial variations in NDVI and foliar traits identified favorable conditions in the sites affected by the extreme wet event (RF). The larch forest in RF with lower NDVI (lower stand density) had higher light (higher $\delta^{13}C$) and nitrogen (lower foliar C/N) availabilities for one mature larch tree than that in unaffected areas (TF) because of reduced competition for light and soil nitrogen among trees. Such favorable conditions and the presence of a large number of young larch trees may lead to further succession of RF after an extreme wet event. But since

the weather extremes are expected to be more frequent and intensive, the period between the extremes may exceed the period of recovery after the extremes. Therefore, the forest may be rather damaged than recovered in the future. Regarding to the prediction of tree growth in this dry region, there is a discrepancy between different vegetation models. In eastern Siberia, dynamic global vegetation model (DGVM) simulated increased forest production in the nearest century, while RWI-based model showed an opposite result (Tei et al. 2017). Some of models may overestimate the production because they do not include important parameters, such soil moisture, soil N production, N uptake by trees. In order to better understand changes in the forest, long-term observation of variation in the soil N availability depending soil moisture and other factors is necessary.

Acknowledgements

First of all, I would like to express my deep and sincere gratitude to my supervisor Prof. Atsuko Sugimoto for the continuous support of Doctoral Course study and research, for her patience, enthusiasm, and sharing knowledge. It would be impossible to write this thesis without help of my supervisor. I also appreciate Profs. Masanobu Yamamoto, Yoshito Chikaraishi, Youhei Yamashita and Tomohisa Irino for all their encouragements, comments and advice on my thesis and presentation. I would like to thank Prof. T.C. Maximov, Prof. A. Kononov, Dr. E. Starostin, Dr. R. Petrov, Mr. M. Grigorev, and other members of the IBPC for supporting our fieldwork in Spasskaya Pad Station. Also, I want to thank Drs. R. Shakhmatov, S. Tei, Y. Miyamoto for their assistance in both field and labworks. I also appreciate the help of Ms. Y. Hoshino and S. Nunohashi, Drs. T. Morozumi, R. Fang, S. Takano and R. Shingubara for their support in labworks. I also appreciate Dr. A. Kotani and Dr. S. Nagai for providing observation data. Finally, I would like to express my gratitude to my parents Alena and Vladimir, my sister Dayaana and other families for giving me heartfelt support. (This work was supported by the International Priority Graduate Programs (IPGP) funded by the Ministry of Education, Culture, Sports, Science and Technology-Japan (MEXT), the Belmont Forum Arctic program COPERA (C budget of ecosystems and cities and villages on permafrost in eastern Russian Arctic) project, and the Hokkaido University DX Doctoral Fellowship (Grant No. JPMJSP2119) funded by the Japan Science and Technology Agency.)

References

Abaimov, A.P., Lesinski, J.A., Martinsson, O., & Milyutin, L.I. (1998). *Variability and ecology of Siberian larch species*. Umeå: Swedish University of Agricultural Sciences. Departament of Silviculture. Reports.

Ale, R., Zhang, L., Li, X., Raskoti, B.B., Pugnaire, F.I., & Luo, T.X. (2018). Water Shortage Drives Interactions Between Cushion and Beneficiary Species Along Elevation Gradients in Dry Himalayas. *Journal of Geophysical Research-Biogeosciences, 123*, 226-238

Anderegg, W.R.L., Berry, J.A., Smith, D.D., Sperry, J.S., Anderegg, L.D.L., & Field, C.B. (2012). The roles of hydraulic and carbon stress in a widespread climate-induced forest die-off. *Proceedings of the National Academy of Sciences of the United States of America, 109*, 233-237

Andreu-Hayles, L., D'Arrigo, R., Anchukaitis, K.J., Beck, P.S.A., Frank, D., & Goetz, S. (2011). Varying boreal forest response to Arctic environmental change at the Firth River, Alaska. *Environmental Research Letters, 6*

Archibold, O.W. (1995). The coniferous forests. *Ecology of World Vegetation* (pp. 238–279)

Bahru, T., & Ding, Y.L. (2020). Effect of stand density, canopy leaf area index and growth variables on Dendrocalamus brandisii (Munro) Kurz litter production at Simao District of Yunnan Province, southwestern China. *Global Ecology and Conservation, 23*

Barber, V.A., Juday, G.P., & Finney, B.P. (2000). Reduced growth of Alaskan white spruce in the twentieth century from temperature-induced drought stress. *Nature, 405*, 668-673

Beck, P.S.A., Andreu-Hayles, L., D'Arrigo, R., Anchukaitis, K.J., Tucker, C.J., Pinzon, J.E., & Goetz, S.J. (2013). A large-scale coherent signal of canopy status in maximum latewood density of tree rings at arctic treeline in North America. *Global and Planetary Change, 100*, 109-118

Berner, L.T., Beck, P.S.A., Bunn, A.G., & Goetz, S.J. (2013). Plant response to climate change along the forest-tundra ecotone in northeastern Siberia. *Global Change Biology, 19*, 3449-3462

Berner, L.T., Beck, P.S.A., Bunn, A.G., Lloyd, A.H., & Goetz, S.J. (2011). High-latitude tree

growth and satellite vegetation indices: Correlations and trends in Russia and Canada (1982-2008). *Journal of Geophysical Research-Biogeosciences, 116*

Blok, D., Schaepman-Strub, G., Bartholomeus, H., Heijmans, M., Maximov, T.C., & Berendse, F. (2011). The response of Arctic vegetation to the summer climate: relation between shrub cover, NDVI, surface albedo and temperature. *Environmental Research Letters, 6*

Burry, L.S., Palacio, P.I., Somoza, M., de Mandri, M.E.T., Lindskoug, H.B., Marconetto, M.B., & D'Antoni, H.L. (2018). Dynamics of fire, precipitation, vegetation and NDVI in dry forest environments in NW Argentina. Contributions to environmental archaeology. *Journal of Archaeological Science-Reports, 18*, 747-757

Callaghan, T.V., Bergholm, F., Christensen, T.R., Jonasson, C., Kokfelt, U., & Johansson, M. (2010). A new climate era in the sub-Arctic: Accelerating climate changes and multiple impacts. *Geophysical Research Letters, 37*

Camberlin, P., Martiny, N., Philippon, N., & Richard, Y. (2007). Determinants of the interannual relationships between remote sensed photosynthetic activity and rainfall in tropical Africa. *Remote Sensing of Environment, 106*, 199-216

Chen, J.M., & Cihlar, J. (1996). Retrieving leaf area index of boreal conifer forests using landsat TM images. *Remote Sensing of Environment, 55*, 153-162

Clevers, J., & Gitelson, A.A. (2013). Remote estimation of crop and grass chlorophyll and nitrogen content using red-edge bands on Sentinel-2 and-3. *International Journal of Applied Earth Observation and Geoinformation, 23*, 344-351

Constable, A.J., Harper, S., Dawson, J., Holsman, K., Mustonen, T., Piepenburg, D., & Rost, B. (2022). Cross-Chapter Paper 6: Polar Regions. In D.C.R. H.-O. Pörtner, M. Tignor, E.S. Poloczanska, K. Mintenbeck, A. Alegría, M. Craig, S. Langsdorf, S. Löschke, V. Möller, A. Okem, B. Rama (Ed.), *Climate Change 2022: Impacts, Adaptation and Vulnerability. Contribution of Working Group II to the Sixth Assessment Report of the Intergovernmental Panel on Climate Change* (pp. 2319–2368). Cambridge, UK and New York, NY, USA: Cambridge University Press

Dearborn, K.D., & Baltzer, J.L. (2021). Unexpected greening in a boreal permafrost peatland

undergoing forest loss is partially attributable to tree species turnover. *Global Change Biology, 27*, 2867-2882

del Castillo, J., Voltas, J., & Ferrio, J.P. (2015). Carbon isotope discrimination, radial growth, and NDVI share spatiotemporal responses to precipitation in Aleppo pine. *Trees-Structure and Function, 29*, 223-233

Douville, H., Raghavan, K., Renwick, J., Allan, R.P., Arias, P.A., Barlow, M., Cerezo-Mota, R., Cherchi, A., Gan, T.Y., Gergis, J., Jiang, D., Khan, A., Pokam Mba, W., Rosenfeld, D., Tierney, J., & Zolina, O. (2021). Water Cycle Changes. In V. Masson-Delmotte, P. Zhai, A. Pirani, S.L. Connors, C. Péan, S. Berger, N. Caud, Y. Chen, L. Goldfarb, M.I. Gomis, M. Huang, K. Leitzell, E. Lonnoy, J.B.R. Matthews, T.K. Maycock, T. Waterfield, O. Yelekçi, R. Yu, & B. Zhou (Eds.), *Climate Change 2021: The Physical Science Basis. Contribution of Working Group I to the Sixth Assessment Report of the Intergovernmental Panel on Climate Change* (pp. 1055–1210). Cambridge, United Kingdom and New York Cambridge University Press

Duursma, R.A., & Marshall, J.D. (2006). Vertical canopy gradients in delta C-13 correspond with leaf nitrogen content in a mixed-species conifer forest. *Trees-Structure and Function, 20*, 496-506

Dyer, M.I., Turner, C.L., & Seastedt, T.R. (1991). Mowing and fertilization effects on productivity and spectral reflectance in Bromus-inermis plots. *Ecological Applications, 1*, 443-452

Ehleringer, J.R., Field, C.B., Lin, Z.F., & Kuo, C.Y. (1986). Leaf carbon isotope and mineral-composition in subtropical plants along an irradiance cline. *Oecologia, 70*, 520-526

Erasmi, S., Klinge, M., Dulamsuren, C., Schneider, F., & Hauck, M. (2021). Modelling the productivity of Siberian larch forests from Landsat NDVI time series in fragmented forest stands of the Mongolian forest-steppe. *Environmental Monitoring and Assessment, 193*

Evans, R.D. (2001). Physiological mechanisms influencing plant nitrogen isotope composition. *Trends in Plant Science, 6*, 121-126

FAO (2020). Global Forest Resources Assessment 2020 – Key findings. In. Rome

Farquhar, G.D., Ehleringer, J.R., & Hubick, K.T. (1989). Carbon isotope discrimination and photosynthesis. *Annual Review of Plant Physiology and Plant Molecular Biology, 40*, 503-537

Friedlingstein, P., Jones, M.W., O'Sullivan, M., Andrew, R.M., Bakker, D.C.E., Hauck, J., Le Quere, C., Peters, G.P., Peters, W., Pongratz, J., Sitch, S., Canadell, J.G., Ciais, P., Jackson, R.B., Alin, S.R., Anthoni, P., Bates, N.R., Becker, M., Bellouin, N., Bopp, L., Chau, T.T.T., Chevallier, F., Chini, L.P., Cronin, M., Currie, K.I., Decharme, B., Djeutchouang, L.M., Dou, X.Y., Evans, W., Feely, R.A., Feng, L., Gasser, T., Gilfillan, D., Gkritzalis, T., Grassi, G., Gregor, L., Gruber, N., Gurses, O., Harris, I., Houghton, R.A., Hurtt, G.C., Iida, Y., Ilyina, T., Luijkx, I.T., Jain, A., Jones, S.D., Kato, E., Kennedy, D., Goldewijk, K.K., Knauer, J., Korsbakken, J.I., Kortzinger, A., Landschutzer, P., Lauvset, S.K., Lefevre, N., Lienert, S., Liu, J.J., Marland, G., McGuire, P.C., Melton, J.R., Munro, D.R., Nabel, J., Nakaoka, S.I., Niwa, Y., Ono, T., Pierrot, D., Poulter, B., Rehder, G., Resplandy, L., Robertson, E., Rodenbeck, C., Rosan, T.M., Schwinger, J., Schwingshackl, C., Seferian, R., Sutton, A.J., Sweeney, C., Tanhua, T., Tans, P.P., Tian, H.Q., Tilbrook, B., Tubiello, F., van der Werf, G.R., Vuichard, N., Wada, C., Wanninkhof, R., Watson, A.J., Willis, D., Wiltshire, A.J., Yuan, W.P., Yue, C., Yue, X., Zaehle, S., & Zeng, J.Y. (2022). Global Carbon Budget 2021. *Earth System Science Data, 14*, 1917-2005

Fujiyoshi, L., Sugimoto, A., Tsukuura, A., Kitayama, A., Caceres, M.L.L., Mijidsuren, B., Saraadanbazar, A., & Tsujimura, M. (2017). Spatial variations in larch needle and soil N-15 at a forest-grassland boundary in northern Mongolia. *Isotopes in Environmental and Health Studies, 53*, 54-69

Gamon, J.A., Field, C.B., Goulden, M.L., Griffin, K.L., Hartley, A.E., Joel, G., Penuelas, J., & Valentini, R. (1995). Relationships between NDVI, canopy structure, and photosynthesis in 3 Californian vegetation types. *Ecological Applications, 5*, 28-41

Garten, C.T., & Taylor, G.E. (1992). Foliar delta C-13 within a temperature deciduous forest - spatial, temporal, and species sources of variation. *Oecologia, 90*, 1-7

Guo, G.M., & Xie, G.D. (2006). The relationship between plant stable carbon isotope

composition, precipitation and satellite data, Tibet Plateau, China. *Quaternary International, 144*, 68-71

Hall, F.G., Shimabukuro, Y.E., & Huemmrich, K.F. (1995). Remote-sensing of forest biophysical structure using mixture decomposition and geometric reflectance models. *Ecological Applications, 5*, 993-1013

Handley, L.L., Austin, A.T., Robinson, D., Scrimgeour, C.M., Raven, J.A., Heaton, T.H.E., Schmidt, S., & Stewart, G.R. (1999a). The N-15 natural abundance (delta N-15) of ecosystem samples reflects measures of water availability. *Australian Journal of Plant Physiology, 26*, 185-199

Handley, L.L., Azcon, R., Lozano, J.M.R., & Scrimgeour, C.M. (1999b). Plant delta N-15 associated with arbuscular mycorrhization, drought and nitrogen deficiency. *Rapid Communications in Mass Spectrometry, 13*, 1320-1324

Heisler-White, J.L., Blair, J.M., Kelly, E.F., Harmoney, K., & Knapp, A.K. (2009). Contingent productivity responses to more extreme rainfall regimes across a grassland biome. *Global Change Biology, 15*, 2894-2904

Homolova, L., Maenovsky, Z., Clevers, J., Garcia-Santos, G., & Schaeprnan, M.E. (2013). Review of optical-based remote sensing for plant trait mapping. *Ecological Complexity, 15*, 1-16

Iijima, Y., Ohta, T., Kotani, A., Fedorov, A.N., Kodama, Y., & Maximov, T.C. (2014). Sap flow changes in relation to permafrost degradation under increasing precipitation in an eastern Siberian larch forest. *Ecohydrology, 7*, 177-187

Iwasaki, H., Saito, H., Kuwao, K., Maximov, T.C., & Hasegawa, S. (2010). Forest decline caused by high soil water conditions in a permafrost region. *Hydrology and Earth System Sciences, 14*, 301-307

Jiang, P., Liu, H.Y., Piao, S.L., Ciais, P., Wu, X.C., Yin, Y., & Wang, H.Y. (2019). Enhanced growth after extreme wetness compensates for post-drought carbon loss in dry forests. *Nature Communications, 10*

Ju, J.C., & Masek, J.G. (2016). The vegetation greenness trend in Canada and US Alaska from

1984-2012 Landsat data. *Remote Sensing of Environment, 176*, 1-16

Kagawa, A., Sugimoto, A., & Maximov, T.C. (2006). Seasonal course of translocation, storage and remobilization of C-13 pulse-labeled photoassimilate in naturally growing Larix gmelinii saplings. *New Phytologist, 171*, 793-804

Kannenberg, S.A., Novick, K.A., Alexander, M.R., Maxwell, J.T., Moore, D.J.P., Phillips, R.P., & Anderegg, W.R.L. (2019). Linking drought legacy effects across scales: From leaves to tree rings to ecosystems. *Global Change Biology, 25*, 2978-2992

Knapp, A.K., Beier, C., Briske, D.D., Classen, A.T., Luo, Y., Reichstein, M., Smith, M.D., Smith, S.D., Bell, J.E., Fay, P.A., Heisler, J.L., Leavitt, S.W., Sherry, R., Smith, B., & Weng, E. (2008). Consequences of More Extreme Precipitation Regimes for Terrestrial Ecosystems. *Bioscience, 58*, 811-821

Kotani, A., Saito, A., Kononov, A.V., Petrov, R.E., Maximov, T.C., Iijima, Y., & Ohta, T. (2019). Impact of unusually wet permafrost soil on understory vegetation and CO2 exchange in a larch forest in eastern Siberia. *Agricultural and Forest Meteorology, 265*, 295-309

Lambers, H., Chapin III, F.S., & Pons, T.L. (1998). *Plant physiological ecology*. New York, Berlin, Heidelberg Springer-Verlag

Lee, Y.J., Yang, C.M., Chang, K.W., & Shen, Y. (2008). A simple spectral index using reflectance of 735 nm to assess nitrogen status of rice canopy. *Agronomy Journal, 100*, 205-212

Li, F., & Sugimoto, A. (2018). Effect of waterlogging on carbon isotope discrimination during photosynthesis in Larix gmelinii. *Isotopes in Environmental and Health Studies, 54*, 63-77

Li, S.G., Tsujimura, M., Sugimoto, A., Davaa, G., Oyunbaatar, D., & Sugita, M. (2007). Temporal variation of delta C-13 of larch leaves from a montane boreal forest in Mongolia. *Trees-Structure and Function, 21*, 479-490

Liang, M.C., Sugimoto, A., Tei, S., Bragin, I.V., Takano, S., Morozumi, T., Shingubara, R., Maximov, T.C., Kiyashko, S.I., Velivetskaya, T.A., & Ignatiev, A.V. (2014). Importance of soil moisture and N availability to larch growth and distribution in the Arctic taiga-

tundra boundary ecosystem, northeastern Siberia. *Polar Science, 8*, 327-341

Liu, J.X., Price, D.T., & Chen, J.A. (2005). Nitrogen controls on ecosystem carbon sequestration: a model implementation and application to Saskatchewan, Canada. *Ecological Modelling, 186*, 178-195

Liu, S.L., Zhang, Y.Q., Cheng, F.Y., Hou, X.Y., & Zhao, S. (2017). Response of Grassland Degradation to Drought at Different Time-Scales in Qinghai Province: Spatio-Temporal Characteristics, Correlation, and Implications. *Remote Sensing, 9*

Lloyd, A.H., Bunn, A.G., & Berner, L. (2011). A latitudinal gradient in tree growth response to climate warming in the Siberian taiga. *Global Change Biology, 17*, 1935-1945

Lopatin, E., Kolstrom, T., & Spiecker, H. (2006). Determination of forest growth trends in Komi Republic (northwestern Russia): combination of tree-ring analysis and remote sensing data. *Boreal Environment Research, 11*, 341-353

Lopes, M.S., & Araus, J.L. (2006). Nitrogen source and water regime effects on durum wheat photosynthesis and stable carbon and nitrogen isotope composition. *Physiologia Plantarum, 126*, 435-445

Loranty, M.M., Davydov, S.P., Kropp, H., Alexander, H.D., Mack, M.C., Natali, S.M., & Zimov, N.S. (2018). Vegetation Indices Do Not Capture Forest Cover Variation in Upland Siberian Larch Forests. *Remote Sensing, 10*

Makarov, M.I., Malysheva, T.I., Cornelissen, J.H.C., van Logtestijn, R.S.P., & Glasser, B. (2008). Consistent patterns of N-15 distribution through soil profiles in diverse alpine and tundra ecosystems. *Soil Biology & Biochemistry, 40*, 1082-1089

Matsushima, M., Choi, W.J., & Chang, S.X. (2012). White spruce foliar delta C-13 and delta N-15 indicate changed soil N availability by understory removal and N fertilization in a 13-year-old boreal plantation. *Plant and Soil, 361*, 375-384

McGuire, A.D., Anderson, L.G., Christensen, T.R., Dallimore, S., Guo, L.D., Hayes, D.J., Heimann, M., Lorenson, T.D., Macdonald, R.W., & Roulet, N. (2009). Sensitivity of the carbon cycle in the Arctic to climate change. *Ecological Monographs, 79*, 523-555

Michaelian, M., Hogg, E.H., Hall, R.J., & Arsenault, E. (2011). Massive mortality of aspen

following severe drought along the southern edge of the Canadian boreal forest. *Global Change Biology, 17*, 2084-2094

Michelsen, A., Schmidt, I.K., Jonasson, S., Quarmby, C., & Sleep, D. (1996). Leaf N-15 abundance of subarctic plants provides field evidence that ericoid, ectomycorrhizal and non- and arbuscular mycorrhizal species access different sources of soil nitrogen. *Oecologia, 105*, 53-63

Myneni, R.B., & Williams, D.L. (1994). On the relationship between FAPAR and NDVI. *Remote Sensing of Environment, 49*, 200-211

Nagano, H., Kotani, A., Mizuochi, H., Ichii, K., Kanamori, H., & Hiyama, T. (2022). Contrasting 20-year trends in NDVI at two Siberian larch forests with and without multiyear waterlogging-induced disturbances. *Environmental Research Letters, 17*

Nakai, T., Hiyama, T., Petrov, R.E., Kotani, A., Ohta, T., & Maximov, T.C. (2020). Application of an open-path eddy covariance methane flux measurement system to a larch forest in eastern Siberia. *Agricultural and Forest Meteorology, 282*

Ogaya, R., & Penuelas, J. (2008). Changes in leaf delta C-13 and delta N-15 for three Mediterranean tree species in relation to soil water availability. *Acta Oecologica-International Journal of Ecology, 34*, 331-338

Ohta, T., Kotani, A., Iijima, Y., Maximov, T.C., Ito, S., Hanamura, M., Kononov, A.V., & Maximov, A.P. (2014). Effects of waterlogging on water and carbon dioxide fluxes and environmental variables in a Siberian larch forest, 1998-2011. *Agricultural and Forest Meteorology, 188*, 64-75

Penuelas, J., Filella, I., Lloret, F., Pinol, J., & Siscart, D. (2000). Effects of a severe drought on water and nitrogen use by Quercus ilex and Phillyrea latifolia. *Biologia Plantarum, 43*, 47-53

Pezeshki, S.R. (2001). Wetland plant responses to soil flooding. *Environmental and Experimental Botany, 46*, 299-312

Pezeshki, S.R., & DeLaune, R.D. (2012). Soil Oxidation-Reduction in Wetlands and Its Impact on Plant Functioning. In (pp. 196-221): Biology

Popova, A.S., Tokuchi, N., Ohte, N., Ueda, M.U., Osaka, K., Maximov, T.C., & Sugimoto, A. (2013). Nitrogen availability in the taiga forest ecosystem of northeastern Siberia. *Soil Science and Plant Nutrition, 59*, 427-441

Richardson, A.D., Keenan, T.F., Migliavacca, M., Ryu, Y., Sonnentag, O., & Toomey, M. (2013). Climate change, phenology, and phenological control of vegetation feedbacks to the climate system. *Agricultural and Forest Meteorology, 169*, 156-173

Roy, D.P., Kovalskyy, V., Zhang, H.K., Vermote, E.F., Yan, L., Kumar, S.S., & Egorov, A. (2016). Characterization of Landsat-7 to Landsat-8 reflective wavelength and normalized difference vegetation index continuity. *Remote Sensing of Environment, 185*, 57-70

Rozas, V., & Garcia-Gonzalez, I. (2012). Too wet for oaks? Inter-tree competition and recent persistent wetness predispose oaks to rainfall-induced dieback in Atlantic rainy forest. *Global and Planetary Change, 94-95*, 62-71

Santos, G.O., Rosalen, D.L., & De Faria, R.T. (2017). Use of active optical sensor in the characteristics analysis of the fertigated Brachiaria with treated sewage. *Engenharia Agricola, 37*, 1213-1221

Schuur, E.A.G., McGuire, A.D., Schadel, C., Grosse, G., Harden, J.W., Hayes, D.J., Hugelius, G., Koven, C.D., Kuhry, P., Lawrence, D.M., Natali, S.M., Olefeldt, D., Romanovsky, V.E., Schaefer, K., Turetsky, M.R., Treat, C.C., & Vonk, J.E. (2015). Climate change and the permafrost carbon feedback. *Nature, 520*, 171-179

Serreze, M.C., & Barry, R.G. (2011). Processes and impacts of Arctic amplification: A research synthesis. *Global and Planetary Change, 77*, 85-96

Shakhmatov, R., Hashiguchi, S., Maximov, T.C., & Sugimoto, A. (2022). Effects of snow manipulation on larch trees in the taiga forest ecosystem in northeastern Siberia. *Progress in Earth and Planetary Science, 9*

Stamatiadis, S., Taskos, D., Tsadila, E., Christofides, C., Tsadilas, C., & Schepers, J.S. (2010). Comparison of passive and active canopy sensors for the estimation of vine biomass production. *Precision Agriculture, 11*, 306-315

Stocker, B.D., Roth, R., Joos, F., Spahni, R., Steinacher, M., Zaehle, S., Bouwman, L., Xu, R.,

& Prentice, I.C. (2013). Multiple greenhouse-gas feedbacks from the land biosphere under future climate change scenarios. *Nature Climate Change, 3*, 666-672

Sugimoto, A. (2019). Stable Isotopes of Water in Permafrost Ecosystem. In T. Ohta, T. Hiyama, Y. Iijima, A. Kotani, & T. Maximov (Eds.), *Water-Carbon Dynamics in Eastern Siberia. Ecological Studies (Analysis and Synthesis)*. Singapore: Springer

Sugimoto, A., Naito, D., Yanagisawa, N., Ichiyanagi, K., Kurita, N., Kubota, J., Kotake, T., Ohata, T., Maximov, T.C., & Fedorov, A.N. (2003). Characteristics of soil moisture in permafrost observed in East Siberian taiga with stable isotopes of water. *Hydrological Processes, 17*, 1073-1092

Sugimoto, A., Yanagisawa, N., Naito, D., Fujita, N., & Maximov, T.C. (2002). Importance of permafrost as a source of water for plants in east Siberian taiga. *Ecological Research, 17*, 493-503

Suzuki, R., Nomaki, T., & Yasunari, T. (2001). Spatial distribution and its seasonality of satellite-derived vegetation index (NDVI) and climate in Siberia. *International Journal of Climatology, 21*, 1321-1335

Takata, K., Patra, P.K., Kotani, A., Mori, J., Belikov, D., Ichii, K., Saeki, T., Ohta, T., Saito, K., Ueyama, M., Ito, A., Maksyutov, S., Miyazaki, S., Burke, E.J., Ganshin, A., Iijima, Y., Ise, T., Machiya, H., Maximov, T.C., Niwa, Y., O'Ishi, R., Park, H., Sasai, T., Sato, H., Tei, S., Zhuravlev, R., Machida, T., Sugimoto, A., & Aoki, S. (2017). Reconciliation of top-down and bottom-up CO2 fluxes in Siberian larch forest. *Environmental Research Letters, 12*

Takenaka, C., Miyahara, M., Ohta, T., & Maximov, T.C. (2016). Response of larch root development to annual changes of water conditions in eastern Siberia. *Polar Science, 10*, 160-166

Tei, S., & Sugimoto, A. (2018). Time lag and negative responses of forest greenness and tree growth to warming over circumboreal forests. *Global Change Biology, 24*, 4225-4237

Tei, S., Sugimoto, A., Kotani, A., Ohta, T., Morozumi, T., Saito, S., Hashiguchi, S., & Maximov, T. (2019a). Strong and stable relationships between tree-ring parameters and forest-level

carbon fluxes in a Siberian larch forest. *Polar Science, 21*, 146-157

Tei, S., Sugimoto, A., Yonenobu, H., Kotani, A., & Maximov, T.C. (2019b). Effects of extreme drought and wet events for tree mortality: Insights from tree-ring width and carbon isotope ratio in a Siberian larch forest. *Ecohydrology, 12*

Tei, S., Sugimoto, A., Yonenobu, H., Matsuura, Y., Osawa, A., Sato, H., Fujinuma, J., & Maximov, T. (2017). Tree-ring analysis and modeling approaches yield contrary response of circumboreal forest productivity to climate change. *Global Change Biology, 23*, 5179-5188

Tei, S., Sugimoto, A., Yonenobu, H., Yamazaki, T., & Maximov, T.C. (2013). Reconstruction of soil moisture for the past 100 years in eastern Siberia by using delta C-13 of larch tree rings. *Journal of Geophysical Research-Biogeosciences, 118*, 1256-1265

Turner, C.L., Seastedt, T.R., Dyer, M.I., Kittel, T.G.F., & Schimel, D.S. (1992). Effects of management and topography on the radiometric response of a tallgrass prairie. *Journal of Geophysical Research-Atmospheres, 97*, 18855-18866

Verbyla, D. (2015). Remote sensing of interannual boreal forest NDVI in relation to climatic conditions in interior Alaska. *Environmental Research Letters, 10*

Wang, Q., Adiku, S., Tenhunen, J., & Granier, A. (2005). On the relationship of NDVI with leaf area index in a deciduous forest site. *Remote Sensing of Environment, 94*, 244-255

Wang, Z.H., Wang, T.J., Darvishzadeh, R., Skidmore, A.K., Jones, S., Suarez, L., Woodgate, W., Heiden, U., Heurich, M., & Hearne, J. (2016). Vegetation Indices for Mapping Canopy Foliar Nitrogen in a Mixed Temperate Forest. *Remote Sensing, 8*

Will, R.E., Narahari, N.V., Shiver, B.D., & Teskey, R.O. (2005). Effects of planting density on canopy dynamics and stem growth for intensively managed loblolly pine stands. *Forest Ecology and Management, 205*, 29-41

Yousfi, S., Kellas, N., Saidi, L., Benlakehal, Z., Chaou, L., Siad, D., Herda, F., Karrou, M., Vergara, O., Gracia, A., Araus, J.L., & Serret, M.D. (2016). Comparative performance of remote sensing methods in assessing wheat performance under Mediterranean conditions. *Agricultural Water Management, 164*, 137-147

Zhu, Y., Tian, Y.C., Yao, X., Liu, X.J., & Cao, W.X. (2007). Analysis of common canopy reflectance spectra for indicating leaf nitrogen concentrations in wheat and rice. *Plant Production Science, 10*, 400-411

Figures

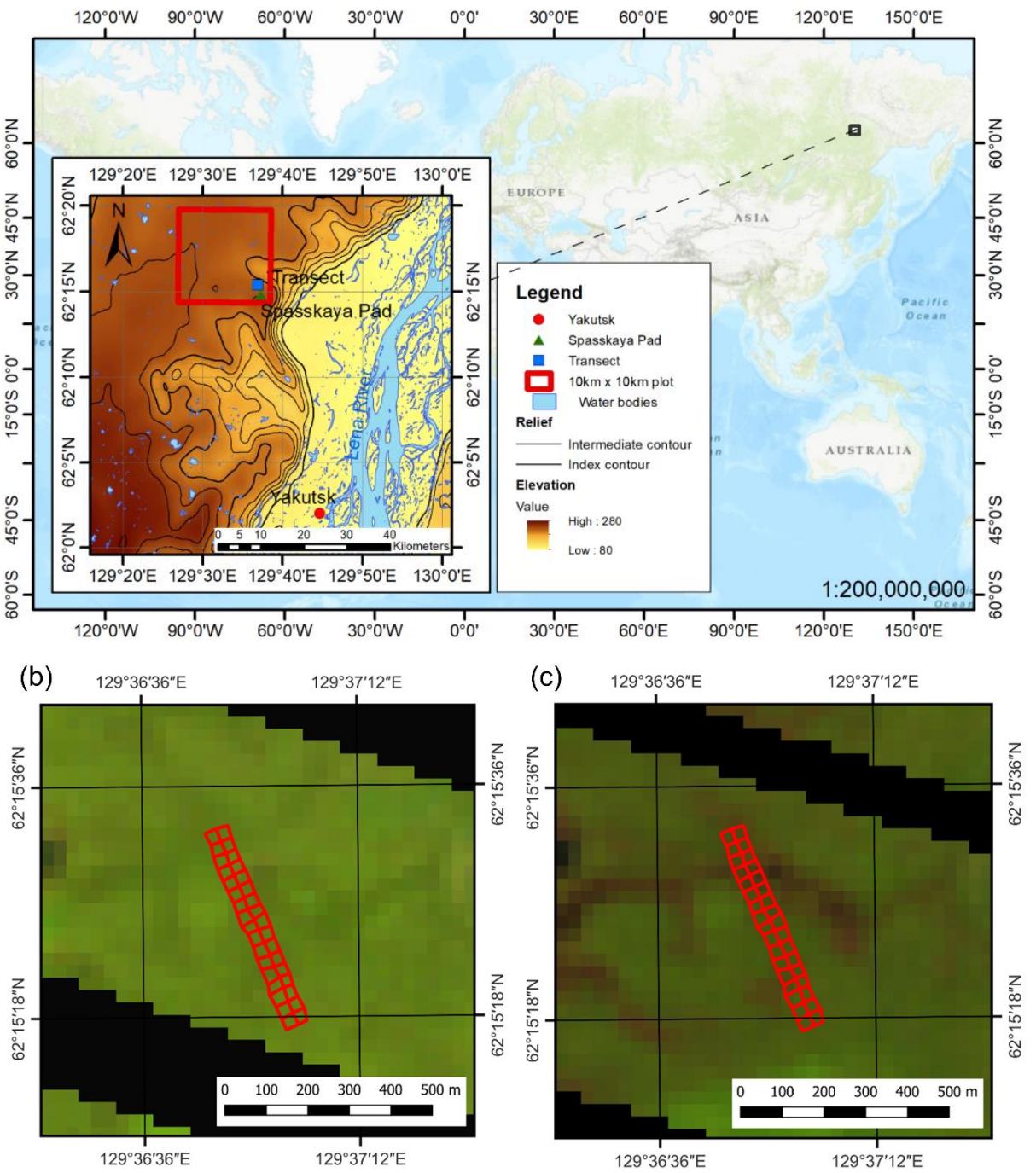

Figure 2.1. Location of the Spasskaya Pad Station (62°25′ N, 129°62′ E), the study transect and 10-km plot near Yakutsk in the topographical map zoomed from a global map (**a**). The study transects 60 m × 510 m in Landsat 7 ETM+ Natural Color Images with a spatial resolution of 30 m before the wet event on 11 June 2006 (**b**) and after the wet event on 9 June 2008 (**c**). The red polygons represent the 34 plots. The black stripes in the last two figures represent the Landsat 7 scan-line error (no data).

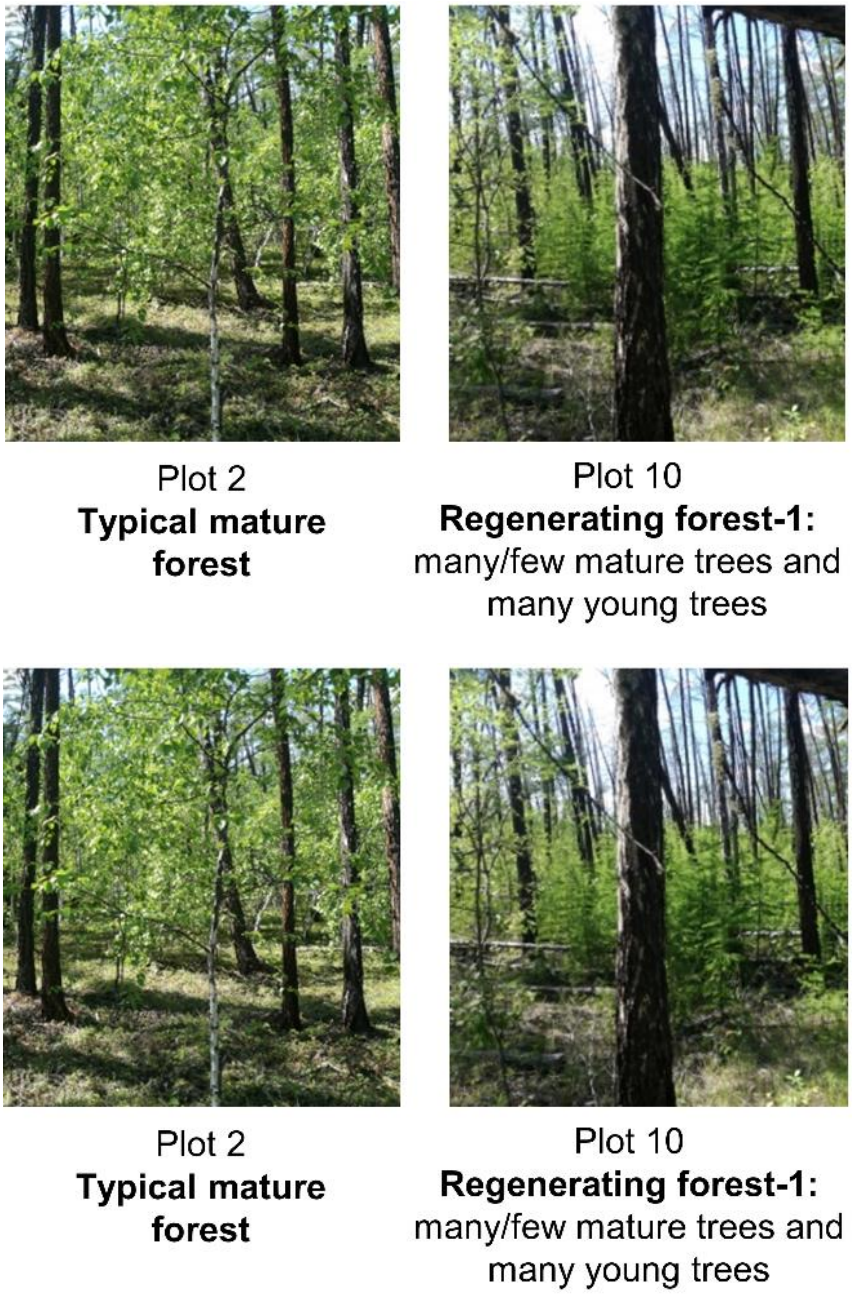

Figure 2.2. Four larch forest types on damage levels observed along the transect: typical mature forest (TF), two types of regenerating forest (RF-1 and RF-2), and damaged forest (DF). Each forest type is demonstrated as a photograph taken at a representative plot.

Figure 2.3. Detailed view of the Spasskaya Pad Forest: the station, the 60 m x 510 m transect for studying spatial variations, points of soil moisture measurement and larch needle sampling for $\delta^{13}C$, $\delta^{15}N$, and C/N for studying historical variations.

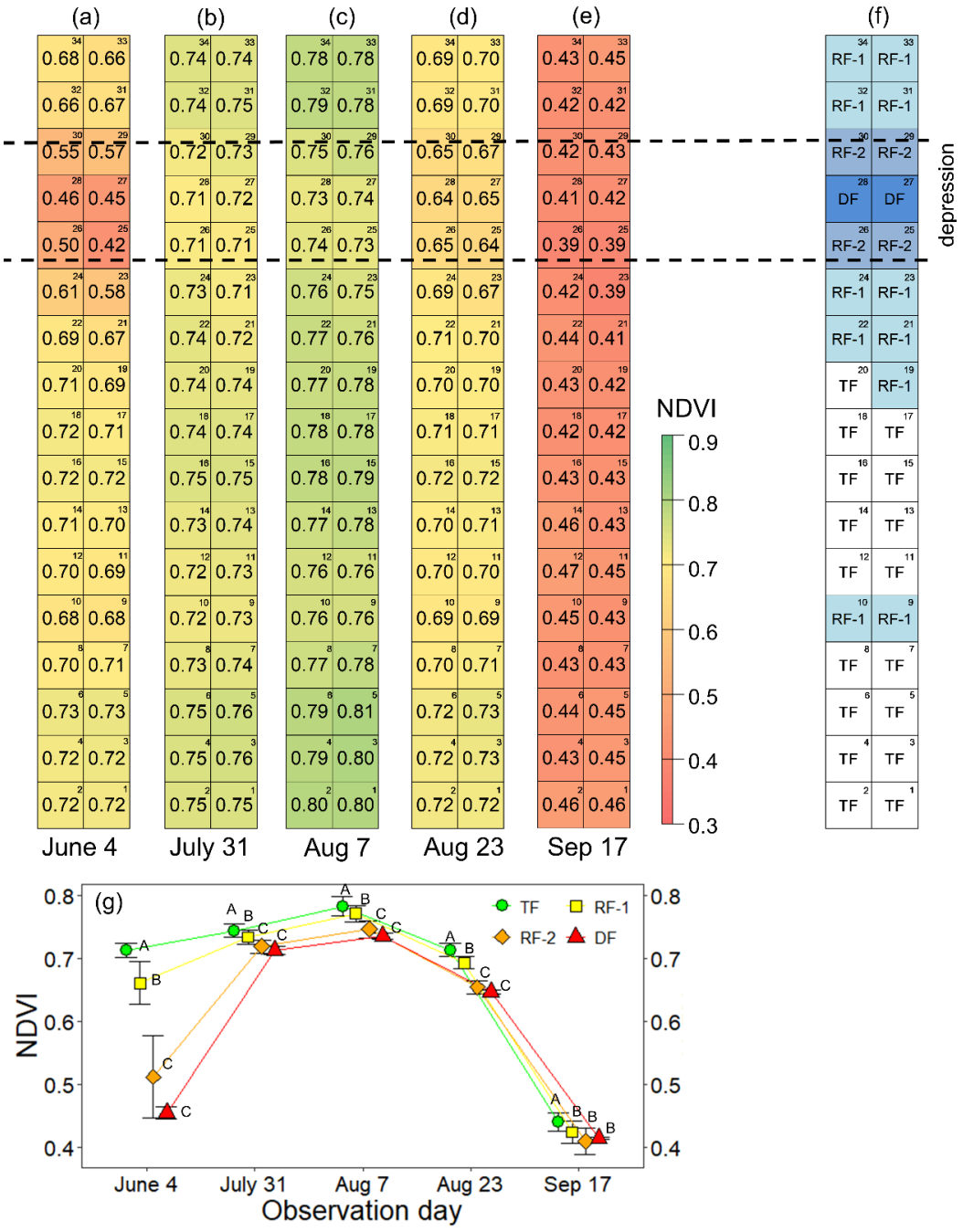

Figure 3.1. Spatial variations in the NDVI along the transect calculated based on the Landsat 8 images captured in the summer of 2018: (**a**) on 4 June; (**b**) on 31 July; (**c**) on 7 August; (**d**) on 23 August; (**e**) and on 17 September. Variations are presented as the heat maps with the color scale bar. The central number shows an average value of the NDVI within the plot. Serial numbers of the plots are shown at the top right corners. (**f**) Scheme of the distribution of the four larch forest types on damage levels observed along the transect: typical forest (TF), two types of regenerating forest (RF-1 and RF-2), and damaged forest (DF). The transect plot numbers are shown at the top right corners of the plots. The black dash lines display the conditional borders of the depression in the transect (plots from No. 25 to 30). (**g**) Seasonal variations in the NDVI of the forest types. Different upper-case letters (A, B, C) mean the statistical significance in the comparison among forest types on an observation day.

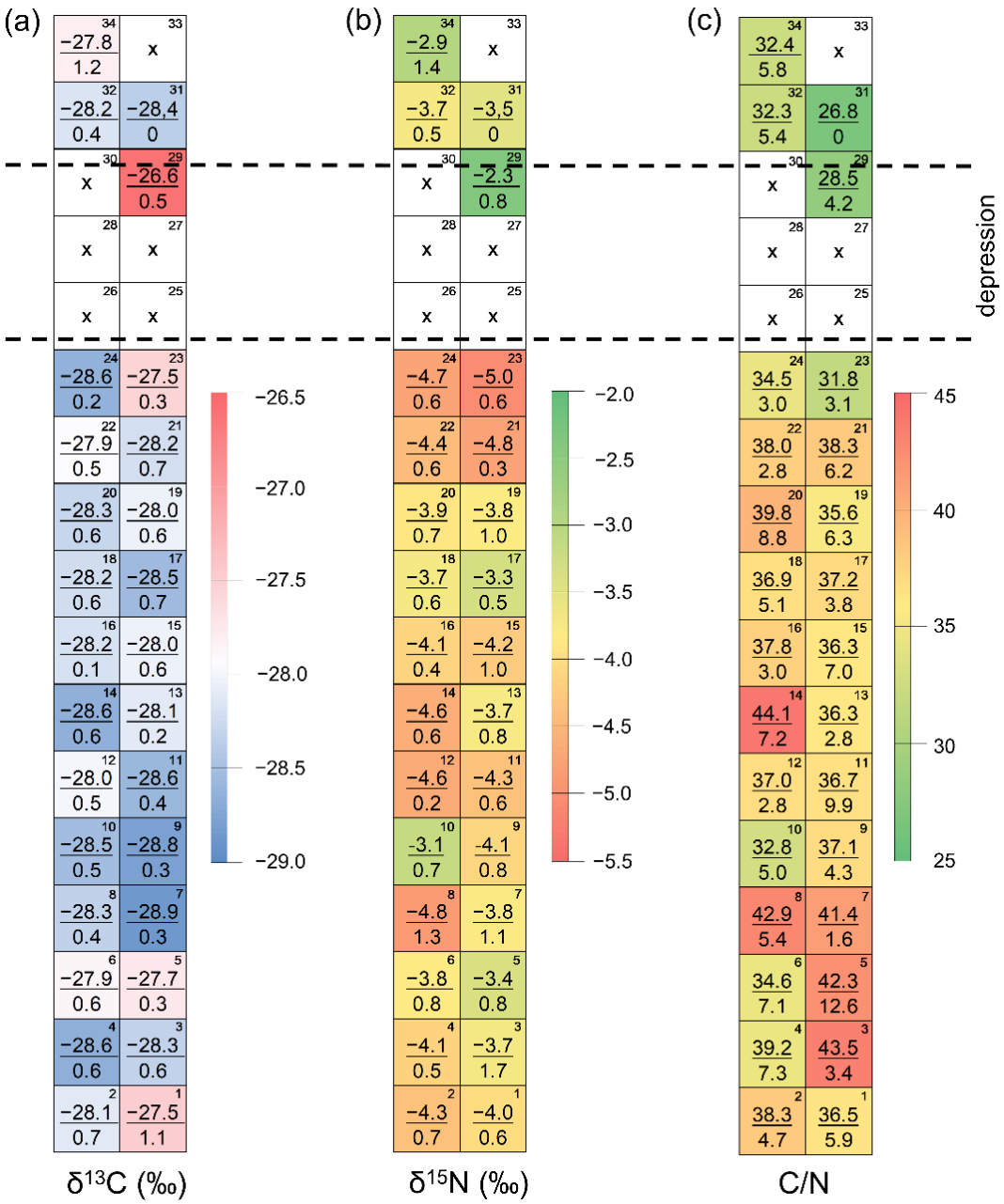

Figure 3.2. Spatial variations in (**a**) the foliar $\delta^{13}C$ (‰), (**b**) the foliar $\delta^{15}N$ (‰), and (**c**) the foliar C/N ratio averaged in each plot (average and standard deviation values are shown as numerator and denominator, respectively). Variations are presented as the heat maps with color scale bars. Serial numbers of the plots are shown at the top right corners. Number of samples from the plots was $n = 1$ for the RF-1 plot No. 31, $n = 2$ for the RF-1 plots No. 23 and 24, $n = 4$ for all other plots (results from No. 25 to 28, 30, and 33 are not shown because mature trees were not available). Black dash lines display the conditional borders of the depression in the transect (plots from No. 25 to 30).

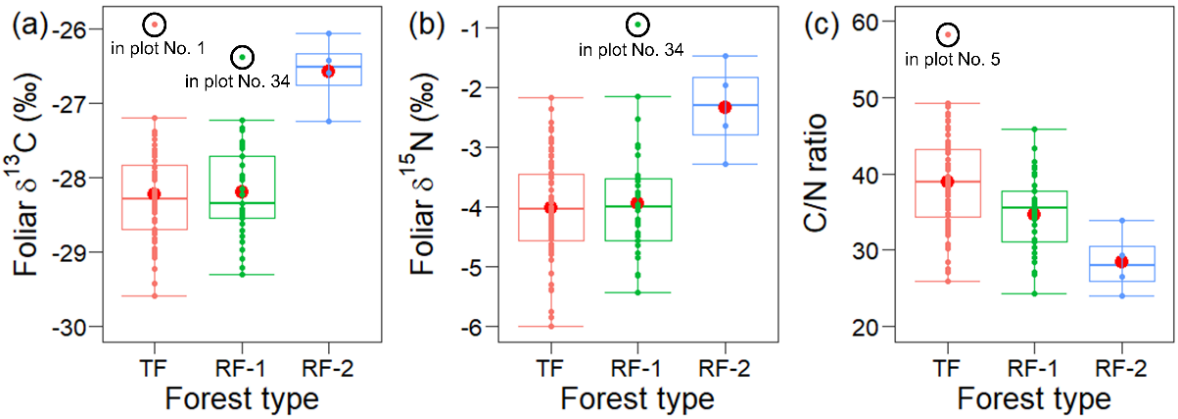

Figure 3.3. Box plots of the (**a**) $\delta^{13}C$ (‰), (**b**) $\delta^{15}N$ (‰), and (**c**) C/N ratio of each tree sample from the TF (n = 68), RF-1 (n = 33), and RF-2 (n = 4). Box encompasses the 25th through 75th percentiles (inter-quartile range IQR) with the median 50%. *Lower (higher)* whisker corresponds to the *smallest (largest)* observation within 1.5 times IQR *below the lower quartile (above the upper quartile)*. Boxplot outliers are circled with the plot number. Red dot in a box indicates mean value of all samples from a forest type.

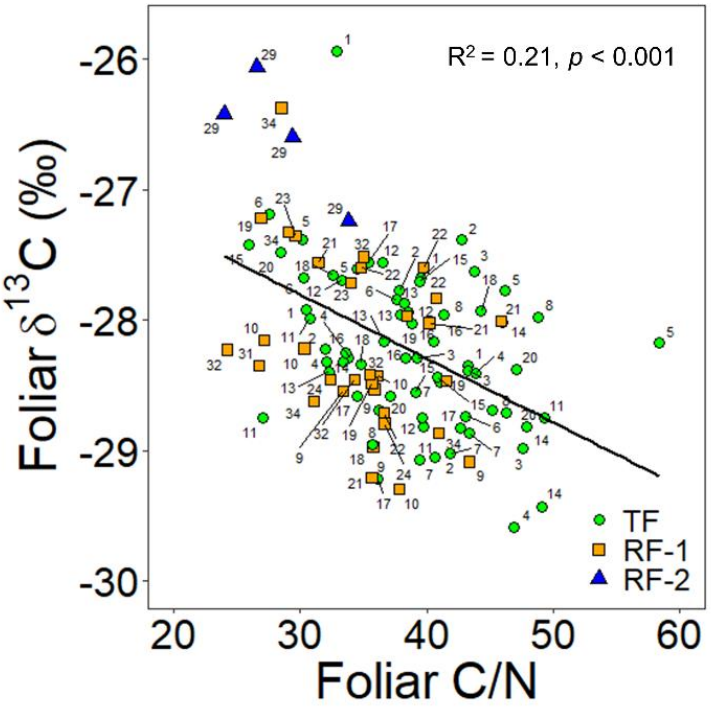

Figure 3.4. Relationships between the foliar $\delta^{13}C$ and C/N for each tree sample from the TF (*n* = 68), the RF-1 (*n* = 33), and the RF-2 (*n* = 4). Each sample was labeled with a plot number. Black solid line shows the linear regression line for all samples in the transect.

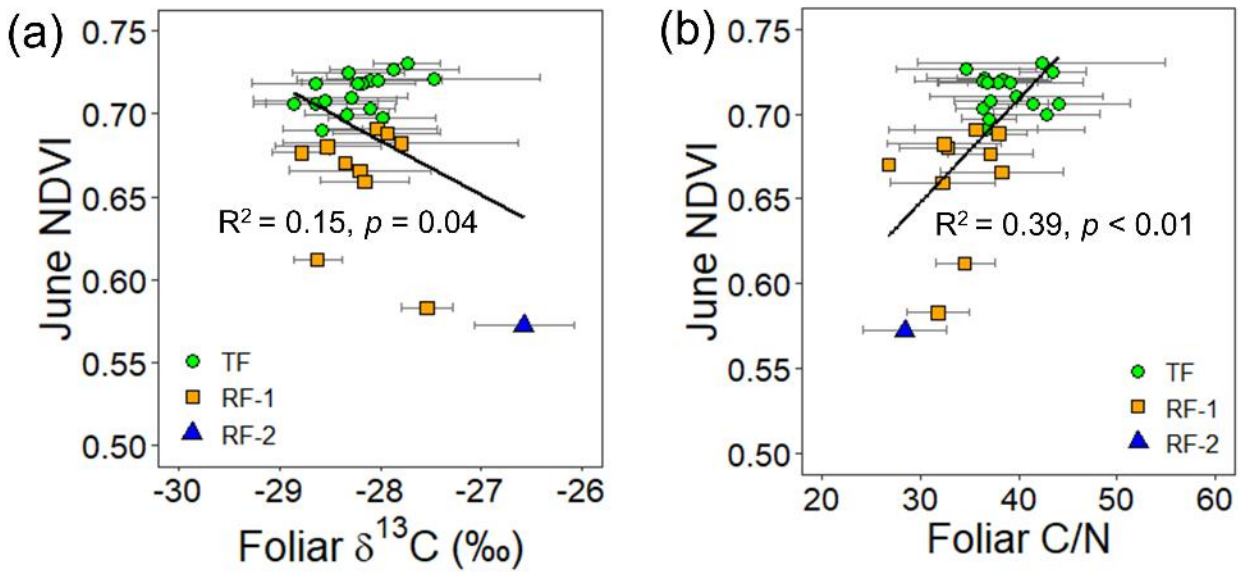

Figure 3.5. Relationships between the NDVI on 4 June 2018, the $\delta^{13}C$ (**a**) and the C/N (**b**) at each plot for the TF (n = 17), the RF-1 (n = 10), and the RF-2 (n = 1). Horizontal error bars represent standard deviations. Black solid line shows the linear regression line for all plots in the transect.

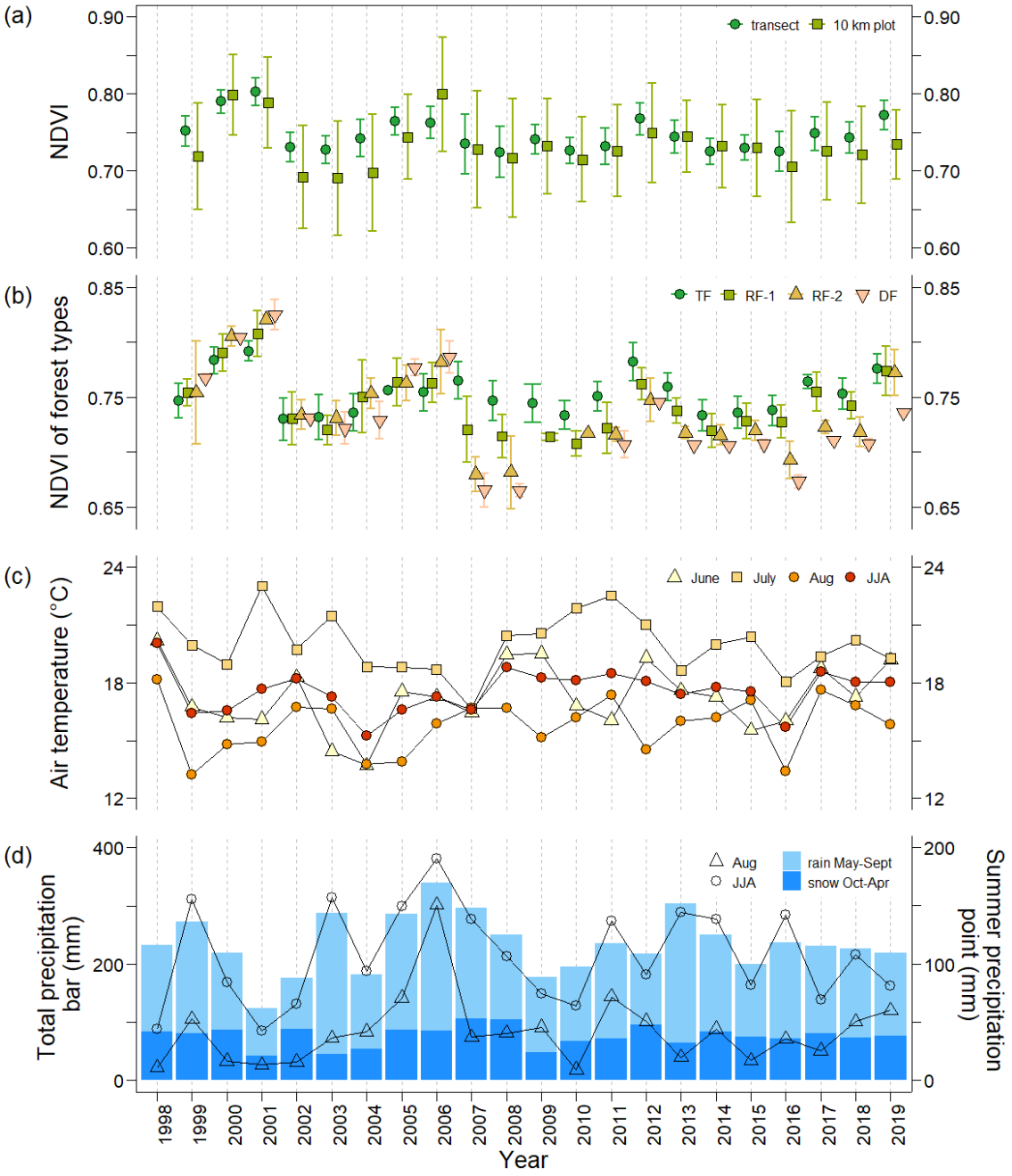

Figure 4.1. The temporal variations from 1999 to 2019 in (a) seasonal maximum NDVI averaged for the plots in the transect and for the representative 10 km × 10 km forest plot calculated from available Landsat 5, 7, 8 images; (b) NDVI of four forest types, typical mature forest (TF), regenerating forests (RF-1 and FR-2), and damaged forest (DF); (c) mean air temperature in June, July, August and whole summer period JJA (June-July-August); (d) the amount of precipitation during previous October-current April (snow) and current May-September (rain) shown with blue bars, in August and whole summer period JJA (June-July-August) shown with triangles and circles.

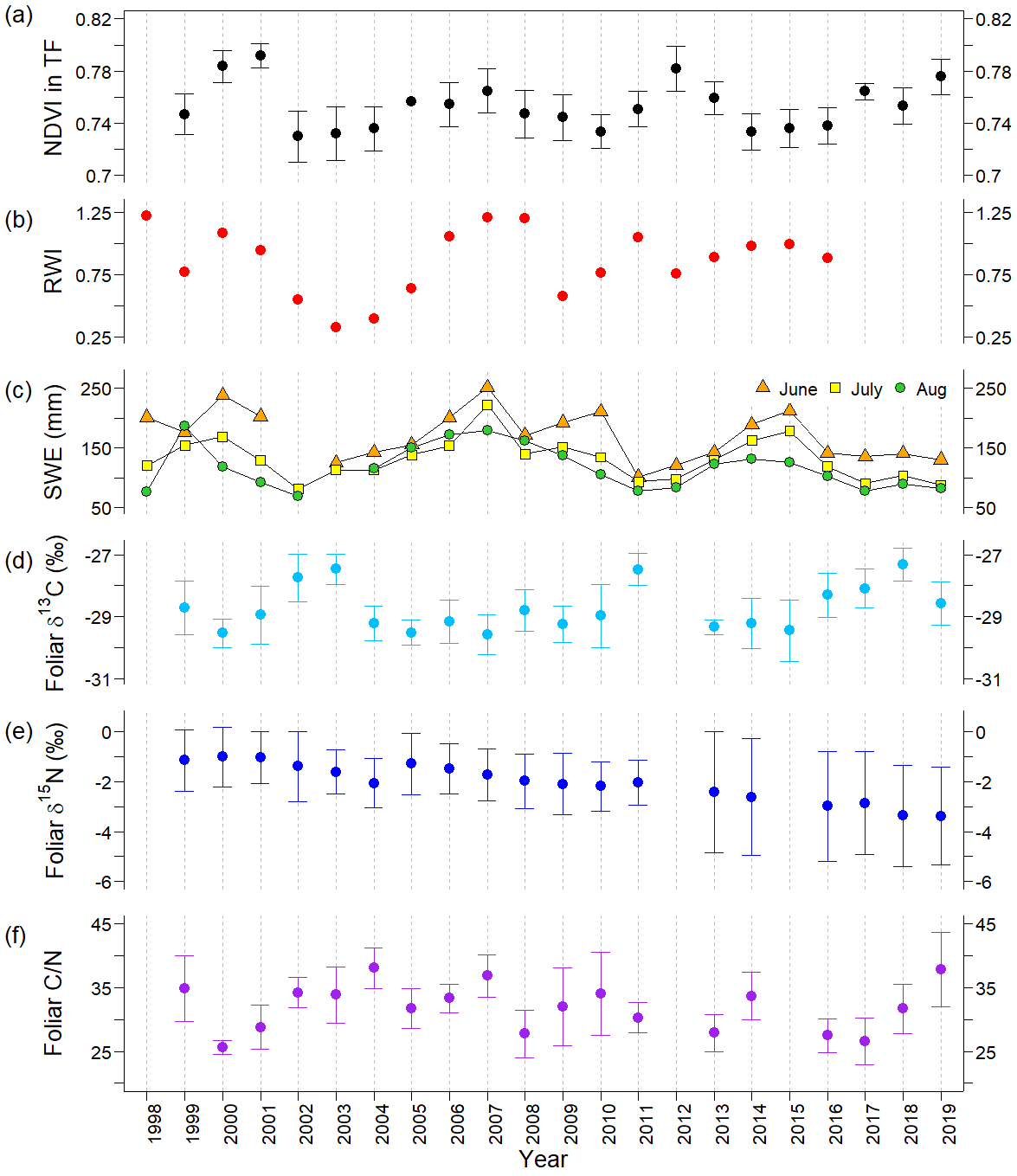

Figure 4.2. The temporal variations in ecosystem parameters at typical forest (TF) observed during 1998-2019: (a) NDVI, (b) larch ring-width index (RWI), (c) soil moisture water equivalent (SWE) at the depth of 0-60 cm in June, July and August, (d) average foliar $\delta^{13}C$, (e) $\delta^{15}N$, (f) C/N ratio. Error bars represent standard deviations. There were no data for NDVI in 1998, RWI in 2017-2019, June SWE in 2002, Aug SWE in 2003, foliar δ13C in 1998 and 2012, foliar δ15N and C/N in 1998, 2012 and 2015.

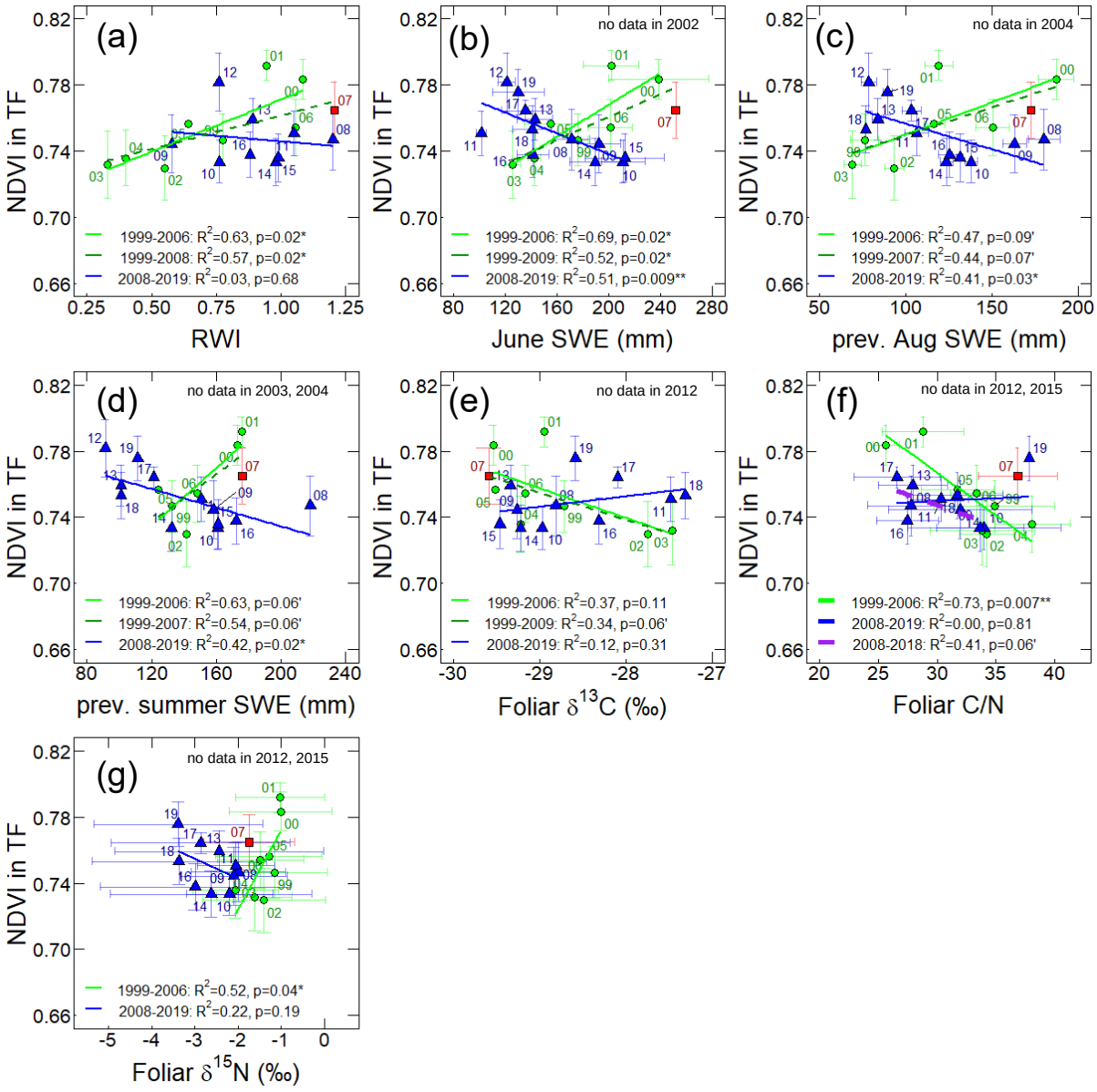

Figure 4.3. The relationships between the TF NDVI in transect and (a) larch ring-width index (RWI) during 1999-2016, monthly average of SWE (mm) in (b) June and (c) previous August, (d) averaged monthly SWE for June-August of previous year, (e) foliar $\delta^{13}C$, (f) C/N, (g) $\delta^{15}N$ during 1999-2019. The green circles, red square and blue triangles show data points in 1999-2006, 2007 and 2008-2019, respectively. Labels nearby the data points are observation years of the TF NDVI. Horizontal and vertical error bars represent standard deviations. Green and blue solid lines show linear regressions for the periods 1999-2006 (before the wet event) and 2008-2019 (after the wet event), and dark green and purple dotted lines represent other periods. p-values and R^2 describe the significance and the degree of variability of the regression models, respectively.

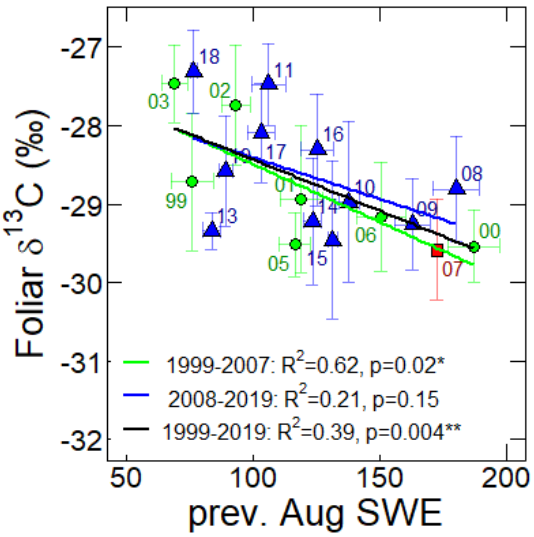

Figure 4.4. The relationship between the foliar $\delta^{13}C$ and monthly mean SWE in previous August (mm) during 1999-2019. The green circles, red square and blue triangles show data points in 1999-2006, 2007 and 2008-2019, respectively. Labels nearby the data points are observation years of the foliar $\delta^{13}C$. Vertical error bars represent standard deviations. The linear regressions for periods 1999-2007, 2008-2019 and 1999-2019 are presented by green, blue and black solid lines. p-values and R^2 describe the significance and the degree of variability of the regression models, respectively.

Tables

Table 3.1. Comparisons between the mean NDVI in two different forest types on 4 June, 31 July, 7 August, 23 August, and 17 September using two parametric unpaired two-sample tests, such as the classical Student's equal variances *t*-test and the Welch unequal variances *t*-test, and one non-parametric Wilcoxon rank-sum test. The results of these three tests are presented as their significance values (*p* values).

Day	Forest types	NDVI (mean ± SD)	RF-1	RF-2	DF	RF-2 & DF[+]
4 June	TF	0.71 ± 0.01	**<0.001 *** **	**0.008 ** **	**0.012 * **	**<0.001 *** **
	RF-1	0.66 ± 0.03		**0.002 ** **	**0.026 * **	**<0.001 *** **
	RF-2	0.51 ± 0.06			0.533 ns	
	DF	0.46 ± 0.01				
	RF-2 & DF	0.49 ± 0.06				
31 July	TF	0.74 ± 0.01	**0.02 * **	**<0.001 *** **	**0.012 * **	**<0.001 *** **
	RF-1	0.73 ± 0.01		**0.03 * **	**0.051 ′**	**0.006 ** **
	RF-2	0.72 ± 0.01			0.533 ns	
	DF	0.71 ± 0.01				
	RF-2 & DF	0.72 ± 0.01				
7 August	TF	0.78 ± 0.01	**0.04 * **	**<0.001 *** **	**0.012 * **	**<0.001 *** **
	RF-1	0.77 ± 0.01		**0.006 ** **	**0.026 * **	**<0.001 *** **
	RF-2	0.75 ± 0.01			0.533 ns	
	DF	0.74 ± 0.00				
	RF-2 & DF	0.74 ± 0.01				
23 August	TF	0.71 ± 0.01	**<0.001 *** **	**<0.001 *** **	**0.012 * **	**<0.001 *** **
	RF-1	0.69 ± 0.01		**0.002 ** **	**0.026 * **	**<0.001 *** **
	RF-2	0.65 ± 0.01			0.533 ns	
	DF	0.65 ± 0.00				
	RF-2 & DF	0.65 ± 0.01				
17 September	TF	0.44 ± 0.01	**0.02 * **	**0.003 ** **	**0.012 * **	**<0.001 *** **
	RF-1	0.42 ± 0.02		0.21 ns	0.231 ns	0.17 ns
	RF-2	0.41 ± 0.02			1 ns	
	DF	0.42 ± 0.00				
	RF-2 & DF	0.41 ± 0.02				

Bold font indicates a significant difference between the NDVI means. Significance levels were flagged as the following: $'p < 0.1$, $*p < 0.05$; $**p < 0.01$, $***p < 0.001$, ns—not significant.
[+] Because of the small sample sizes in the RF-2 ($n = 4$) and DF ($n = 2$) and the statistically insignificant difference in the NDVI between them on each observation day, the RF-2 and DF were brought together as one group ($n = 6$).

Table 3.2. Linear regression models between the plot NDVI which were calculated from the Landsat-8 OLI images on 4 June, July 31, 7 August, 23 August, and 17 September (independent variables) and the plot-averaged $\delta^{13}C$, $\delta^{15}N$, and C/N of the larch needles sampled (dependent variable x). Models were described by the R-squared and *p* value. Number of plots used in the models is 28 out of 34: with the TF (n = 17), the RF-1 (n = 10), and the RF-2 (n = 1).

Day	Foliar $\delta^{13}C$ (‰)			Foliar $\delta^{13}N$ (‰)			Foliar C/N		
	NDVI = $b_1x + b_0$	**R^2**	***p***	**NDVI = $b_1x + b_0$**	**R^2**	***p***	**NDVI = $b_1x + b_0$**	**R^2**	***p***
4 June	**−0.240x − 0.033**	**0.15**	**0.04 ***		<0.01	0.93 ns	**0.006x + 0.465**	**0.39**	**<0.01 ****
31 July		0.01	0.64 ns	**0.007x + 0.769**	**0.16**	**0.04 ***		0.04	0.30 ns
7 August		0.01	0.64 ns		0.10	0.11 ns		0.06	0.20 ns
23 August		0.06	0.20 ns		0.00	1.00 ns	**0.002x + 0.618**	**0.39**	**<0.01 ****
17 September		0.00	0.90 ns		0.01	0.63 ns	**0.002x + 0.376**	**0.15**	**0.04 ***

Bold font indicates a significant relationship. Significance levels (*p* values) were flagged as *$p < 0.05$, **$p < 0.01$, ns—not significant.

Table 4.1. Mean and standard deviation of seasonal maximum NDVI of all plots in the TF and RF-1 in the periods before (1999-2006), during (2007) and after (2008-2019) the extreme wet event. Averaged NDVI was also calculated for wet and dry periods before the event. Different letters in the superscript (a, b, c, d) indicate a statistical difference between the means, calculated using either Student t-test, Welch t-test or Wilcoxon rank-sum test. The sample size (n) indicates a number of plots in a NDVI data group.

Forest type	before the wet event			2007	after the wet event
	wet period (2000, 2001, 2006)	dry period (2002)	all years		
Typical	0.78±0.02	0.73±0.02	0.75±0.03	0.76±0.02	0.75±0.02
Regenerating-1	0.79±0.03	0.73±0.02	0.76±0.03	0.72±0.03	0.74±0.03

Supplementary materials

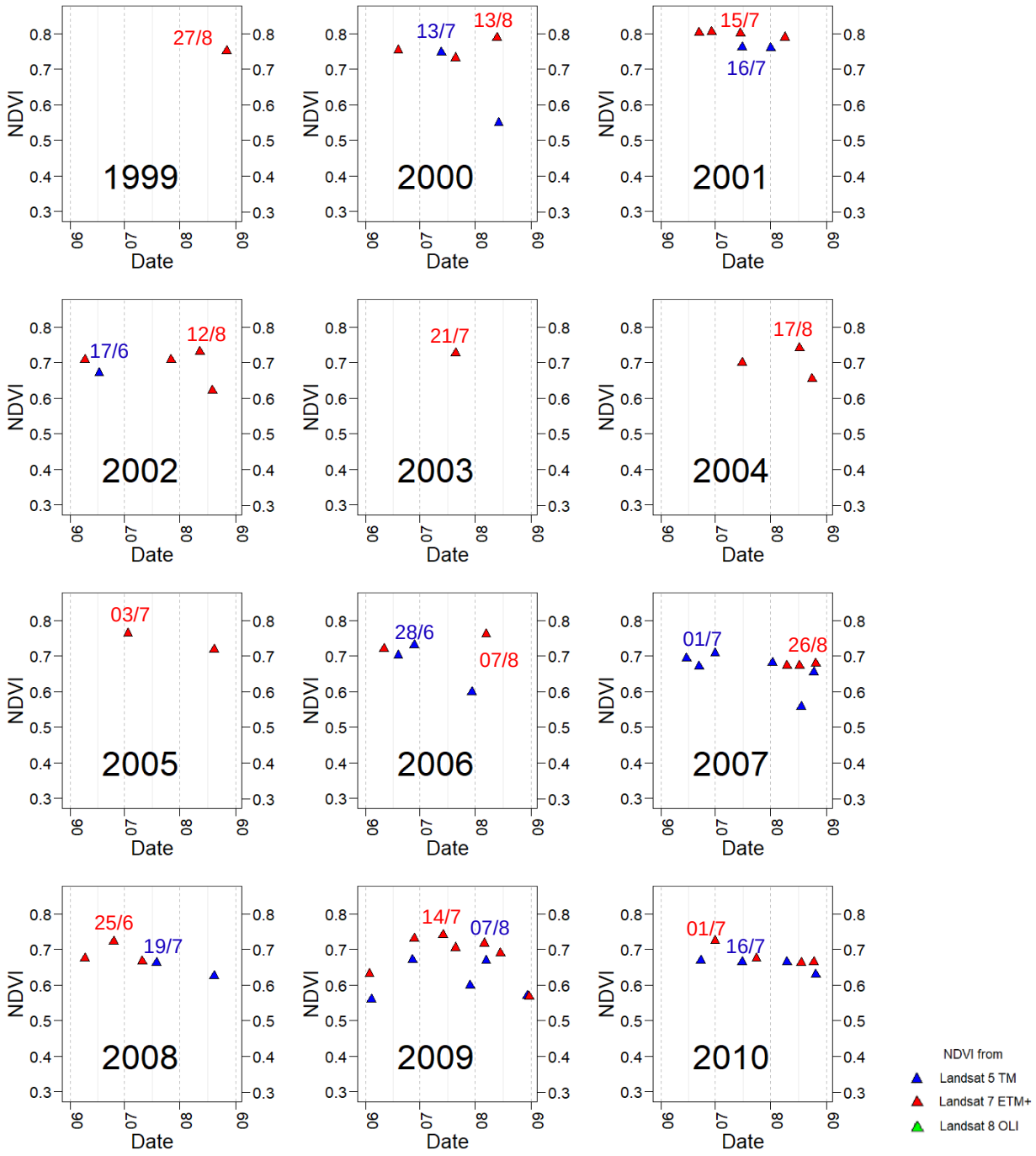

Figure S1. The seasonal variation in the raw transect NDVI in each year of the period 1999-2019. The blue, and green triangles indicate the transect NDVI calculated from Landsat 5, 7 and 8 images, respectively. For available observation days, the transect NDVI value was calculated as average of only quality plots (cloud-free according to Landsat Quality Assessment band). In the figure, only days with a number of quality plots of higher than n = 16 (maximum n = 34) were shown. The seasonal maximum date was found for each of dataset groups (Landsat 5, 7, 8), shown by blue, red and green colors, respectively.

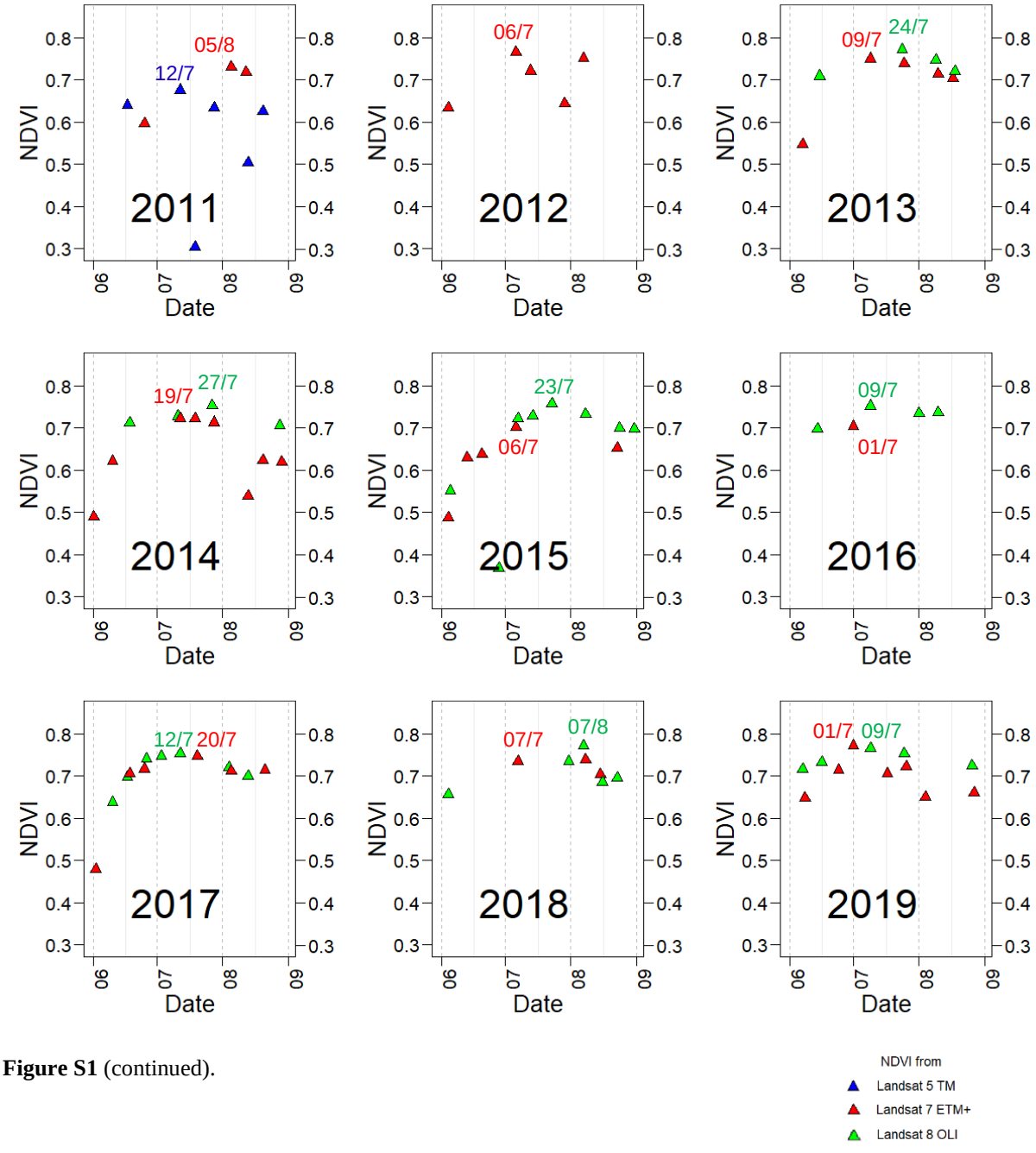

Figure S1 (continued).

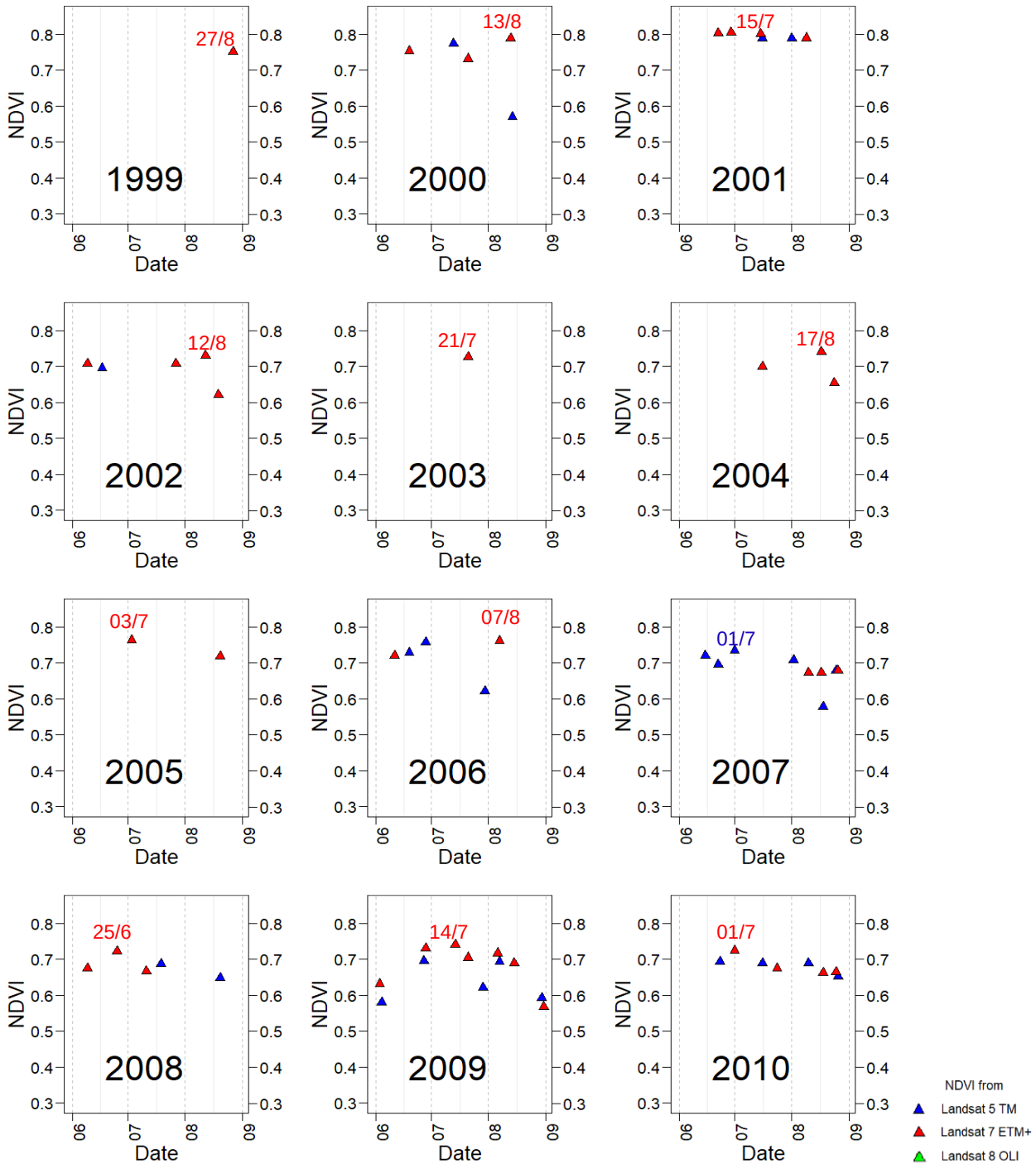

Figure S2. The seasonal variation in the transect NDVI in each year of the period 1999-2019 after conversions of NDVI data shown in Figure S1. The conversions of NDVI data were made from Landsat 5 TM and 8 OLI to Landsat 7 ETM according to the equations developed by Ju and Masek (2016) and Roy et al. (2016). The seasonal maximum was found for each year. To determine a difference among mean NDVI of the transect on observation days of each year, paired sample t-test was applied. In case of statistically insignificant difference among observation days, the day with higher number of quality pixels was selected.

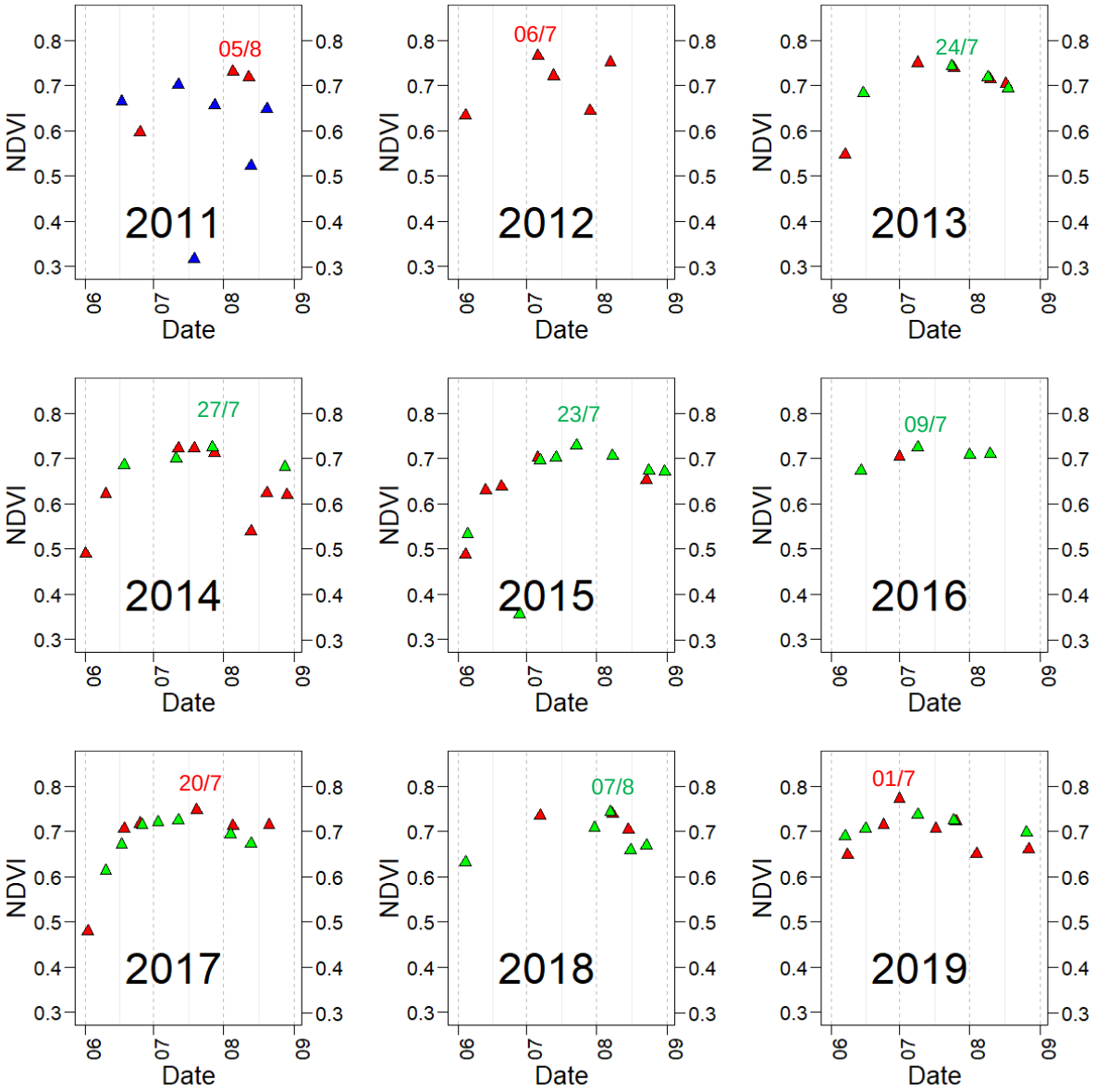

Figure S2 (continued).

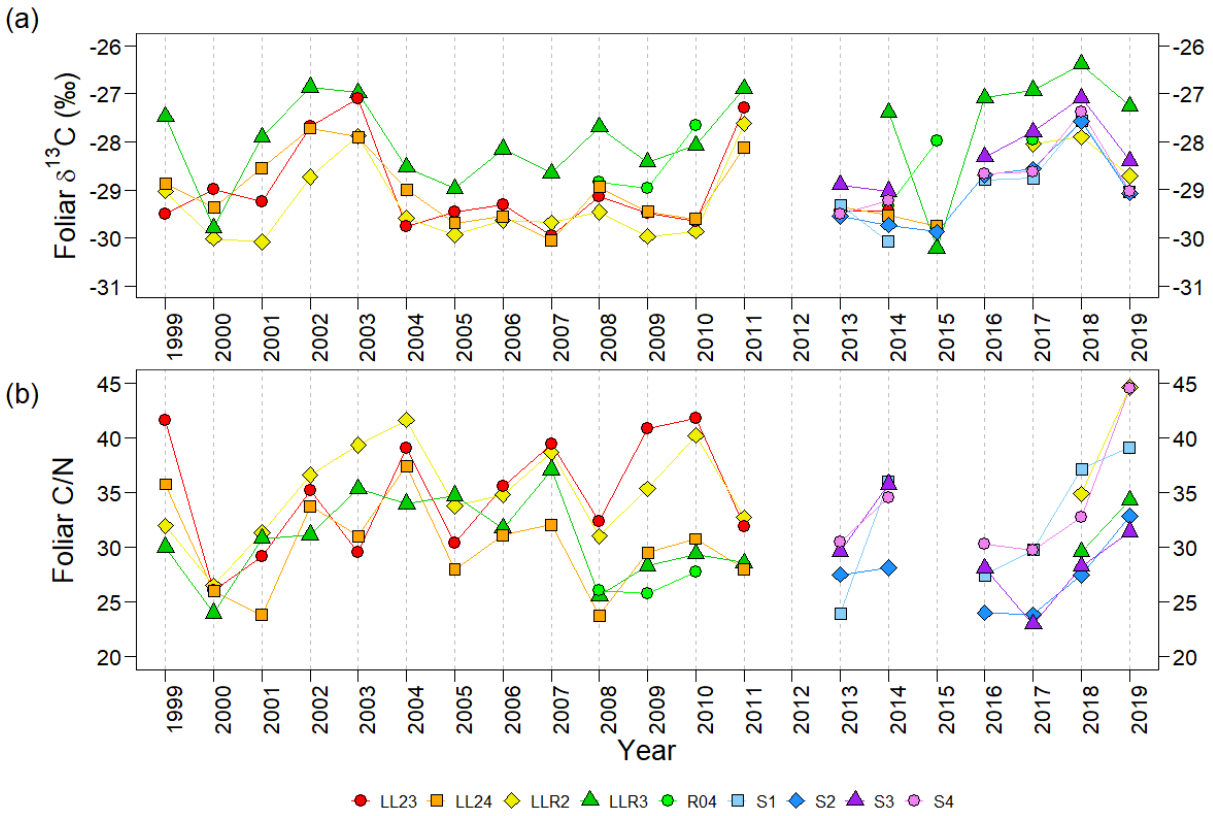

Figure S3. Temporal variations of raw data in (a) the foliar $\delta^{13}C$ and (b) C/N of nine trees in the typical forest during 1999-2019. The five trees LL23, LL24, LLR2 and LLR3 were continuously sampled from 1999 to 2011, and the tree R04 was sampled in 2008-2010, 2014, 2015 and 2017. The four trees S1, S2, S3 and S4 were sampled from 2013. The number of sampled trees for the foliar $\delta^{13}C$ (a) in every year were: n=0 in 2012; n=4 in 1999-2007, 2011 and 2015; n=5 in 2008-2010, 2016; n=6 in 2013, 2018 and 2019; n=7 in 2017; n=8 in 2014. The number of sampled trees for the foliar C/N (b) in every year were: n=0 in 2012 and 2015; n=4 in 1999-2007, 2011, 2013, 2014, 2016-2017; n=5 in 2008-2010; n=6 in 2018 and 2019. From each tree four stems were taken, and leaves were mixed well before the analyses. All data obtained in each year was averaged, in order to build a successive temporal variation in the foliar $\delta^{13}C$ and C/N (Figure 4.2d and f)

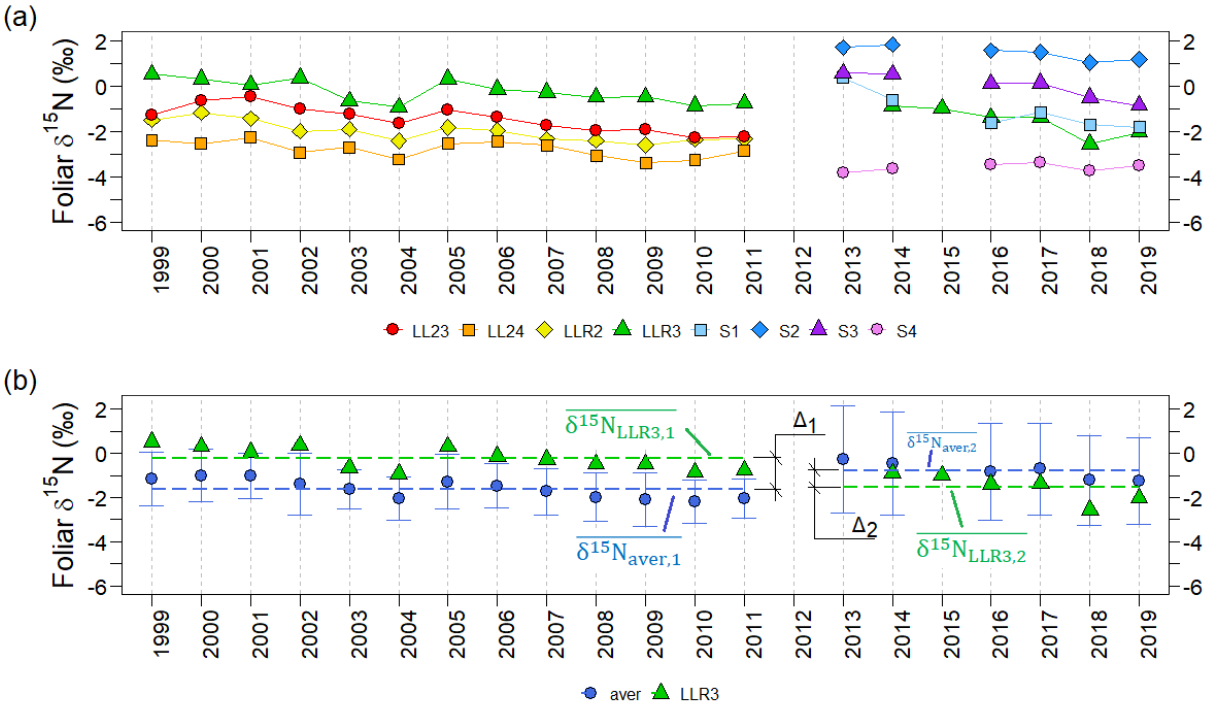

Figure S4. Temporal variations of raw data in (a) the foliar $\delta^{15}N$ of the same trees as in Figure S2, and (b) method of calculation to obtain successive temporal variation in the foliar $\delta^{15}N$. The $\delta^{15}N$ value differs from tree to tree because of different source of nitrogen for the tree. To obtain continuous temporal variation, first, the average values from LL23, LL24, LLR2 and LLR3 in 1999-2011 ($\delta^{15}N_{aver,1}$) and S1-S4 in 2013-2019 ($\delta^{15}N_{aver,2}$) were calculated, and, second, the differences between the average and LLR3 (Δ_1 and Δ_2) were obtained. Then, continuous average value was calculated by adding Δ_1 and Δ_2 to $\delta^{15}N_{aver,2}$ (Figure 3c).

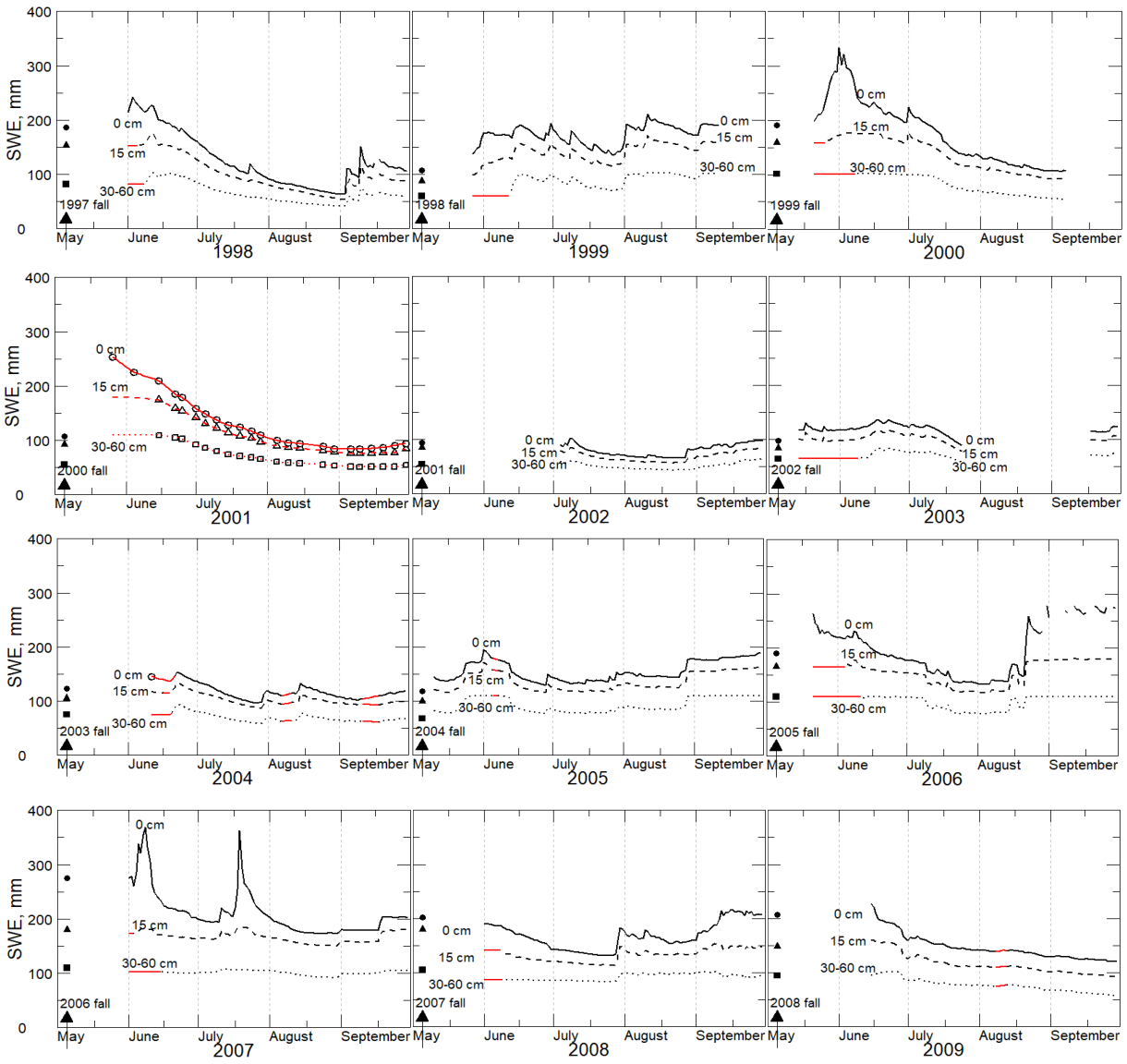

Figure S5. Daily variation of soil moisture water equivalent (SWE, mm) including ice from surface of mineral soil layer to 60 cm in May to September from 1998 to 2019. Cumulative SWE from a depth of 60 cm to 30 cm, 30 to 15 cm, and 15 to 0 cm are shown in the figure. Black dotted, dashed and solid lines show continuous daily data, and empty circle, triangle and square shown in 2001 and 2004 are one day data. Filled circle, triangle and square with arrow in the left side of each figure are SWE in previous September (before freeze). The SWE was calculated with the same or similar methods by Sugimoto et al. (2003), that is from volumetric soil water content (VSWC, m3/m3) observed by TDR by multiplying by layer thickness (mm). The SWE was estimated from regression relationships of TDR measurements between manual (Moisture Point, Environmental Sensors Inc., Canada) and automatic observations. Three automatic measurement systems were used in different years: TRIME IMKO P2 sensors (IMKO Micromodultechnik GmbH, Germany) at depths of 10, 20, 40 cm in 1998, 1999, 2002-2008, Decagon ECH2O sensors (Meter Environment, USA) at 7.5, 22.5, 45 cm in 2009, 2012, 2013 and 2016-2019 and Sentek EnviroSmart (Campbell Scientific Inc, Canada) at 10, 20, 30, 40, 50, 60 cm in 2010, 2014 and 2015. In 2001, SWE observed by Moisture Point were shown. Red lines show estimated values by comparison of previously observed data.

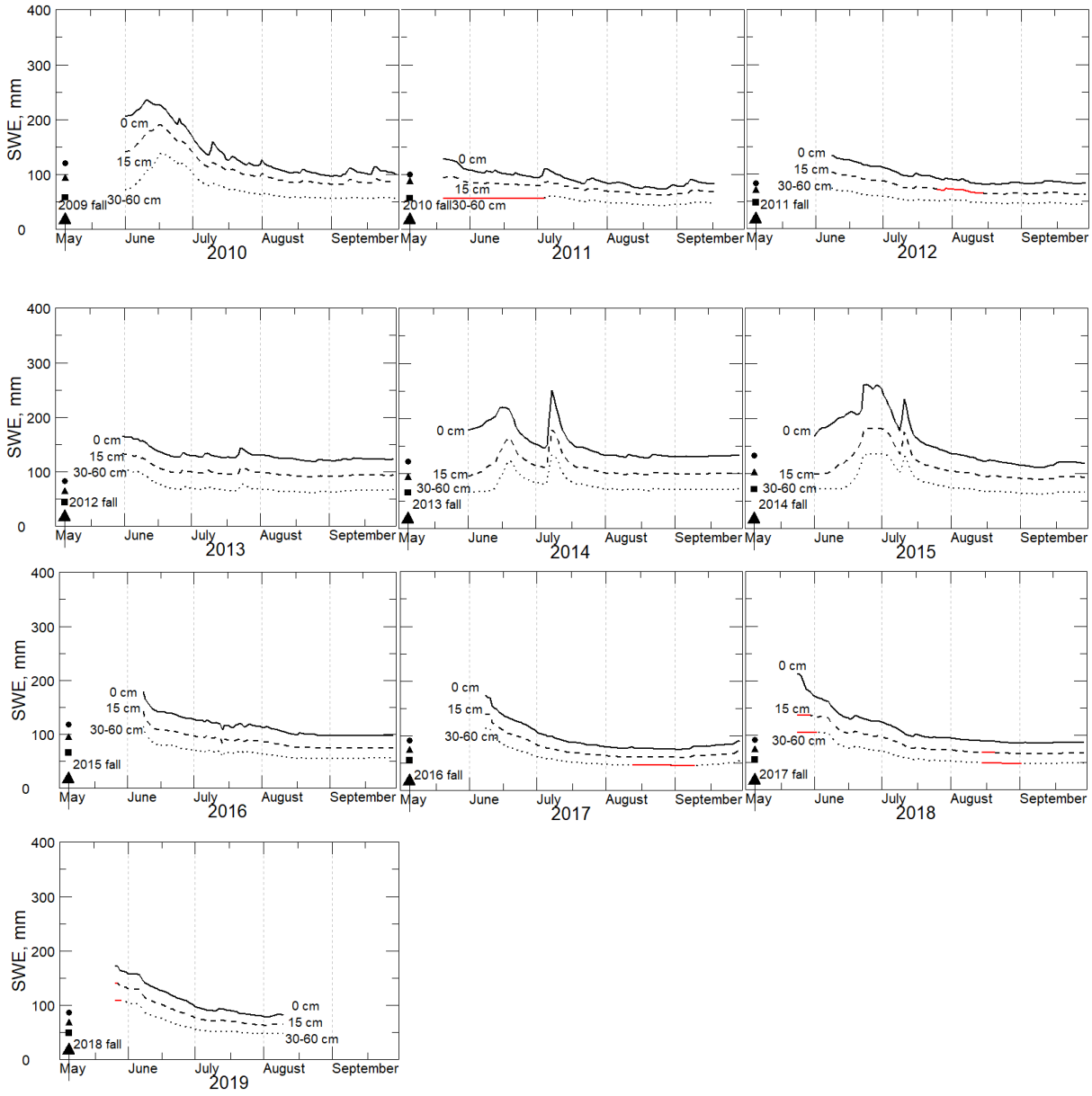

Figure S5 (continued).

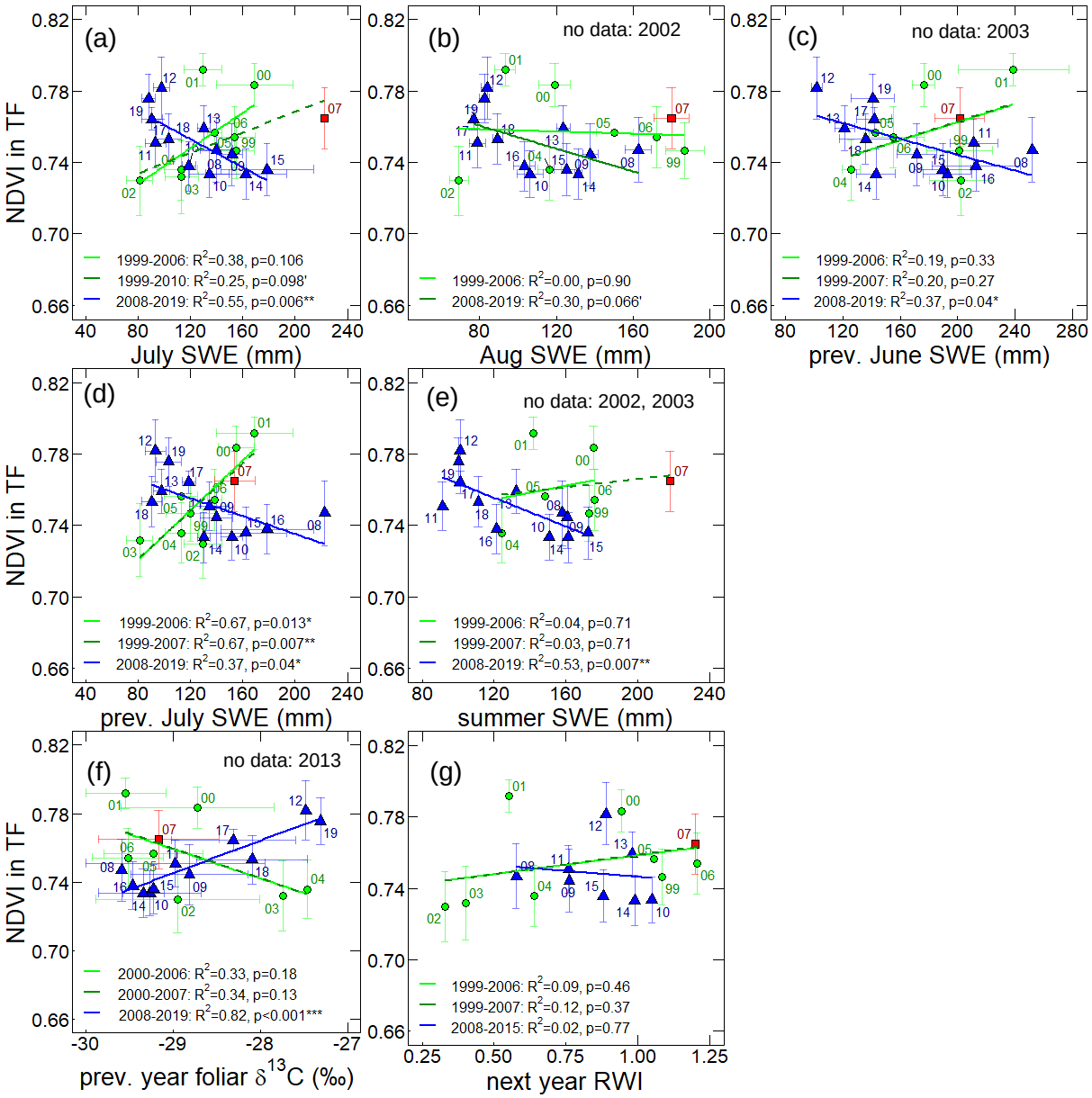

Figure S6. The relationships between the TF NDVI in transect and ecological parameters: monthly average soil moisture water equivalent (SWE mm) in (a) July, (b) August, (c) previous June, (d) previous July, (e) averaged June, July and August SWE, (f) previous year's foliar $\delta^{13}C$ (‰) during 2000-2019, (g) next year's RWI during 1999-2015. Green circles and blue triangles are the data before (1999-2006) and after (2008-2019) the wet event, and red square are the data observed in 2007. Labels nearby the data points are observation years of NDVI. Horizontal and vertical error bars represent standard deviations. Green, dark green dotted and blue solid lines show linear regressions for periods 1999-2006 (before the wet event), including 2007 (the wet event), and 2008-2019 (after the wet event). For the figure S6 (e), dark green dotted line is the linear regression for the period 1999-2010. The p-values and R^2 describe the significance and the degree of variability of the regression are also shown.

Table S1. Seasonal maximum of NDVI (mean and standards deviation) observed for four forest types (TF, RF-1, RF-2, and DF) within the transect and 10 km plot during 1999-2019. NDVI was calculated from available Landsat 5 TM, 7 ETM+ and 8 OLI images. All the NDVI values from Landsat 5 and 8 were converted to Landsat 7 ETM+ using the methods of Ju and Masek (2016) and Roi et al. (2016), respectively. The value n shows number of the quality plots among 17 (TF), 11 (RF-1), 4 (RF-2), and 2 (DF), respectively (total n = 34). The n for the 10 km plot shows percentage of the quality pixels among 111556 pixels.

Satellite (transect /plot)	Year	Day of maximum NDVI		Typical forest			Regenerating forest-1			Regenerating forest-2			Damaged forest			Transect			10 km plot		
		transect	plot	aver	std	n	aver	std	n	aver	std	n	aver	std	n	aver	std	n	aver	std	n, %
L7 ETM+	1999	27.08		0.75	0.02	17	0.75	0.01	11	0.75	0.05	4	0.77	0.00	2	0.75	0.02	34	0.72	0.07	100.0
L7 ETM+	2000	13.08		0.78	0.01	17	0.79	0.02	11	0.81	0.01	4	0.80	0.00	2	0.79	0.02	34	0.80	0.05	100.0
L7 ETM+	2001	15.07		0.79	0.01	17	0.81	0.02	11	0.82	0.00	4	0.82	0.01	2	0.80	0.02	34	0.79	0.06	95.3
L7 ETM+	2002	12.08		0.73	0.02	17	0.73	0.02	11	0.73	0.01	4	0.73	0.00	2	0.73	0.02	34	0.69	0.07	100.0
L7 ETM+	2003	21.07		0.73	0.02	17	0.72	0.01	11	0.73	0.02	4	0.72	0.01	2	0.73	0.02	34	0.69	0.07	76.7
L7 ETM+	2004	17.08		0.74	0.02	17	0.75	0.03	11	0.75	0.01	4	0.73	0.02	2	0.74	0.02	34	0.70	0.08	83.1
L7 ETM+	2005	03.07		0.76		1	0.76	0.02	9	0.76	0.02	4	0.78	0.01	2	0.76	0.02	16	0.74	0.06	82.5
L7 ETM+	2006	07.08	29.07	0.75	0.02	17	0.76	0.02	11	0.78	0.03	4	0.79	0.01	2	0.76	0.02	34	0.80	0.07	76.9
L5 TM/ L7 ETM+	2007	01.07	25.07	0.76	0.02	17	0.72	0.03	11	0.68	0.02	4	0.67	0.02	2	0.73	0.04	34	0.73	0.08	51.6
L7 ETM+	2008	25.06		0.75	0.02	17	0.71	0.02	11	0.68	0.03	4	0.66	0.01	2	0.72	0.03	34	0.72	0.08	79.3
L7 ETM+	2009	14.07		0.74	0.02	16	0.71	0.00	2			0			0	0.74	0.02	18	0.73	0.06	67.7
L7 ETM+/ L5 TM	2010	01.07	16.07	0.73	0.01	17	0.71	0.01	7	0.72		1			0	0.73	0.02	25	0.72	0.06	97.9
L7 ETM+	2011	05.08	12.08	0.75	0.01	12	0.72	0.02	11	0.72	0.01	4	0.71	0.01	2	0.73	0.02	29	0.73	0.06	78.2
L7 ETM+	2012	06.07		0.78	0.02	12	0.76	0.01	11	0.75	0.02	4	0.75	0.00	2	0.77	0.02	29	0.75	0.06	81.8
L8 OLI	2013	24.07		0.76	0.01	17	0.74	0.01	11	0.72	0.01	4	0.71	0.00	2	0.74	0.02	34	0.74	0.05	98.8
L8 OLI	2014	27.07		0.73	0.01	17	0.72	0.02	11	0.72	0.01	4	0.71	0.00	2	0.73	0.02	34	0.73	0.05	99.7
L8 OLI/ L7 ETM+	2015	23.07	31.07	0.74	0.01	17	0.73	0.02	11	0.72	0.01	4	0.71	0.00	2	0.73	0.02	34	0.73	0.06	50.7
L8 OLI	2016	09.07		0.74	0.01	14	0.73	0.01	9	0.69	0.02	4	0.67	0.01	2	0.72	0.03	31	0.71	0.07	87.8
L7 ETM+	2017	20.07		0.76	0.01	7	0.75	0.02	9	0.72	0.01	4	0.71	0.00	2	0.75	0.02	22	0.73	0.06	83.6
L8 OLI	2018	07.08		0.75	0.01	17	0.74	0.01	11	0.72	0.01	4	0.71	0.00	2	0.74	0.02	34	0.72	0.06	100.0
L7 ETM+/ L8 OLI	2019	01.07	09.07	0.78	0.01	17	0.77	0.02	11	0.77	0.02	4	0.74	0.00	2	0.77	0.02	34	0.73	0.05	100.0

Table S2. The results of Shapiro-Wilk test, a normality test, for seasonal maximum NDVI data in each forest type, presented as the test statistic W and its significance level p-value. The data distribution was normal at $p > 0.05$ and non-normal at $p < 0.05$* (shown by bold font). The dash "−" means no result because of either a small number of samples in a forest type ($n < 3$) or no samples.

Date	TF		RF-1		RF-2		DF	
	W	p	W	p	W	p	W	p
1999	0.94	0.36	0.94	0.46	0.91	0.48	_	_
2000	0.97	0.78	0.88	0.09	0.89	0.36	_	_
2001	0.90	0.08	0.98	0.98	0.96	0.76	_	_
2002	0.93	0.19	0.97	0.88	0.97	0.85	_	_
2003	0.98	0.93	0.91	0.27	0.97	0.85	_	_
2004	0.97	0.75	0.88	0.12	0.89	0.37	_	_
2005	_	_	0.93	0.44	0.83	0.16	_	_
2006	0.95	0.52	0.95	0.68	0.77	0.06	_	_
2007	0.94	0.30	**0.81**	**0.01***	0.93	0.57	_	_
2008	0.95	0.42	0.92	0.32	0.92	0.54	_	_
2009	0.93	0.23	_	_	_	_	_	_
2010	0.96	0.68	0.94	0.62	_	_	_	_
2011	0.95	0.65	0.97	0.89	0.84	0.19	_	_
2012	0.96	0.78	0.81	0.11	_	_	_	_
2013	**0.86**	**0.02***	0.91	0.27	0.96	0.77	_	_
2014	0.96	0.66	0.92	0.31	0.97	0.85	_	_
2015	0.98	0.94	0.95	0.61	0.82	0.15	_	_
2016	0.92	0.20	0.91	0.35	0.95	0.71	_	_
2017	0.90	0.32	0.96	0.79	0.79	0.08	_	_
2018	0.97	0.80	0.90	0.21	0.94	0.68	_	_
2019	0.98	0.92	0.97	0.93	0.93	0.59	_	_

Table S3. The results of F-test, a test of equality of variances, for two normally distributed seasonal maximum NDVI datasets of two forest types (see Table S2), presented as the test statistic F and its significance level p-value. The variances of two NDVI datasets were equal at $p > 0.05$ and unequal at $p < 0.05$* (shown by bold font). The dash "**–**" means no result because of a non-normally distributed NDVI dataset in at least one of the two forest types being compared.

Date	Forest types	RF-1		RF-2		DF	
		F	p	F	p	F	p
1999	TF	0.59	0.40	**8.93**	**<0.01***	–	–
	RF-1			**0.07**	**<0.01***	–	–
	RF-2					–	–
2000	TF	2.01	0.21	0.57	0.71	–	–
	RF-1			3.53	0.33	–	–
	RF-2					–	–
2001	TF	**5.27**	**<0.01***	0.20	0.21	–	–
	RF-1			**26.27**	**0.02***	–	–
	RF-2					–	–
2002	TF	1.49	0.46	0.46	0.57	–	–
	RF-1			3.24	0.36	–	–
	RF-2					–	–
2003	TF	0.41	0.15	0.58	0.72	–	–
	RF-1			0.70	0.59	–	–
	RF-2					–	–
2004	TF	**3.82**	**0.02***	0.66	0.82	–	–
	RF-1			5.80	0.18	–	–
	RF-2					–	–
2005	TF	–	–	–	–	–	–
	RF-1			1.81	0.68	–	–
	RF-2					–	–
2006	TF	1.11	0.82	2.86	0.14	–	–
	RF-1			0.39	0.22	–	–
	RF-2					–	–
2007	TF	–	–	0.84	0.98	–	–
	RF-1			–	–	–	–
	RF-2					–	–
2008	TF	1.15	0.78	3.30	0.09	–	–
	RF-1			0.35	0.18	–	–
	RF-2					–	–
2009	TF	–	–	–	–	–	–
	RF-1			–	–	–	–
	RF-2					–	–
2010	TF	0.80	0.83	–	–	–	–
	RF-1			–	–	–	–
	RF-2					–	–
2011	TF	2.99	0.09	0.21	0.22	–	–
	RF-1			**14.54**	**0.05***	–	–
	RF-2					–	–
2012	TF	0.71	0.60	1.25	0.68	–	–
	RF-1			0.57	0.44	–	–
	RF-2					–	–
2013	TF	–	–	–	–	–	–
	RF-1			4.35	0.25	–	–
	RF-2					–	–
2014	TF	1.15	0.77	0.41	0.50	–	–
	RF-1			2.82	0.43	–	–
	RF-2					–	–
2015	TF	1.22	0.70	0.36	0.43	–	–
	RF-1			3.41	0.34	–	–
	RF-2					–	–
2016	TF	1.16	0.76	1.46	0.53	–	–
	RF-1			0.80	0.71	–	–
	RF-2					–	–
2017	TF	**7.85**	**0.02***	0.84	0.96	–	–
	RF-1			9.30	0.09	–	–
	RF-2					–	–
2018	TF	0.74	0.64	0.90	0.92	–	–
	RF-1			0.82	0.71	–	–
	RF-2					–	–
2019	TF	2.75	0.07	2.32	0.23	–	–
	RF-1			1.19	1.00	–	–
	RF-2					–	–

Table S4. Comparisons of seasonal maximum NDVI averaged for each forest type between two different forest types in years from 1999-2019 using two parametric unpaired two-sample tests, such as classical Student's equal variances

t-test and Welch unequal variances t-test, and one non-parametric Wilcoxon rank-sum test. The results of these three tests are presented as their significance values (p-values) and test statistics (t, t_w and W, respectively). Bold font indicates a significant difference flagged as 'p <0.1, *p <0.05, **p <0.01, ***p <0.001, and ns – not significant.

Date	Forest types	RF-1		RF-2		DF	
		Statistic	p	Statistic	p	Statistic	p
1999	TF	t = 1.38	0.179^{ns}	t_w = 0.33	0.764^{ns}	W = 30	0.105^{ns}
	RF-1			t_w = -0.004	0.997^{ns}	W = 19	0.154^{ns}
	RF-2					W = 4	1^{ns}
2000	TF	t = 1.28	0.212^{ns}	**t = 3.37**	**0.003****	**W = 34**	**0.012***
	RF-1			t = -1.62	0.128^{ns}	W = 17	0.308^{ns}
	RF-2					W = 4	1^{ns}
2001	TF	**t_w = 2.40**	**0.033***	**t = 6.12**	**<0.001*****	**W = 34**	**0.012***
	RF-1			**t_w = -1.95**	**0.075'**	W = 18	0.231^{ns}
	RF-2					W = 5	0.8^{ns}
2002	TF	t = 0.11	0.914^{ns}	t = 0.39	0.698^{ns}	W = 20	0.749^{ns}
	RF-1			t = -0.25	0.806^{ns}	W = 10	0.923^{ns}
	RF-2					W = 3	0.8^{ns}
2003	TF	t = -1.70	0.100^{ns}	t = -0.06	0.951^{ns}	W = 11	0.491^{ns}
	RF-1			t = -1.40	0.185^{ns}	W = 12	0.923^{ns}
	RF-2					W = 2	0.533^{ns}
2004	TF	t_w = 1.35	0.199^{ns}	**t = 1.91**	**0.072'**	W = 13	0.655^{ns}
	RF-1			t = -0.17	0.869^{ns}	W = 7	0.513^{ns}
	RF-2					W = 0	0.133^{ns}
2005	TF	W = 4	1^{ns}	W = 2	1^{ns}	W = 2	0.667^{ns}
	RF-1			t = 0.07	0.943^{ns}	W = 13	0.436^{ns}
	RF-2					W = 6	0.533^{ns}
2006	TF	t = 1.29	0.210^{ns}	**t = 2.55**	**0.02***	**W = 32**	**0.047***
	RF-1			t = -1.53	0.149^{ns}	W = 20	0.103^{ns}
	RF-2					W = 6	0.533^{ns}
2007	TF	**W = 10**	**<0.001*****	**t = -9.12**	**<0.001*****	**W = 0**	**0.012***
	RF-1			**W = 39**	**0.026***	W = 2	0.103^{ns}
	RF-2					W = 1	0.267^{ns}
2008	TF	**t = -4.50**	**<0.001*****	**t = -5.53**	**<0.001*****	**W = 0**	**0.012***
	RF-1			**t = 2.40**	**0.032***	**W = 0**	**0.026***
	RF-2					W = 3	0.8^{ns}
2009	TF	**W = 1**	**0.026***	–	–	–	–
	RF-1			–	–	–	–
	RF-2					–	–
2010	TF	**t = -4.52**	**<0.001*****	W = 3	0.444^{ns}	–	–
	RF-1			W = 2	0.75^{ns}	–	–
	RF-2					–	–
2011	TF	**t = -3.68**	**0.001****	**t = -4.86**	**<0.001*****	**W = 0**	**0.022***
	RF-1			t_w = 0.73	0.479^{ns}	W = 6	0.410^{ns}
	RF-2					W = 2	0.533^{ns}
2012	TF	**t = -2.93**	**0.008****	**t = -3.35**	**0.005****	**W = 0**	**0.022***
	RF-1			t = 1.59	0.136^{ns}	W = 4	0.231^{ns}
	RF-2					W = 4	1^{ns}
2013	TF	**W = 17**	**<0.001*****	**W = 1**	**<0.001*****	**W = 0**	**0.012***
	RF-1			**t = 3.43**	**0.004****	**W = 0**	**0.026***
	RF-2					W = 0	0.133^{ns}
2014	TF	**t = -2.49**	**0.020***	**t = -2.42**	**0.026***	**W = 0**	**0.012***
	RF-1			0.50	0.625^{ns}	W = 6	0.410^{ns}
	RF-2					W = 2	0.533^{ns}
2015	TF	t = -1.32	0.199^{ns}	**t = -2.13**	**0.047***	**W = 1**	**0.023***
	RF-1			t = 1.00	0.335^{ns}	W = 3	0.154^{ns}
	RF-2					W = 0	0.133^{ns}

Table S4 (continue)

Date	Forest types	RF-1		RF-2		DF	
		Statistic	p	Statistic	p	Statistic	p
2016	TF	**t = -1.72**	**0.098'**	**t = -5.60**	**<0.001*** **	**W = 0**	**0.013***
	RF-1			**t = 3.75**	**0.003****	**W = 0**	**0.036***
	RF-2					W = 1	0.267^{ns}
2017	TF	t_w = -1.50	0.162^{ns}	**t = -10.84**	**<0.001*** **	**W = 0**	**0.056'**
	RF-1			**t = 3.48**	**0.005****	**W = 0**	**0.036***
	RF-2					W = 0	0.133^{ns}
2018	TF	**t = -2.14**	**0.042***	**t = -4.48**	**<0.001*** **	**W = 0**	**0.012***
	RF-1			**t = 3.27**	**0.006****	**W = 0**	**0.026***
	RF-2					W = 2	0.533^{ns}
2019	TF	t = -0.24	0.810^{ns}	t = -0.40	0.691^{ns}	**W = 0**	**0.012***
	RF-1			t = 0.13	0.897^{ns}	W = 2	0.103^{ns}
	RF-2					W = 0	0.133^{ns}

Table S5. Pearson correlation (r) between TF NDVI and ecosystem and climatic parameters with 0-,1- and 2-year time lag of the TF NDVI before the wet event (1999-2006). Bold font indicates a significant correlation. Significance levels were flagged as 'p <0.1, *p <0.05, **p <0.01, ***p <0.001. The number (n) indicates sample size of observed years.

Ecosystem and climatic parameters in the current year (i year)				Mean transect TF NDVI in the current year (i year)			the following year (i+1 year)			two years later (i+2 year)		
	Parameter	Observation Month	unit	r	p-value	n	r	p-value	n	r	p-value	n
Needle parameters	$\delta^{13}C$		‰	-0.61	0.11	8	-0.57	0.177	7	0.13	0.8	6
	$\delta^{15}N$		‰	**0.72**	**0.043***	**8**	0.27	0.565	7	-0.18	0.727	6
	C/N		‰	**-0.85**	**0.007****	**8**	-0.24	0.604	7	0.59	0.216	6
Soil moisture water equivalent (SWE)	June SWE	June	mm	**0.83**	**0.020***	**7**	0.43	0.333	7	-0.30	0.567	6
	July SWE	July	mm	0.61	0.106	8	**0.82**	**0.013***	**8**	0.13	0.775	7
	Aug SWE	August	mm	-0.06	0.901	7	**0.69**	**0.089'**	**7**	0.48	0.333	6
	summer SWE	JJA	mm	0.20	0.711	6	**0.79**	**0.060'**	**6**	-0.03	0.962	5
Tree-ring width index	RWI			**0.79**	**0.019***	**8**	0.31	0.448	8	0.03	0.938	8
Precipitation	Jan prec	January	mm	-0.53	0.177	8	0.01	0.973	8	0.34	0.408	8
	Feb prec	February	mm	-0.43	0.293	8	-0.19	0.66	8	0.30	0.473	8
	Mar prec	March	mm	-0.60	0.118	8	**-0.66**	**0.072'**	**8**	0.04	0.933	8
	Apr prec	April	mm	0.59	0.124	8	0.30	0.472	8	0.33	0.432	8
	May prec	May	mm	0.56	0.151	8	-0.06	0.896	8	-0.40	0.321	8
	June prec	June	mm	0.26	0.534	8	**0.75**	**0.033***	**8**	0.23	0.59	8
	July prec	July	mm	-0.61	0.109	8	-0.10	0.811	8	0.15	0.728	8
	Aug prec	August	mm	-0.14	0.739	8	0.27	0.522	8	0.42	0.297	8
	Sep prec	September	mm	-0.37	0.373	8	-0.13	0.765	8	**0.62**	**0.099'**	**8**
	Oct prec	October	mm	-0.02	0.956	8	0.42	0.298	8	**0.91**	**0.002****	**8**
	Nov prec	November	mm	-0.02	0.965	8	-0.10	0.809	8	0.04	0.916	8
	Dec prec	December	mm	-0.23	0.583	8	-0.11	0.797	8	0.34	0.41	8
	snow before summer	previous Oct - current Apr	mm	-0.05	0.899	8	0.47	0.243	8	0.18	0.662	8
	rain	MJJAS	mm	-0.31	0.452	8	0.21	0.619	8	0.52	0.187	8
	summer (JJA) rain	JJA	mm	-0.38	0.358	8	0.32	0.438	8	0.33	0.421	8
Air temperature	Jan temp	January	ºC	-0.07	0.874	8	0.57	0.142	8	0.29	0.494	8
	Feb temp	February	ºC	-0.40	0.322	8	-0.02	0.97	8	0.11	0.802	8
	Mar temp	March	ºC	-0.24	0.568	8	**-0.67**	**0.071'**	8	-0.50	0.212	8
	Apr temp	April	ºC	-0.22	0.6	8	0.20	0.637	8	-0.42	0.301	8
	May temp	May	ºC	0.49	0.215	8	0.18	0.672	8	-0.52	0.19	8
	June temp	June	ºC	0.12	0.776	8	-0.09	0.828	8	0.30	0.465	8
	July temp	July	ºC	0.30	0.466	8	-0.57	0.144	8	0.11	0.798	8
	Aug temp	August	ºC	-0.25	0.547	8	-0.54	0.171	8	-0.03	0.939	8
	Sep temp	September	ºC	-0.62	0.103	8	0.07	0.873	8	0.28	0.501	8
	Oct temp	October	ºC	-0.11	0.794	8	**-0.67**	**0.070'**	8	-0.16	0.705	8
	Nov temp	November	ºC	-0.02	0.958	8	-0.45	0.266	8	-0.38	0.347	8
	Dec temp	December	ºC	0.17	0.684	8	-0.03	0.938	8	0.24	0.573	8
	summer (JJA) temp	JJA	ºC	0.12	0.775	8	-0.48	0.228	8	0.18	0.672	8
	MJJAS temp	MJJAS	ºC	-0.04	0.926	8	-0.45	0.262	8	0.09	0.838	8

Table S6. Pearson correlation (r) between the mean TF NDVI and ecosystem (or climatic) parameters with 0-,1- and 2-year time lag of the TF NDVI after the wet event (2008-2019). Bold font indicates a significant correlation. Significance levels were flagged as the following: 'p <0.1, *p <0.05, **p <0.01, ***p <0.001. The number (n) indicates a sample size of observed years.

Ecosystem and climatic parameters in the current year (i year)				Transect TF NDVI								
				the current year (i year)			the following year (i+1 year)			two years later (i+2 year)		
	Parameter	Observation Month	unit	r	p-value	n	r	p-value	n	r	p-value	n
Needle parameters	$\delta^{13}C$		‰	0.34	0.306	11	**0.91**	**<0.001*** **	11	0.36	0.274	11
	$\delta^{15}N$		‰	-0.46	0.176	10	-0.36	0.311	10	-0.24	0.505	10
	C/N		‰	0.09	0.807	10	-0.12	0.733	10	-0.02	0.961	10
Soil water equivalent (SWE)	June SWE	June	mm	**-0.71**	**0.009****	**12**	**-0.61**	**0.036***	**12**	0.08	0.794	12
	July SWE	July	mm	**-0.74**	**0.006***	**12**	**-0.61**	**0.036***	**12**	-0.19	0.553	12
	Aug SWE	August	mm	**-0.55**	**0.066'**	**12**	**-0.64**	**0.026***	**12**	-0.43	0.159	12
	summer SWE	JJA	mm	**-0.73**	**0.008****	**12**	**-0.65**	**0.023***	**12**	-0.17	0.598	12
Tree-ring width index	RWI			-0.16	0.683	9	0.15	0.689	10	-0.25	0.450	11
Precipitation	Jan prec	January	mm	0.30	0.341	12	0.22	0.483	12	-0.17	0.587	12
	Feb prec	February	mm	0.30	0.341	12	0.05	0.887	12	-0.10	0.767	12
	Mar prec	March	mm	-0.20	0.538	12	-0.28	0.380	12	-0.26	0.413	12
	Apr prec	April	mm	0.19	0.560	12	0.18	0.582	12	0.16	0.627	12
	May prec	May	mm	-0.01	0.974	12	-0.41	0.187	12	0.27	0.401	12
	June prec	June	mm	-0.24	0.458	12	-0.12	0.699	12	0.05	0.877	12
	July prec	July	mm	-0.41	0.182	12	-0.15	0.648	12	-0.48	0.115	12
	Aug prec	August	mm	0.40	0.199	12	**0.57**	**0.053'**	12	-0.27	0.401	12
	Sep prec	September	mm	0.41	0.183	12	-0.23	0.480	12	0.06	0.865	12
	Oct prec	October	mm	0.25	0.426	12	0.14	0.667	12	0.11	0.731	12
	Nov prec	November	mm	-0.05	0.875	12	-0.23	0.479	12	-0.18	0.586	12
	Dec prec	December	mm	-0.06	0.858	12	0.41	0.187	12	0.19	0.559	12
	snow before summer	previous Oct - current Apr	mm	0.27	0.401	12	0.07	0.840	12	-0.41	0.189	12
	rain	MJJAS	mm	0.02	0.949	12	-0.14	0.663	12	-0.34	0.285	12
	summer (JJA) rain	JJA	mm	-0.18	0.566	12	0.15	0.636	12	**-0.50**	**0.097'**	**12**
Air temperature	Jan temp	January	ºC	0.22	0.500	12	0.19	0.554	12	0.38	0.221	12
	Feb temp	February	ºC	0.07	0.836	12	-0.19	0.546	12	0.17	0.597	12
	Mar temp	March	ºC	-0.21	0.519	12	0.01	0.986	12	0.27	0.396	12
	Apr temp	April	ºC	0.07	0.827	12	0.22	0.492	12	0.05	0.876	12
	May temp	May	ºC	0.10	0.748	12	0.11	0.739	12	-0.46	0.137	12
	June temp	June	ºC	**0.60**	**0.038***	**12**	-0.26	0.414	12	-0.36	0.254	12
	July temp	July	ºC	-0.12	0.710	12	0.29	0.361	12	0.31	0.334	12
	Aug temp	August	ºC	-0.07	0.824	12	0.03	0.916	12	0.34	0.283	12
	Sep temp	September	ºC	**0.52**	**0.087'**	**12**	-0.23	0.464	12	-0.18	0.574	12
	Oct temp	October	ºC	0.30	0.344	12	0.17	0.592	12	-0.30	0.335	12
	Nov temp	November	ºC	-0.30	0.345	12	0.05	0.869	12	0.19	0.547	12
	Dec temp	December	ºC	0.12	0.720	12	-0.05	0.884	12	-0.18	0.569	12
	summer (JJA) temp	JJA	ºC	0.27	0.401	12	0.05	0.878	12	0.15	0.647	12
	MJJAS temp	MJJAS	ºC	**0.50**	**0.097'**	**12**	-0.01	0.979	12	-0.13	0.679	12

Table S7. Pearson correlation (r) between the mean TF NDVI and ecosystem (or climatic) parameters with 0-,1- and 2-year time lag of the TF NDVI for the observation period of the NDVI (1999-2019). Bold font indicates a significant correlation. Significance levels were flagged as the following: 'p <0.1, *p <0.05, **p <0.01, ***p <0.001. The number (n) indicates a sample size of observed years.

Ecosystem and climatic parameters in the current year (i year)				Transect TF NDVI								
				the current year (i year)			the following year (i+1 year)			two years later (i+2 year)		
	Parameter	Observation Month	unit	r	p-value	n	r	p-value	n	r	p-value	n
Needle parameters	$\delta^{13}C$		‰	-0.23	0.326	20	0.17	0.495	19	0.18	0.478	18
	$\delta^{15}N$		‰	0.15	0.550	19	0.02	0.940	18	-0.13	0.613	17
	C/N		‰	-0.33	0.167	19	-0.14	0.566	18	0.27	0.291	17
Soil water equivalent (SWE)	June SWE	June	mm	0.09	0.712	20	-0.13	0.582	20	-0.06	0.791	19
	July SWE	July	mm	0.00	0.983	21	-0.04	0.872	21	-0.07	0.763	20
	Aug SWE	August	mm	-0.15	0.542	20	0.07	0.761	20	0.02	0.934	19
	summer SWE	JJA	mm	-0.14	0.569	19	-0.16	0.517	19	-0.10	0.685	18
Tree-ring width index	RWI			**0.41**	**0.092'**	**18**	0.21	0.381	19	-0.13	0.599	20
Precipitation	Jan prec	January	mm	0.03	0.884	21	0.07	0.762	21	-0.02	0.928	21
	Feb prec	February	mm	-0.13	0.562	21	-0.11	0.626	21	0.13	0.587	21
	Mar prec	March	mm	-0.30	0.180	21	**-0.40**	**0.072'**	**21**	-0.13	0.574	21
	Apr prec	April	mm	0.27	0.231	21	0.11	0.649	21	0.15	0.525	21
	May prec	May	mm	0.20	0.384	21	-0.27	0.229	21	0.06	0.810	21
	June prec	June	mm	0.03	0.903	21	0.26	0.253	21	0.11	0.636	21
	July prec	July	mm	**-0.46**	**0.034***	**21**	-0.14	0.550	21	-0.10	0.662	21
	Aug prec	August	mm	0.03	0.903	21	0.35	0.120	21	-0.04	0.875	21
	Sep prec	September	mm	0.00	0.990	21	-0.11	0.631	21	0.35	0.125	21
	Oct prec	October	mm	0.13	0.587	21	0.27	0.240	21	**0.49**	**0.024***	21
	Nov prec	November	mm	-0.02	0.932	21	-0.07	0.776	21	-0.01	0.950	21
	Dec prec	December	mm	-0.16	0.492	21	0.11	0.627	21	0.25	0.284	21
	snow before summer	previous Oct - current Apr	mm	0.13	0.575	21	0.27	0.244	21	-0.10	0.675	21
	rain	MJJAS	mm	-0.16	0.494	21	0.13	0.583	21	0.13	0.575	21
	summer (JJA) rain	JJA	mm	-0.25	0.268	21	0.28	0.219	21	-0.04	0.864	21
Air temperature	Jan temp	January	ºC	0.08	0.731	21	0.19	0.407	21	0.27	0.238	21
	Feb temp	February	ºC	-0.20	0.378	21	-0.13	0.576	21	0.11	0.623	21
	Mar temp	March	ºC	-0.22	0.340	21	-0.29	0.197	21	-0.10	0.655	21
	Apr temp	April	ºC	-0.06	0.809	21	0.17	0.469	21	-0.11	0.647	21
	May temp	May	ºC	0.22	0.340	21	0.07	0.779	21	**-0.43**	**0.049***	**21**
	June temp	June	ºC	0.27	0.229	21	-0.17	0.461	21	0.01	0.975	21
	July temp	July	ºC	0.01	0.964	21	-0.13	0.560	21	0.19	0.420	21
	Aug temp	August	ºC	-0.14	0.542	21	-0.29	0.210	21	0.07	0.777	21
	Sep temp	September	ºC	-0.09	0.700	21	-0.05	0.844	21	0.10	0.676	21
	Oct temp	October	ºC	0.07	0.758	21	-0.20	0.383	21	-0.24	0.289	21
	Nov temp	November	ºC	-0.13	0.581	21	-0.24	0.292	21	-0.05	0.827	21
	Dec temp	December	ºC	0.17	0.468	21	-0.04	0.847	21	0.02	0.915	21
	summer (JJA) temp	JJA	ºC	0.09	0.684	21	-0.28	0.224	21	0.12	0.597	21
	MJJAS temp	MJJAS	ºC	0.13	0.575	21	-0.25	0.267	21	-0.03	0.880	21

Table S8. Pearson correlation (r) between the foliar $\delta^{13}C$ and soil moisture water equivalent (SWE) in the surface layer of 0-60 cm with 0-,1- and 2-year time lag of the foliar $\delta^{13}C$ for three periods, 1999-2007, 2008-2019 and 1999-2019. Bold font indicates a significant correlation. Significance levels were shown as 'p <0.1, *p <0.05, **p <0.01, ***p <0.001. The number (n) indicates a sample size of observed years.

Period	Soil moisture water equivalent in the current year (i year)	Foliar $\delta^{13}C$								
		the current year (i year)			the following year (i+1 year)			two years later (i+2 year)		
		r	p-value	n	r	p-value	n	r	p-value	n
1999-2007	June SWE	**-0.63**	**0.093'**	**8**	0.39	0.345	8	**0.70**	**0.078'**	**7**
	July SWE	**-0.68**	**0.042***	**9**	-0.55	0.124	9	0.47	0.242	8
	Aug SWE	-0.53	0.178	8	**-0.79**	**0.020***	**8**	-0.07	0.879	7
	summer SWE	-0.33	0.476	7	-0.32	0.487	7	0.38	0.457	6
2008-2019	June SWE	**-0.74**	**0.009****	**11**	0.03	0.924	11	0.17	0.608	11
	July SWE	**-0.79**	**0.004****	**11**	-0.25	0.450	11	0.08	0.824	11
	Aug SWE	**-0.70**	**0.016***	**11**	-0.46	0.153	11	-0.04	0.901	11
	summer SWE	**-0.81**	**0.002****	**11**	-0.22	0.513	11	0.08	0.816	11
1999-2019	June SWE	**-0.71**	**<0.001*****	**19**	0.12	0.628	19	0.35	0.150	18
	July SWE	**-0.74**	**<0.001*****	**20**	-0.32	0.162	20	0.23	0.338	19
	Aug SWE	**-0.63**	**0.004****	**19**	**-0.62**	**0.004****	**19**	-0.04	0.876	18
	summer SWE	**-0.74**	**<0.001*****	**18**	-0.27	0.279	18	0.14	0.593	17

Table S9. Pearson correlation (r) between the foliar C/N and soil moisture water equivalent (SWE) in the surface layer of 0-60 cm with 0-,1- and 2-year time lag of the foliar C/N for three periods, 1999-2006, 2008-2018 and 1999-2019. Bold font indicates a significant correlation. Significance levels were shown as 'p <0.1, *p <0.05. The sample size (n) indicates a number of observed years.

Period	Soil moisture water equivalent in the current year (i year)	Foliar C/N								
		the current year (i year)			the following year (i+1 year)			two years later (i+2 year)		
		r	p-value	n	r	p-value	n	r	p-value	n
1999-2006	June SWE	**-0.77**	**0.045***	7	-0.41	0.358	7	0.02	0.964	6
	July SWE	-0.51	0.192	8	**-0.65**	**0.082'**	**8**	-0.34	0.452	7
	Aug SWE	0.18	0.702	7	**-0.78**	**0.037***	**7**	-0.30	0.565	6
	summer SWE	-0.41	0.422	6	**-0.78**	**0.067'**	**6**	0.12	0.852	5
2008-2018 (excluding 2007 and 2019)	June SWE	**0.60**	**0.089'**	**9**	0.08	0.859	8	-0.34	0.455	7
	July SWE	0.47	0.197	9	0.04	0.927	8	-0.46	0.300	7
	Aug SWE	0.08	0.833	9	0.40	0.322	8	0.11	0.816	7
	summer SWE	0.43	0.245	9	0.19	0.660	8	-0.26	0.574	7
1999-2019	June SWE	0.04	0.888	18	-0.24	0.338	18	-0.22	0.392	17
	July SWE	0.07	0.766	19	**-0.39**	**0.100'**	**19**	-0.36	0.140	18
	Aug SWE	0.19	0.445	18	-0.24	0.341	18	-0.22	0.404	17
	summer SWE	0.18	0.491	17	-0.25	0.339	17	-0.21	0.437	16